Modeling and optimization of a gas transmission network for supplying natural gas with hydrogen injection.

by

Pronob Das

B.Sc., Rajshahi University of Engineering and Technology, 2017

A Thesis Submitted in Partial Fulfillment
of the Requirements for the Degree of

MASTER OF APPLIED SCIENCE

In the Department of Mechanical Engineering

University of Victoria

Supervisory Committee

Modeling and optimization of a gas transmission network for supplying natural gas with hydrogen injection.

by

Pronob Das

B.Sc., Rajshahi University of Engineering and Technology, 2017

Supervisory Committee

Dr. Andrew Rowe, Department of Mechanical Engineering, UVic
Supervisor

Dr. Peter Wild, Department of Mechanical Engineering, UVic
Departmental Member

ABSTRACT

This study focuses on optimizing natural gas transmission pipelines transporting methane-hydrogen mixtures to minimize compressor fuel consumption. The optimization problem employs MATLAB and genetic algorithm for the modeling and optimization of the pipeline. The study targets both single and multi-delivery point pipelines for the optimization. For an 800 km pipeline, the fuel consumption for delivering 8 GW of power is 2.98% for single delivery considering natural gas transmission. Around 2.7% fuel is consumed for multi-delivery pipelines to delivery same power for natural gas considering six delivery points. Introducing hydrogen into the natural gas mixture increases fuel consumption proportionally, with 5-20vol% hydrogen injections resulting in fuel consumptions of 3-3.8%, respectively, for multi-delivery pipelines. Pure hydrogen (100% H_2) injection leads to a significant increase in fuel consumption up to 19.9%. The study also explores the impact of maximum allowable operating pressure (MAOP) on pipeline performance. The operating pressure of the pipeline increases with the increasing hydrogen content while maintaining the constant power delivery. This highlights the need for higher pressures to transport hydrogen-enriched natural gas efficiently. Because hydrogen has a lower energy density, mixtures containing it tend to cause a higher pressure to drop when delivering energy at a desired rate leading higher compressor fuel consumption. The study finds that blending hydrogen reduces CO_2 emissions significantly from compressor fuel consumption, with reductions of 1.85-7.25% for 5-20vol% hydrogen injections, respectively. In terms of economic implications, transitioning from natural gas to electric compressors reduces emissions due to compressor fuel consumption from 430 ktCO_2/year to 31.9 ktCO_2/year, albeit with a cost increase for compressor power supply from $15.39 million to $178 million annually. The results underscore the usefulness of the optimization approach in enhancing fuel efficiency and reducing emissions.

Table of Contents

List of Figures

List of Tables

Nomenclature

A	Area, m^2
C	Sonic velocity, m/s
CH_4	Methane gas
CO_2	Carbon-di-oxide gas
C_p	Specific heat capacity at constant pressure, J/(kmol.K)
C_v	Specific heat capacity at constant volume, J/kg·K
D	Pipeline internal diameter, m
F	Darcy friction factor
f_E	Seam joint factor
f_F	Design factor
f_T	Temperature direction factor
G	Gravity acceleration, m/s^2
G	Pipeline arc
H	Compressor isentropic head, KJ/kg
H	Pipeline elevation, m
H_2	Hydrogen gas
K	Isentropic exponent
L	Pipeline length, km
L_e	Equivalent pipe length, km
M	Mass flow rate, kg/s
M	Molecular mass, g/mol
m_d	Delivered mass flow rate, kg/s
m_f	Compressor fuel consumption rate, kg/s
n_c	Number of compressors
P	Average pressure, Pa
P	Compressor required power, kw
P_b	Base pressure, kPa
P_c	Pseudo critical pressure, Pa
p_d	Delivery pressure, Pa
P_r	Reduced pressure, Pa
p_s	Supply pressure, Pa
Q	Volumetric flow rate, m^3/s
R	Universal gas constant, 8314 J/kmol-K
S	Elevation adjustment parameter
T	Pipe wall thickness, m
T	Temperature, K
T_c	Pseudo critical temperature, K
T_r	Reduced temperature, K
V	Gas velocity, m/s

v_e	Erosional velocity, m/s
Z	Compressibility factor
A	Acute angle, degrees
E	Material roughness, μm
P	Density, kg/m^3
η_d	Driver efficiency, %
η_i	Isentropic efficiency, %
η_m	Mechanical efficiency, %

Acronyms

ACO	Ant Colony Optimization
AHP	Analytic Hierarchy Method
CAPEX	Capital expenditure
CCC	Committee on Climate Change
CCS	Carbon capture and sequestration
CFC	Compressor fuel consumption
GA	Genetic Algorithm
GHG	Greenhouse gas
GRG	Generalized Reduced Gradient
HHV	Higher heating value, kJ/kg
LHV	Lower heating value, kJ/kg
LNG	Liquefied natural gas
MAOP	Maximum Allowable Operating Pressure
MILP	Mixed-Integer Linear Programming
NG	Natural gas
NPS	Nominal pipe size
PSO	Particle swarm optimization
Re	Reynolds number
SMR	Steam methane reformation
SMYS	Stipulated minimum yield strength
TSOs	Transmission system operators

ACKNOWLEDGEMENTS

All praise be to Lord Krishna, the Most Gracious, the Most Merciful, for blessing me with the knowledge, strength, and patience that sustained me throughout my MASc. journey.

I am deeply grateful to my supervisor, Dr. Andrew Rowe, for guiding me through the state-of-the-art in my research journey. His deep knowledge, willingness to explain complex concepts, constructive criticism, and continuous support have greatly influenced the shaping of my thesis. I am particularly thankful for his encouragement and trust in my ability to explore novel ideas and make them a reality.

I would like to thank:
Our research group advisor, Dr. Peter Wild, whose contributions have left a roadmap to plan and begin my research.
Mr. Chiradeep Majumder, for his helpful suggestions and support, which greatly encouraged me throughout my studies.

Last but not least, I am grateful to my parents, lovely wife, and siblings for their sacrifice, dedication, and emotional support for my higher studies in abroad.

DEDICATION

I dedicate this thesis to my late father, **Madhusudan Das**, my mother, **Ruposree Das**, father-in-law, mother-in-law, and my beloved wife, **Shusmita Rani**, whose love, support, and encouragement have been my greatest source of strength and inspiration throughout this journey.

Chapter 1

Introduction and problem formulation

This chapter presents the common characteristics of natural gas pipeline networks with their essential elements and explores the innovative integration of hydrogen gas injection into these systems. The modeling background for pipeline transmission systems is then reviewed and analyzed. Following this, the major contributions are stated with the research gap from previous literature.

1.1 Introduction

1.1.1 Natural gas pipeline

Relatively clean fuels have emerged as a result of public awareness of the pollution produced by excessive use of fossil fuels and the pressing need to rebuild the global energy infrastructure. Natural gas is regarded as a promising energy choice for 21st-century demands because of its low emission rates, energy efficiency, and availability [1, 2]. As a result, the amount of natural gas consumed worldwide increased by 5.3% between 1984 and 2018, to 195 billion cubic meters. Natural gas is currently the largest contributor to primary energy growth, accounting for 23% of global energy consumption; by 2050, that percentage is predicted to jump to 69% [2]. The annual global natural gas consumption trends are shown in **Fig. 1.1**. From the figure, it is clear that natural gas demand is going to be more in near future. The combination of increasing global energy demand, environmental and economic benefits, technological advancements, supportive policies, and the versatile nature of natural gas contributes to its rising consumption. However, due to the significant operational expenses associated with supply chains in moving natural gas from production centers to consumers, the resource has not been fully utilized despite its potential.

Pipeline networks play a major role in the transportation of natural gas [3, 4]. Today, natural gas pipelines are critical to the energy infrastructure, playing a pivotal role in the transportation of natural gas from production sites to consumers. This infrastructure provides a reliable means of transporting large volumes of natural gas over long distances, ensuring a steady supply of energy to residential, commercial, and industrial users. According to studies, globally ~93% of natural gas is transported via pipeline networks [2]. As a result, the effectiveness and safety of the pipeline network are important [5]. Unpredictable gas consumption rates and restricted permitted pressure

might cause certain natural gas pipeline networks to function effectively outside their ideal operating range. Medium- and long-term operating deficiencies may result from the excessive use of natural gas to meet the levels of intense energy demand.

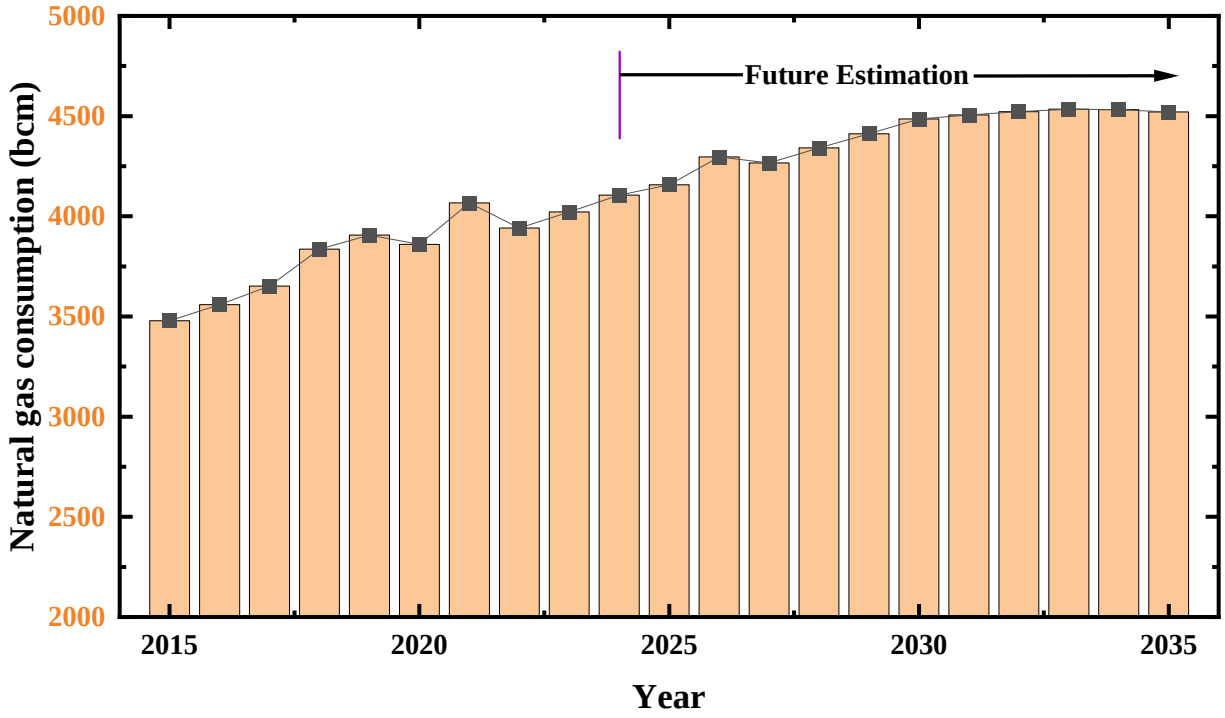

Fig. 1.1: Global annual natural gas consumption scenarios [6, 7].

A natural gas pipeline network must operate safely and cost-effectively, which necessitates an understanding of operating variables to determine the best operating strategy [8]. A comprehensive process of natural gas production, transmission, and delivery to end users is shown in **Fig. 1.2**. It starts with the extraction of oil and gas from wells, followed by the separation of oil, gas, and water. The gas then moves to a processing plant where nonhydrocarbon gases are removed, and some by-products are vented, flared, or returned to the field. The processed natural gas is then compressed at compressor stations to ensure it moves efficiently through the pipelines. An odorant is added to the gas for safety reasons before it continues through the main transmission lines. Along the way, the gas can be stored in underground storage reservoirs or liquefied natural gas (LNG) storage facilities. Finally, the gas is delivered to consumers, which include industrial plants, commercial buildings, and residential homes, through distribution pipelines managed by natural gas companies. This entire system ensures a steady and reliable supply of natural gas from production to consumption.

Gas is delivered to the distribution side and consumers via a network of medium-, high-, and low-pressure pipelines. Compressors are used by pipeline networks in this context to recover the pressure loss due to elevation, friction, and energy losses from gas to the environment. For instance, natural gas flowing via pipelines is consumed to provide energy for compressor stations powered by turbines. Typically, these gas stations are estimated to consume between 3-5% of their transported fuel [9] and constitutes around half of the total operational costs [10]. Reducing natural gas use will help reduce greenhouse gas emissions while also improving the supply chain's sustainability [11]. Moreover, since gas turbines or electricity are typically used to power natural gas compressors, changes in compressor energy consumption will also result in changes to the surrounding environment. Thus, optimizing the performance of the pipeline network greatly depends on the efficient operation of compressor stations.

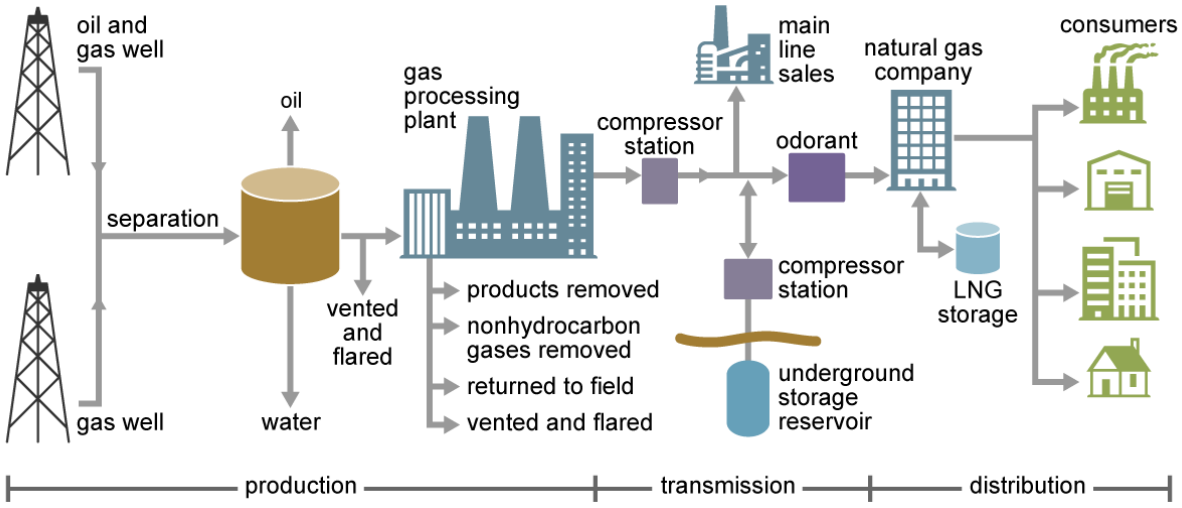

Fig. 1.2: Natural gas production, transmission, and distribution process [12].

Natural gas pipeline modeling is essential for ensuring the efficient, safe, and reliable operation of the natural gas transmission system. By simulating various operational scenarios, modeling allows for optimization of flow rates, pressure levels, and compressor station usage, which enhances overall operational efficiency and reduces costs. By anticipating possible problems like leaks or ruptures, it also plays a crucial part in safety and risk management by enabling proactive maintenance and risk reduction. Moreover, accurate modeling is crucial for regulatory compliance, design and planning of new infrastructure, and assessing the impact of integrating hydrogen gas into existing pipelines. Additionally, real-time modeling capabilities support immediate operator decision-making, enhancing responsiveness to dynamic conditions and emergencies. Overall,

natural gas pipeline modeling is a cornerstone of effective pipeline management, contributing to the sustainability and resilience of the energy supply chain.

1.1.2 Hydrogen gas into natural gas pipeline

The world is consuming more energy than ever before due to population and economic growth. Fossil fuels account for a large portion of the world's energy consumption, and excessive carbon dioxide emissions have created serious ecological issues. Countries all over the world are attempting to move non-fossil energy sources and optimize their energy structure in response to the severe difficulties posed by climatic anomalies and environmental pollution. Hydrogen energy holds significant importance as a sustainable and versatile energy source that can play a crucial role in addressing global energy challenges with its zero-emission ability. The global consumption of hydrogen is increasing at a pace of about 3-4% per year due to the growing demand for transportation fuels and the increased usage of heavy unconventional resources like oil sands [13]. Notably, the Committee on Climate Change (CCC) foresees hydrogen playing a role in decarbonizing the UK's residential sector through a low-carbon hybrid heating system in line with net-zero goals [14]. The CCC projects that the demand for hydrogen must grow from 27 TWh in 2017 to 270 TWh by 2050 for the UK to achieve its 2050 net-zero carbon target [14]. However, hydrogen faces several limitations, including high infrastructure costs for its production, storage, and distribution. Its low energy density per volume, explosive nature, and tendency to cause embrittlement in metals like steel further complicate its widespread adoption [15].

Researchers are currently attempting to produce hydrogen through thermal processes (natural gas reforming, coal gasification, pyrolysis, etc.) [16-23], electrolytic processes (water electrolysis from renewable energy sources) [24-29], photolytic processes [30-32], and biological & thermochemical processes [33-36]. Currently, fossil fuels provide 95% of the hydrogen produced worldwide. Half of this production comes from steam methane reformation of Natural Gas (SMR) [37, 38], with the majority of the remaining production coming from coal gasification and partial oxidation of natural gas [39]. Although hydrogen offers advantages for energy sector, construction of hydrogen pipelines over long distance pipeline is challenging. Hydrogen pipelines are more capital-intensive than gas pipelines [40], requiring a larger diameters [41] for same energy delivery capacity. These pipelines also are expected to be more costly because of increased requirements for leak testing, welding processes due to corrosion tendency, and compression at many supply chain stages [42]. Due to the more difficult maintenance and pipeline deterioration,

Schoots et al. [43] reports that the labor expenses for hydrogen pipes would be 28% more than those for natural gas. All things considered, building hydrogen pipelines may cost between 19% and 8% more than building CH_4 and CO_2 pipelines [43]. The capital expenditure (CAPEX) for new hydrogen pipelines could be 10%–50% higher than that of natural gas pipelines [44]. On the other hand, repurposing existing pipelines may prove to be 10%–25% less expensive than installing new hydrogen pipes, according to estimates made by European transmission system operators (TSOs) [44].

Theoretically, it is possible to blend hydrogen at percentages of up to 20% and at least 5% with little financial outlay [45]. However, even at fractions of 5%–15%, blend concentration needs to be evaluated case-by-case to take into consideration the unique end-user typology and variations in natural gas composition in pipelines [46]. Furthermore, switching to higher blending percentages will necessitate adjusting the infrastructure and machinery, including new burners [14]. This will raise the hazards associated with the environment, technological difficulties [47], and possible expenses [46].

Combining low-carbon hydrogen with natural gas has the potential to lower the carbon intensity of hard-to-decarbonize industries that are now supplied by natural gas, such as industrial operations, peak power generation for electricity, and heating for homes and businesses. The carbon footprint of natural gas and the applications that depend on it could be decreased by integrating hydrogen generated from low-carbon sources, like solar and wind power, into the system [48]. Hydrogen energy offers the benefit of easy storage as it can be stored in various forms such as compressed gas, liquid hydrogen, or metal hydrides, allowing for high energy density and the ability to store large amounts of energy over extended periods with minimal loss and emissions [49].

Hydrogen has many potential applications such as seasonal energy storage, light-, medium-, and heavy-duty transportation, and heating and power for residential, commercial, and industrial use. An estimated 80EJ (80×10^{18} joules) will be realized by hydrogen in 2050, making up 18% of the total energy required [10]. It can be produced from a range of low-carbon sources, such as biomass, nuclear, and renewable electricity, coal or natural gas with carbon capture and sequestration (CCS), and biomass [50]. However, creating the infrastructure required to support hydrogen for these different uses presents a significant obstacle. Around the world, businesses, governments at all levels, and researchers are exploring the possibility of incorporating hydrogen

into natural gas pipeline networks to reap the benefits of hydrogen without having to shoulder the financial burden of constructing new infrastructure. This strategy has a lot of potential benefits, but it also has a lot of drawbacks.

The development of hydrogen energy is hampered by the high cost of hydrogen storage and delivery [51-53]. Hydrogen is a gas at room temperature and, therefore must be stored at high pressure and/or low temperature to attain high energy densities. Thus, it has drawn a lot of attention as a potential method to transport hydrogen into natural gas pipelines [54-56]. The properties of hydrogen gas are compared with methane, ethane, and propane in **Table 1.1**.

Table 1.1: Comparison of properties of hydrogen, methane, ethane, and propane [54].

Component	**Hydrogen**	**Methane**	**Ethane**	**Propane**
Molecular Weight (g/mol)	2.02	16.04	30.07	44.1
Critical Temperature (K)	33.2	190.6	305.4	369.8
Critical Pressure (bar)	13.15	45.4	48.8	42.5
Critical Volume (cm^3/mol)	64.3	99.2	148.3	99.2
Lower heating value (MJ/kg), weight basis	120	50	47.8	46.35
Higher heating value (MJ/kg), weight basis	142	55.5	51.9	50.35
Molecular diffusivity in air (m^2/s)	6.1×10^{-5}	1.6×10^{-5}	1.453×10^{-5}	1.2043×10^{-5}
Acentric factor	-0.215	0.008	0.099	0.153
Heat Capacity at constant pressure at 25^0C (J/molK)	28.8	35.5	52.84	74.92
Specific heat ratio (C_p/C_v)	1.4	1.31	1.186	1.126
Adiabatic flame temperature in air (K)	2483	2236	2222	2250
Autoignition temperature in air (C)	500	580	515	455

1.2 Literature review on natural gas transmission system with hydrogen injection

Injection of hydrogen into natural gas of various compositions was studied by Deymi-Dashtebayaz et al. [57]. The results indicate that adding hydrogen affects pipeline pressure drop and energy density. The economics and emissions of producing electrolytic hydrogen in Ontario utilizing surplus power for distribution and mixing in natural gas infrastructure were evaluated by Mukherjee et al. According to their findings, providing end users with hydrogen-enriched natural gas could lower CO_2 emissions by 3,504 metric tons without hydrogen storage and 9,429 metric tons with hydrogen storage [58]. Modeling and simulation of the network of natural gas pipelines for hydrogen injection has been studied by numerous researchers as presented in **Table 1.2**.

Table 1.2: Literature review on the natural gas pipeline.

Gas Composition	Year	H_2 blend	Methodology	Objective function	Key findings
NG – H_2 [10]	2024	27.3%	Non-linear optimization	Maximize H_2 injection Minimize CFC	• For every 1% of hydrogen added, cost is reduced 3.29%. • Cost reduction from 24.78 to 22.23 million dollars with an 11.48% decline • Emission reduction from 11.84 to 10.63 kt with also an 11.48% decline.
NG – H_2 [54]	2023	-	Simulation (ACO)	Maximize H_2 injection Minimize CFC	• Max. 9.85%-mole H_2 permissible • Energy delivery = 8420 MJ • CFC = 1.01 kg/s
NG – H_2 [59]	2023	30%	Simulation	Optimal hydrogen blends and GHG reduction	• Around 36.3% reduction in GHG • A blend of up to 60% hydrogen with a 35% reduction in energy transmission
NG-H_2 [60]	2021	30%	Simulation (ASPEN)	-	• Reduction of pressure drops for single point H_2 injection. • Increment of pressure drops for multi-point H_2 injection.
NG – H_2 [61]	2018	10%	Simulation (MILP)	Minimization of cost	• Total cost increases with the addition of H_2
NG [62]	2018	-	Simulation (MILP)	Minimization of cost	• Around 7.5% cost reduction
NG [63]	2014	-	Simulation (MILP)	Minimization of cost	• Reduction of total cost • Improvement of system efficiency

Considering rising natural gas demand, Alves et al. [64] presented a multi-objective optimization model for designing natural gas transmission pipelines that minimizes transportation costs and maximizes the volume of gas carried. Compressor station and gas flow constraints were taken into account, and the Generalized Reduced Gradient (GRG) approach was employed to solve the problem. In order to optimize the design parameters of a natural gas transmission pipeline, Sanaye and Mahmoudimehr [65] presented an optimization tool consisting of Genetic Algorithm (GA) and optimal attributes of individual pipelines. To achieve a balance between the highest throughput and the maximum operation profit, Wu et al. [66] developed an optimization model for the trunk natural gas pipelines. Two goals were combined into a single objective function and the weight value was determined using the Analytic Hierarchy Method (AHP). The non-linear model mentioned above was solved using particle swarm optimization (PSO).

Chebouba et al. [67] optimized a NG transmission system using ant colony optimization (ACO) algorithm considering fuel consumption minimization as the objective function. Guandalini et al. [68] created an unsteady model of a gas pipeline segment to evaluate the dynamic impacts of injecting and blending hydrogen into the gas network. They compared a scenario with

only natural gas (NG) to one where hydrogen was mixed with NG within the same network. The analysis revealed significant effects on the higher heating value, Wobbe index, and density, though these effects remained within acceptable quality assurance limits. Additionally, the study demonstrated that the permissible hydrogen fractions are restricted and highly sensitive to boundary conditions, including user profiles and the size of connected gas supply stations. Natural gas networks are used in the technique known as "hydrogen transportation," which efficiently transports hydrogen to end users by combining it with energy from renewable sources (such as solar and wind) that cannot be balanced in real time [69]. Moreover, it is clear from the literature that up to 20% hydrogen injection is feasible with the natural gas for most end-users [54, 56, 70-72].

While there have been a number of pilot projects utilizing natural gas networks to mix hydrogen [55, 73], the technology for using this mixture in transportation is still in its early stages of development. There is currently insufficient research on the effects of hydrogen on equipment, pipelines, and mixing gas properties.

1.3 Limitations of earlier studies

Compressor stations in gas pipelines consume significant amounts of fuel, necessitating optimization strategies to reduce this fuel consumption. The significant limitations from the previous studies have been discussed here:

- Previous studies have highlighted the challenges in developing a comprehensive set of equations for natural gas transmission systems that comply with physical performance equations and predefined constraints. Despite the availability of various general-purpose optimization algorithms, applying them to pipeline transportation remains challenging due to the intricate integration of algebraic and differential equations required to model gas flow in pipelines. Many optimization algorithms struggle to handle this complexity effectively.
- Previous studies have not clearly established the effect of operating pressure in pipelines when blending H_2.
- No previous studies have examined the impact of using compressors powered by electricity, which do not consume a portion of the flowing gas, on emissions and fuel costs, unlike conventional turbine compressors.

- Most existing research has focused on single-delivery gas supply systems, which do not reflect the real-world scenario of multiple delivery stations supplying natural gas to different regions.

Earlier research in natural gas transmission optimization often narrowly focused on individual factors such as pipeline operational pressure, the effects of hydrogen blending, variations in Maximum Allowable Operating Pressure (MAOP), and the maximum capacity of existing pipeline infrastructure. Although these studies provided valuable insights, they generally did not integrate these factors into a comprehensive framework, potentially missing the synergies and trade-offs between different optimization parameters.

1.4 Objectives of the present study

There are mainly four major objectives in the present study to address the above-mentioned limitations from the previous studies:

- The present study addresses the gap of comprehensive set of equations by formulating all necessary equations mathematically. Motivated by these limitations, this paper conducts a holistic and integrated analysis using MATLAB and Genetic Algorithms (GA). The research aims to optimize the performance of gas pipelines, particularly in terms of reducing the fuel consumption of compressor stations, by leveraging advanced computational tools like MATLAB and GA.
- This study addresses the gap of operating pressure effect in pipelines when blending H_2 by sharply analyzing and optimizing operating pressure to reduce fuel consumption while adhering to pressure constraints.
- The authors also highlight a significant oversight in the literature: an innovative aspect of this paper is its comparison between electric-drive compressors and traditional systems.
- This study considers a complex and multi-delivery gas supply system which reflect real world gas transmission system. Additionally, while previous studies have predominantly focused on gas transmission pipelines, this paper also includes the consideration of low-pressure gas supplied from gas processing plants.

In summary, this thesis aims to address the limitations of earlier research through a comprehensive analysis that integrates multiple optimization parameters using advanced computational tools. This

approach builds on previous studies in natural gas pipeline optimization, offering a more holistic view and filling gaps left by earlier, more isolated research efforts.

1.5 Major contributions of the study

The study focuses on a large-scale and real complex natural gas network system. The major contributions of the present study are stated below:

- The study establishes both single and multi-delivery natural gas transmission models using MATLAB and GA.
- It investigates the effects of hydrogen injection (5-20 vol%) on the performance of the natural gas pipeline system. This is crucial for understanding how introducing hydrogen as a blend affects operational parameters.
- It discusses the maximum possible power delivery with the existing pipeline. This involves assessing the capacity limits and potential enhancements without physical expansion.
- It analyzes how MAOP influences compressor fuel consumption. This likely includes optimizing pressure levels to balance operational efficiency with safety and regulatory compliance.
- It focuses on the electrification of compressors and compares the costs and emissions associated with electrically powered compressors versus those powered by natural gas. This aligns with current trends towards reducing carbon footprints in energy infrastructure.
- The study examines how varying hydrogen injection ratios affect emissions from the pipeline system. This is essential for understanding the environmental impact of hydrogen integration.
- The study also addresses the impacts of pipeline material roughness factor on the fuel consumption.
- Finally, the study examines and analyzes the fuel consumption and emissions from the operational Coastal GasLink Pipeline network in British Columbia, Canada.

1.6 Summary

This chapter provides an overview of natural gas transmission systems, highlighting the growing importance of hydrogen in this sector. A review of the literature on hydrogen injection into natural

gas pipelines, including identification of its limitations, and an outline of the major contributions of the current study are presented.

Chapter 2

Methodology

This chapter describes the mathematical formulation of the pipeline model developed in this thesis paper, covering essential flow equations like continuity and momentum. It validates these with prior research, addressing constraints like pressure and velocity limits. Optimization methods are discussed to minimize fuel consumption and enhance operational efficiency in gas pipeline systems.

2.1 Gas pipeline Modeling

The equations governing the flow of natural gas through a pipeline are based on fluid dynamics and conservation of mass, momentum, and energy. The foundational flow equation relies on solutions derived from partial differential equations. Over the past century, several equations have been proposed to model the flow of compressible gas in lengthy pipelines. Notable among these are the Weymouth equation [74], the Panhandle A equation [75], and the Panhandle B equation [76]. Although these equations are derived from the fundamental energy equation for compressible flows, each incorporates a unique representation of the friction factor, facilitating analytical solutions. Additionally, these equations differ vary in terms of underlying theory and the number of parameters employed in their definition.

A gas transmission line is typically not constructed to handle two phase flow due to operational issues. Gathering systems, separation units, and oil and gas wells are a few examples of exceptions. The transmission line is limited to gas flow in a single phase. The differential momentum balance yields the pressure drop in a gas pipeline, which is the crucial parameter to calculate the compression power necessary for transmission. The friction that occurs between the fluid boundary layer and the tube's interior surface results in energy losses, which in turn lowers the gas pressure. The modeling approach consists of the material balance, the momentum conservation equations on the fundamental components of the network, and the other governing equations. The required formulas and inequalities in the gas transmission network system are established to ascertain the dynamic parameters like pressure and flow rate. The momentum balance for a single pipeline is shown first.

2.1.1 Assumptions for pipeline modelling optimization

The following assumptions are considered by the gas modeling equations:

Steady condition: Steady-state gas flow is assumed. Gas pipelines are known to experience unsteady (transient) flow in which flow parameters fluctuate. However, under many conditions, the steady state assumption produces results that are acceptable [77].

Isothermal flow: The gas flow is considered as isothermal in the present study. It is significant to remember that the heat transfer mechanism in subterranean pipelines modifies the temperature of the gas along their length. Nonetheless, the temperature of the gas eventually exceeds the ambient temperature in a system of lengthy extension lines, such a cross-country pipeline network that spans many kilometers. Because long transmission lines maintain a stable gas temperature that is either the same as or comparable to the surrounding environment's temperature, the common assumption that the flow will be isothermal works well.

Supply Pressure: It is assumed that the supply pressure from gas processing plant to the first compressor is 1.38 MPa (200 psi), and the delivery pressure to all the delivery nodes is equal or greater than 1.38 MPa.

Pipeline Elevation: Since the upstream and downstream locations do not significantly differ in elevation, it is assumed that the pipe segment is horizontal.

Flow direction: The flow always goes from upstream to downstream direction towards the supply node.

Compressors characteristics: Centrifugal compressors are employed in the pipelines to increase the gas pressure again. These kinds of compressor stations are common in today's gas business because of their low operating and maintenance expenses. It was therefore presumed that the compressors had the same features.

Isentropic compression: For the gas, a reversible adiabatic compression process is considered.

2.1.2 One dimensional compressible gas flow

A good approximation for calculating the pressure drop in a gas pipeline is to use a one-dimensional flow model, where the fluid conditions vary only along the pipe. The fact that the cross-section area is constant, and the pipe centerline's curvature is very large in relation to the

cross-sectional dimensions is one of the reasons for this application. A general schema of a pipe section is shown in **Fig. 2.1**. The momentum balance, also known as the equation of motion, equation of continuity, energy balance, and equation of state, is the basis for most fundamental equations describing the flow of gas in pipes. The assumptions made in relation to the operational conditions affect the form of the mathematical model. The foundation of simplified models is the omission of some terms from the original model.

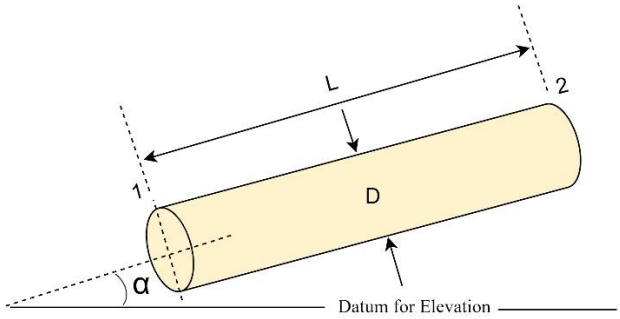

Fig. 2.1: Diagrammatic illustration of a sloped pipe section.

2.1.3 Conservation of mass: continuity equation

The equation of one-dimensional conservation of mass is given in **Equation (2.1)**, where ρ is the gas density in (kg/m^3), v is the average gas velocity in (m/s) in the x direction, and t is the time in (second).

$$\frac{\partial(\rho V)}{\partial \mathrm{t}} + \frac{\partial \rho}{\partial \mathrm{t}} = 0 \tag{2.1}$$

Equation (2.2) expresses the relationship between the mass flow rate, m in (kg/s), commonly known as pipe throughput, and the velocity of gas and density. Gas velocity varies along a pipeline despite constant pipe diameter because it is dependent on pressure, unlike liquid pipelines where it is constant owing to compressibility.

$$m = \frac{\pi}{4} D^2 \rho V \tag{2.2}$$

In this case. The cross-sectional area (m^2) remains constant over the entire length. Here, D means internal diameter of the pipe in m. By include the compressibility factor, Z, in the model, the relationship between gas density and pressure is expressed in the form of the following equation.

$$\rho = \frac{pM}{ZRT} \tag{2.3}$$

In the above equation, M is the average molecular mass of the gas, which varies depending on its composition, and R is the universal gas constant, which is equivalent to 8314 J/k mol-K. A simple

mixing rule [78], represented by the following equation, is used to get the mole mass of the gas. Here, Y_i and M_i stand for the mole fractions and molecular masses of the various species, respectively.

$$M = \sum M_i Y_i \tag{2.4}$$

To account for the compression behavior of gases, the ideal gas equation is modified using the compressibility factor, Z. In high pressure flow, the majority of actual gases must be adjusted using the compressibility factor. An appropriate equation to obtain factor Z, in this case, is Dranchuk-Purvis-Robinson [79] as shown in **Equation (2.5)**. In **Equations (2.6) and (2.7)**, T_r and P_r are reduced temperature and pressure, p is the average pressure of the pipe segment (Pa), T is the gas temperature (K), and T_c and P_c are pseudo critical temperature (K) and pressure (Pa). Based on the critical characteristics of the natural gas components, one can compute T_c and P_c of natural gas itself, using a suitable mixing rule.

$$\mathrm{Z} = 1 + \left(0.31506 - \frac{1.0467}{T_r} - \frac{0.5783}{T_r^3}\right)\rho_r + (0.5353 - \frac{0.6127}{T_r} - \frac{0.6185}{T_r^3})\rho_r{}^2 \tag{2.5}$$

$$T_r = \frac{T}{T_c} \tag{2.6}$$

$$P_r = \frac{p}{P_c} \tag{2.7}$$

where $\rho_r = 0.27\left(\frac{P_r}{ZT_r}\right)$, as natural gas specific density, no dimensional number.

$$T_c = \sum T_{ci} y_i \tag{2.8}$$

$$P_c = \sum P_{ci} y_i \tag{2.9}$$

The conditions at which the differences between the liquid and vapor phases vanish is known as its critical point. The present study employs Kay's rule, a straightforward linear mixing rule illustrated in **Equations (2.8) and (2.9)**, to calculate the average pseudo-critical characteristics of a gas based on the mole fractions of its constituents disclosed. The continuity equation can be rearranged in terms of mass flow rate and pressure using **Equation (2.3)**, which can be stated as the following equation:

$$\frac{1}{A}\frac{\partial m}{\partial x} + \frac{M}{R}\frac{\partial}{\partial t}\left(\frac{p}{ZT}\right) = 0 \tag{2.10}$$

2.1.4 Equation of motion: momentum balance

The pressure fluctuations along a pipe and with time are determined by applying the conservation of momentum equation to a cylindrical control volume. Thus, the following formula can be used to determine the pressure at each location along a pipe:

$$\frac{\partial p}{\partial x} + \frac{f}{2D}\rho v^2 \pm g\rho sin\alpha + \frac{\partial(\rho v^2)}{\partial x} + \frac{\partial(\rho v)}{\partial t} = 0 \tag{2.11}$$

The variables in this equation are pressure (p) in Pa, acceleration due to gravity (g) in m/s^2, and the acute angle (α) between the pipe centerline direction (x) and the horizon. In the preceding equation, the sign of the gravity factor is positive when the gas moves upward and negative when it flows downhill. The relative roughness of the pipeline, expressed as ε/D, and the Reynolds number, Re, determine the dimensionless Darcy friction factor, f. The Reynolds number measures the proportion of viscous to inertial forces under specific flow conditions and aids in the distinction between laminar and turbulent flow.

$$Re = \frac{\rho v D}{\mu} \tag{2.12}$$

The roughness of the pipeline wall has a significant impact on the pressure drop in offshore gas pipelines, where Re has an order of magnitude of 13,000. It is standard procedure in these pipelines to coat the pipe walls to lessen wall roughness and pressure loss [80].

The friction factor as shown in **Equation (2.13)** is evaluated using the equation derived by Prandtl-von Karman, where the friction factor depends only on the relative roughness, because the flow is thought to be fully developed in this case, as is the case with gas pipelines [2].

$$f = \left(-2log\frac{\frac{\varepsilon}{D}}{3.71}\right)^{-2} \tag{2.13}$$

The following formula can be used to express the momentum balance in terms of pressure and throughput:

$$\frac{\partial p}{\partial x} + \frac{f}{2D}\frac{ZRT}{pMA^2}m^2 \pm g\frac{pM}{ZRT}sin\alpha + \frac{2mR}{A^2M}\frac{ZT}{p}\frac{\partial m}{\partial x} + \frac{m^2R}{A^2M}\frac{\partial}{\partial x}\left(\frac{ZT}{p}\right) + \frac{1}{A}\frac{\partial m}{\partial t} = 0 \tag{2.14}$$

The derivation of the equation is shown in the **Appendix A**. At every point along the pipe, the flow characteristics remain constant when the system is in a steady state. **Equations (2.15) and (2.16)** can be used to numerically represent that steady state condition. Consequently, the mass flow rate through the pipe stays constant, using **Equation (2.10)**:

$$\frac{\partial m}{\partial t} = 0 \tag{2.15}$$

$$\frac{\partial}{\partial t}\left(\frac{p}{ZT}\right) = 0 \tag{2.16}$$

$$\frac{1}{A}\frac{dm}{dx} = 0 \Rightarrow m = cte \tag{2.17}$$

As a result, the general **Equation (2.14)** can be expressed as follows in a steady state:

$$\frac{dp}{dx} + \frac{f}{2D}\frac{ZRT}{pMA^2}m^2 \pm g\frac{pM}{ZRT}sin\alpha + \frac{m^2R}{A^2M}\frac{d}{dx}\left(\frac{ZT}{p}\right) = 0 \tag{2.18}$$

Variations in elevation of gas transmission lines may appear to have a negligible effect on the total pressure drop, but this effect can be significant, especially in high pressure lines. **Appendix A** contains the corresponding equation for calculating the pressure drop in a pipe segment with an elevation change. The steady-state pressure drop for a horizontal pipe may be found using the following expression in **Equation (2.19)** if the temperature and compressibility factor are assumed to remain constant between pipe locations 1 and 2.

$$\left(P_2{}^2 - P_1{}^2\right) - \frac{32m^2ZRT}{\pi^2D^4M}\ln\left(\frac{P_2}{P_1}\right) + \frac{16f}{\pi^2D^5}\frac{ZRT}{M}m^2L = 0 \tag{2.19}$$

2.1.5 Maximum allowable operational pressure

When the internal pressure in a pipe reaches the yield strength of the pipe material, irreversible deformation and eventual failure may occur as the pipe wall becomes stressed. In addition to the internal pressure created by the gas passing through the pipe, external pressure may also be present. This external pressure may come from the weight of the soil above the pipe in a buried pipeline as well as potential loads from passing cars. As a pipe descends below the surface of the earth, the pressure it receives from above-ground vehicles will decrease. The effect of internal pressure is typically greater than that of external loads in scenarios involving underground pipelines. Consequently, in a gas pipelines, the internal pressure, typically, determine the minimum wall thickness that is required.

As a design parameter in pipeline engineering, the pressure at every point in the pipeline should be lower than the MAOP. **Equation (2.21)** is utilized to compute the upper limit [54]. According to a hypothetical **Equation (2.22)**, the wall thickness of the pipelines is taken into account while calculating MAOP. This formula provides the thickness, t, in meters for a range of sizes. The planned dimensions for stainless steel pipes given by ASME B36.19M standard are used to generate this equation.

$$p < MAOP \tag{2.20}$$

$$MAOP = SMYS * \frac{2t}{D} * f_F f_E f_T \tag{2.21}$$

$$t = 52 \times 10^{-3} D + 989 \times 10^{-7} \tag{2.22}$$

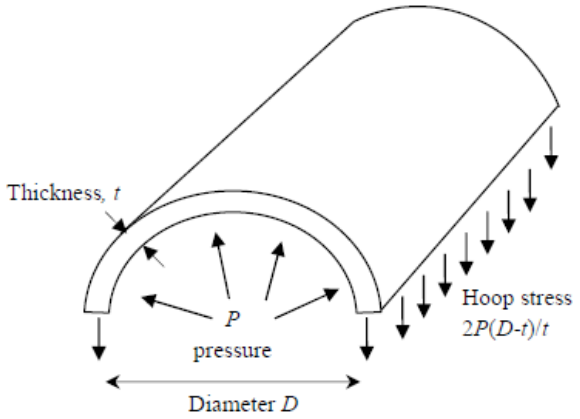

Fig. 2.2: Internal pressure causes stress on the pipeline because of the flow of gas.

This equation states that the minimum wall thickness needed for a gas pipeline to resist internal pressure is dependent on the pipe's internal diameter and material. The specified minimum yield strength (SMYS) of pipe material is the yield stress, a mechanical characteristic of the pipeline material. The design factor is known as factor f_F. For cross-country or offshore gas pipelines, this factor is typically 0.72, but it can be as low as 0.4 based on the class location and construction style [81]. To calculate pipeline MAOP, the stipulated minimum yield strength (SMYS) for the steel is considered as 2000 bar, which is within usual, standard ranges. The population density in the pipeline's immediate area determines the class sites in turn.

The pipe material and junction type affect the seam joint factor, or f_E, a factor which represents the overall strength of a weld seam. The range of seam joint factors for the most widely utilized material kinds is one to six. When the gas temperature is below 120 ºC, the temperature deration factor, or f_T (which is an adjustment factor of the pipeline's MAOP or capacity based on temperature variations), is equal to 1, but above 230 ºC, it increases to 0.867 [81].

2.1.6 Critical velocity

So-called critical flow is a significant factor in the management of compressible fluid flow. The increase in flow for a compressible flow, caused by a rise in pressure drop, is restricted to the fluid's critical velocity, or the speed of sound. The greatest velocity that a compressible fluid in a pipe can

achieve is known as the sonic or critical velocity. At less than half the speed of sound, velocities are maintained for trouble-free operation. **Equation (2.23)** can be used to compute the sonic velocity in a gas, c, with a good approximation. In this instance, k represents the gas's average isentropic exponent. The constant pressure heat capacity, expressed in J/(kmol K), is called C_p.

$$c = \sqrt{\frac{kZRT}{M}} \tag{2.23}$$

$$v < c/2 \tag{2.24}$$

$$k = \frac{\Sigma\left(C_{p_i} y_i\right)}{M\Sigma\left(C_{p_i} y_i\right) - R} \tag{2.25}$$

In a pipeline, increasing gas velocity can have a specific impact on vibrations d noise levels. Additionally, over an extended length of time, faster speeds will erode the inside surfaces of elbows, tubes, and other joints. The maximum velocity range ought to be such that impingement attack or erosion-corrosion cavitations are kept to a minimum. Typically, the following equation is used to compute the upper limit of the gas velocity empirically for design purposes [82]. The erosional velocity, v_e, in the gas always falls below the speed of sound in the pipeline design domain and is represented by Equation (2.27) [54]. It is important to consider that the flow velocity should be within a range that minimizes corrosion. The lowest possible flow velocity range should maintain pollutants suspended in the pipeline, reducing the amount of corrosion-causing material that builds up inside the pipeline.

$$V < v_e \tag{2.26}$$

$$v_e = 122\sqrt{\frac{Z_i RT}{P_{ij} M}} \tag{2.27}$$

where R is the gas constant, Z_i is the compressibility factor, and v_e is the erosional velocity, given in meters per second; T is the gas temperature, given in Kelvin; the average gas pressure in the pipeline, or p_{ij}, is given in bars.

2.2 Compressor characteristics

A centrifugal gas compressor is identified by its pressure ratio, which is the relationship between the compressor's suction side pressure and discharge pressure, as well as its supplied flow rate. An isentropic procedure can be effectively employed to formulate the compression process in a centrifugal compressor with the goal of computing horsepower for a compressor station. Even for compressors, the pressure ratio of a centrifugal compressor is typically given in m and is associated

with a particular term called "head" that is brought over from pump design nomenclature. One definition of the "head" produced by the compressor is the amount of energy delivered to the gas per kg of mass. The isentropic equation of compressor head is stated in **Equation (28)**.

$$h_i = \frac{ZRT}{M}\frac{k}{k-1}\left[\left(\frac{p_d}{p_s}\right)^{\frac{k-1}{k}} - 1\right] \quad (2.28)$$

In the above equation, h_i is compressor isentropic head in kJ/kg, k is the isentropic exponent (considered 1.3), p_d is the delivery pressure from the compressor in Pa, and p_s is the supply pressure to the compressor in Pa. The required power at the compressor in kW can be stated by **Equation (29)**.

$$P_i = \frac{mh_i}{\eta_i} \quad (2.29)$$

Where η_i is the isentropic efficiency of the compressor, m is the compressed gas in kg/s, and h_i is compressor isentropic head in kJ/kg.

Electric motors, steam turbines, or internal combustion engines are frequently used as centrifugal compressor drives. Combustion turbines are another option for supplying the energy needed for the compression process. A little amount of the natural gas that is compressed by turbine compressors is used as energy. The turbine drives a centrifugal compressor, which has a sort of fan inside, to compress and pump natural gas through the pipeline. The same kind of centrifugal compressor is turned at some compressor stations by an electric motor. The usage of any natural gas from the pipe is not necessary for this kind of compression, but a nearby steady supply of electricity is. Several compressor stations are also powered by reciprocating natural gas engines. These engines, which resemble very big automotive engines, are propelled by pipeline-supplied natural gas. The natural gas is compressed by the engine's pistons, which are powered by the gas's combustion and located outside the engine.

In this work, it is assumed that the station's centrifugal compressors are powered by turbines whose energy source is a line of the compressed gas from the pipeline that passes through the station, as illustrated in **Fig. 2.3**. The required power for compression, P, is divided by the isentropic efficiency, η_i (%), mechanical efficiency, η_m (%), driver efficiency, η_d (%), and LHV (lower heating value) to yield the flow rate of the gas used as fuel for the compression process in each compressor. The fuel consumption rate for compressor is stated in **Equation (2.30)** [2, 54].

$$m_f = \frac{10^6 m h_i}{\eta_i \eta_m \eta_d LHV} \tag{2.30}$$

The compressor stations typically consume about 3 to 5% of the transported gas [83]. Isentropic, mechanical and driver efficiencies for the compressors is assumed roughly 0.72, 0.90 and 0.35, respectively, according to the literature. Here, LHV stands for energy released by the gas's mass at its maximum rate of combustion. The mass lower heating values, LHV_i, of the molecules making up the gas are used to compute it at 25 °C and 1 bar in (kJ/kg) [54]:

$$\text{LHV} = \frac{\sum y_i M_i LHV_i}{\sum y_i M_i} \tag{2.31}$$

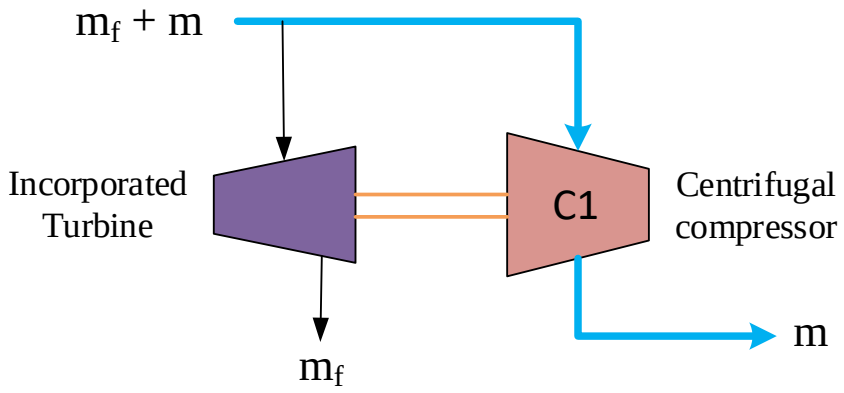

Fig. 2.3: Centrifugal compressor and its incorporated turbine in a compressor station.

Since it is expected that the water emitted following the combustion reactions is in a gaseous condition, HHV (high heating value) is not introduced in this instance. While meeting supply, delivery, and transport requirements as well as other physical limits, the maximum amount of gas that the network can transport is calculated. The transmitted power of a gas pipeline, a linear function of transmitted mass flow rate, m (kg/s), can be calculated by using **Equation (2.32)**. The pipe flow equation with the pipeline elevation difference can be described by **Equation (2.33)** [84].

$$P\ (kW) = m\ \left(\frac{kg}{s}\right) \times LHV\ \left(\frac{kJ}{kg}\right) \tag{2.32}$$

$$\left({P_1}^2 - e^{s_{12}} {P_2}^2\right) = \frac{32 m^2 ZRT}{\pi^2 D^4 M} \ln\left(\frac{P_1}{P_2}\right) - \frac{16 f}{\pi^2 D^5} \frac{ZRT}{M} m^2 L \tag{2.33}$$

Where, elevation adjustment parameter, $s_{12} = 0.0684 \left(\frac{H_2 - H_1}{TZ}\right)$

Equivalent pipe length (km), $L_e = L \left(\frac{e^s - 1}{s}\right)$

2.3 Equation Validation

Equation (2.19) is used mainly for the pipeline gas transmission. This section justify the precision of the equation using a paper on hydrogen blended long distance natural gas transmission simulation published by Clees et al. [85]. Multi-physical Network Simulator (MYNTS) was used in the paper, which is a software that solves transient non-isothermal Euler equations using sophisticated compressor thermodynamics and gas composition models for the purpose of simulating and analyzing gas networks. **Fig. 2.4 (a)** is from the reference paper, and **Fig. 2.4 (b)** is plotted using **Equation (2.19)**. In the analysis, pure H_2 (100% H_2), NG H_2 10%, and biogas low CH_4 gases are considered only due to the lack of proper heating values of other gases. From both figures, the pressure drops for input pressure 5 MPa are 46%, 84.2%, and 89% for biogas with low CH_4, NG H_2 10%, and pure hydrogen gases respectively, which are the same as values noted in **Fig. 2.4 (a)**. Additionally, the pressure drop lines follows the similar trend as the reference paper for inlet pressure 5 MPa to 12 MPa.

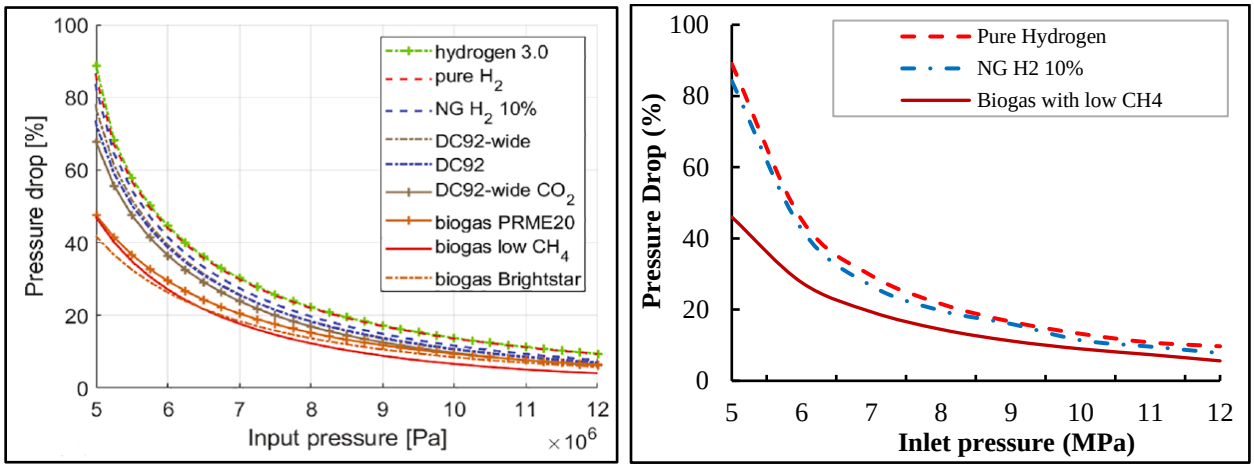

(a) (b)

Fig. 2.4: Pressure drop (%) profile with the variation of input pressure for different gases from (a) reference paper (Cless et al. [85]), and (b) present study.

2.4 Objective function

Depending on the problem definition, various objective functions may be taken into account, such as network design or developments the operational conditions of a gas network. Any of the following objective functions can be selected as the optimality purpose of the gas transmission network such as:

i. minimization of compressor fuel consumption
ii. minimization of total transmission cost
iii. maximize power throughout
iv. minimize emission
v. maximize H_2 injection

Arya et al. [54] considered minimizing compressor fuel consumption and maximizing H_2 injection as the objective functions in their hydrogen blended NG transmission system simulation. Similarly, in another study, Zhang [10] minimized compressor fuel consumption and maximized H_2 injection as the objective functions to optimize H_2 injected NG gas system. Cerniauskas et al. [86] used minimization of cost as the objective function of their NG pipeline modeling with reassignment for hydrogen. In another study, Tabkhi et al. [87] modeled H_2 injected natural gas transmission pipeline system using minimization of compressor fuel consumption as the objective function. Guandalini et al. [68] chosen emission reduction as the objective function for H_2 injected NG pipeline modeling, where compressor operating cost is considered as the objective function by Kazi et al. [73] to optimize steady flow of H_2 injected NG transmission pipeline. Uster and Dilaveroglu [63] conducted a study to optimize a NG transmission system considering minimization of total investment and operating cost as the objective function. Wang et al. [62] considered cost minimization as the objective function of muti-period NG transmission system. Alves and colleagues [64] introduced a multi-objective optimal model for the design of natural gas transmission pipes with the aim of minimizing transportation costs and optimizing the amount of gas transported. Using the ant colony optimization (ACO) technique, Chebouba et al. [67] designed an NG transmission system with the goal of minimizing fuel usage.

From **Table 1.2**, most of the researchers considered minimization of compressor fuel consumption in the optimization process which is also equivalent to the minimization of emissions and energy consumption. The objective function, f of the study can be stated as follows, where n_c means number of compressor stations in the pipeline:

$$f = \min \sum_{1}^{n_c} m_f$$

Where the fuel consumption for all the individual compressor is calculated using **Equation (2.31)**.

2.5 Optimization constraints

All the considered linear and non-linear constraints are stated below:

(1) All the pressure in the pipeline is always lower than pipeline MAOP.
(2) The lowest delivery pressure of the pipeline is equal or greater than 1.38 MPa (200 psi).
(3) The velocity of the gas in the pipeline is lower than the erosional velocity.
(4) The velocity of the gas in the pipeline is lower than the half of the critical velocity.
(5) Mass balance around all nodes.

2.6 Optimization process

Natural gas transmission systems are complex. It is typical, in practice, to simplify natural gas pipeline networks by segmenting them into pipelines, compressor stations, and terminals when modeling these networks. Given that pipelines transport large volumes of natural gas, even minor reductions in gas consumption at compressor stations can lead to substantial resource savings. Therefore, research focused on identifying optimal parameters to minimize energy consumption is crucial for informed decision-making. In this context, researchers have developed various techniques to reduce fuel usage.

Recent studies have employed optimization methods such as GA, ACO, GRG, etc. techniques for different applications and proposals [2]. Gas in the network is routed via intermediate terminals, withdrawn from the system at demand terminals, and then directed into the pipeline at supply terminals. **Fig. 2.5** outlines the main operational and design factors that can enhance pipeline profitability. Additionally, **Fig. 2.6** displays common methods for optimizing various operational parameters. The modeling equations and presumptions used to simulate and optimize the gas pipeline network are covered in this section. GRG methods [88], dynamic programming [89], and nonlinear techniques [63] are among the most commonly used traditional methods. However, these approaches have notable limitations. For instance, GRG methods require calculating a gradient at each point along the objective function curve. As a result, they are ineffective when the objective function is discontinuous or non-differentiable, due to the infinite slope at certain points.

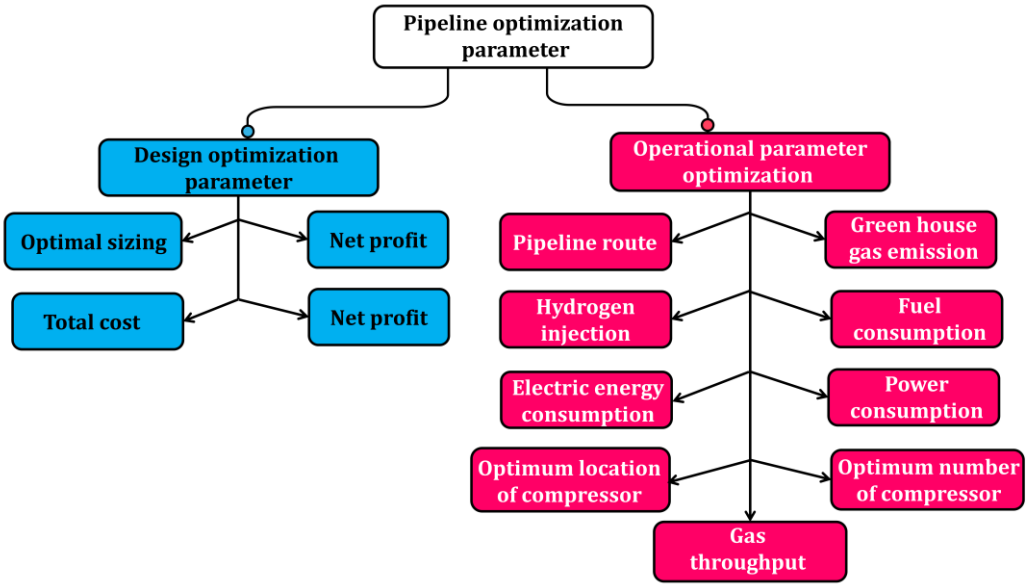

Fig. 2.5: Key operational and design elements that are utilized to maximize pipeline profitability [2].

Based on the literature review, GA was selected to optimize the present model. The flexibility, robustness, and efficiency of GA make it an excellent choice for optimizing natural gas pipeline operations. It offers a comprehensive approach to handle the complex, multi-dimensional, and constrained nature of pipeline systems, making it highly suitable for modeling and optimization tasks in this domain.

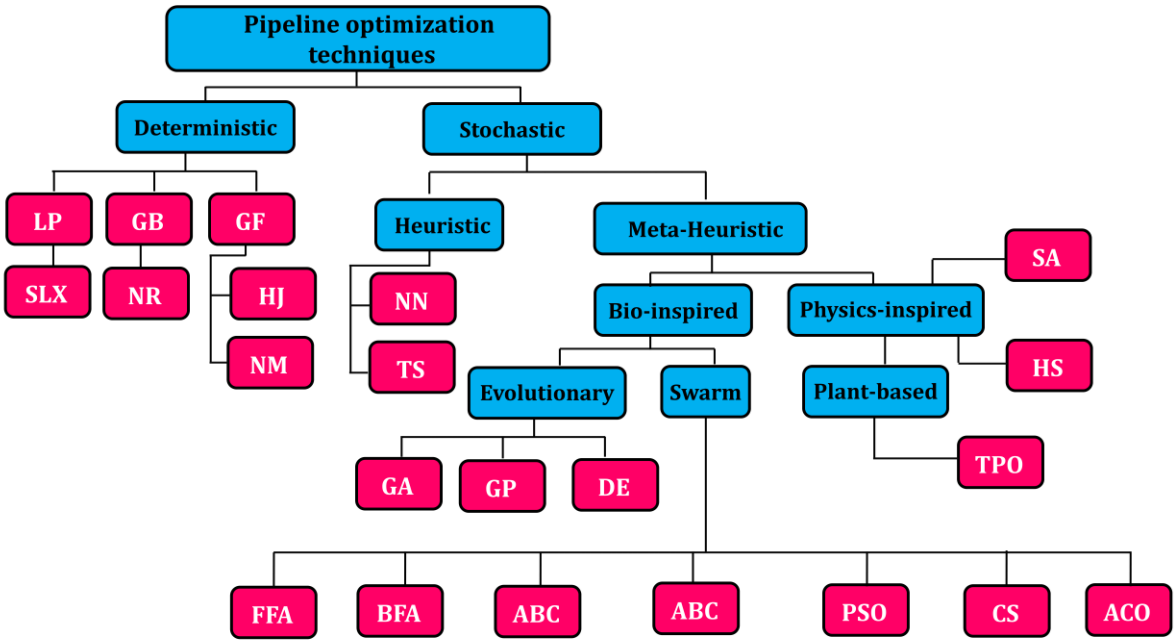

Fig. 2.6: common techniques utilized for optimizing the operational parameters [9].

2.6.1 Genetic Algorithm

Genetic algorithms were initially developed in the 1980s by Robert Goldberg and colleagues to optimize network pipelines. The research conducted by [90] showcased the utilization of the GA technique to reduce the overall power consumption in compressors powered by turbochargers. According to research findings, GA was initially used in 1987 to modernize antiquated pipelines [90]. The study conducted by [91] further improved the efficiency of gas pipeline networks eliminating the need for compressors. Sanaye & Mahmoudimehr employed this tactic to reduce the price of fuel employed by compressors. The concept was expanded into a multi-objective GA technique that was successfully applied for the TransCanada Pipeline [92].

Effective fuel consumption reduction of a gas compressor plant can be achieved by genetic algorithms, as demonstrated by Reference [93]. Using GA to enhance network workflows has been the subject of numerous additional studies [54, 94-96]. Natural selection is a process used by genetic and search-based algorithms [90]. Genetic algorithms have their origins in the adaptation and survival of natural species. The decision variables are configured to provide researchers with an initial trial solution known as a "chromosome" or "string" when utilizing GA in pipeline optimization. For coding, a binary alphabet is established. The fitness function of a genetic algorithm is used to assess the initial trial solutions. A population is the set of trial solutions. Mutation, crossover, and reproduction operators are used by genetic algorithms to optimize results. Reproduction is a perfect example of how selection creates the survival of the fittest. When two parents of binary elements exchange some segments, the result is a crossover, which is necessary to produce offspring from binary components. A useful genetic characteristic is lost when a mutation results in the occasional flipping of bit values. **Fig. 2.7** displays the extensive GA algorithm.

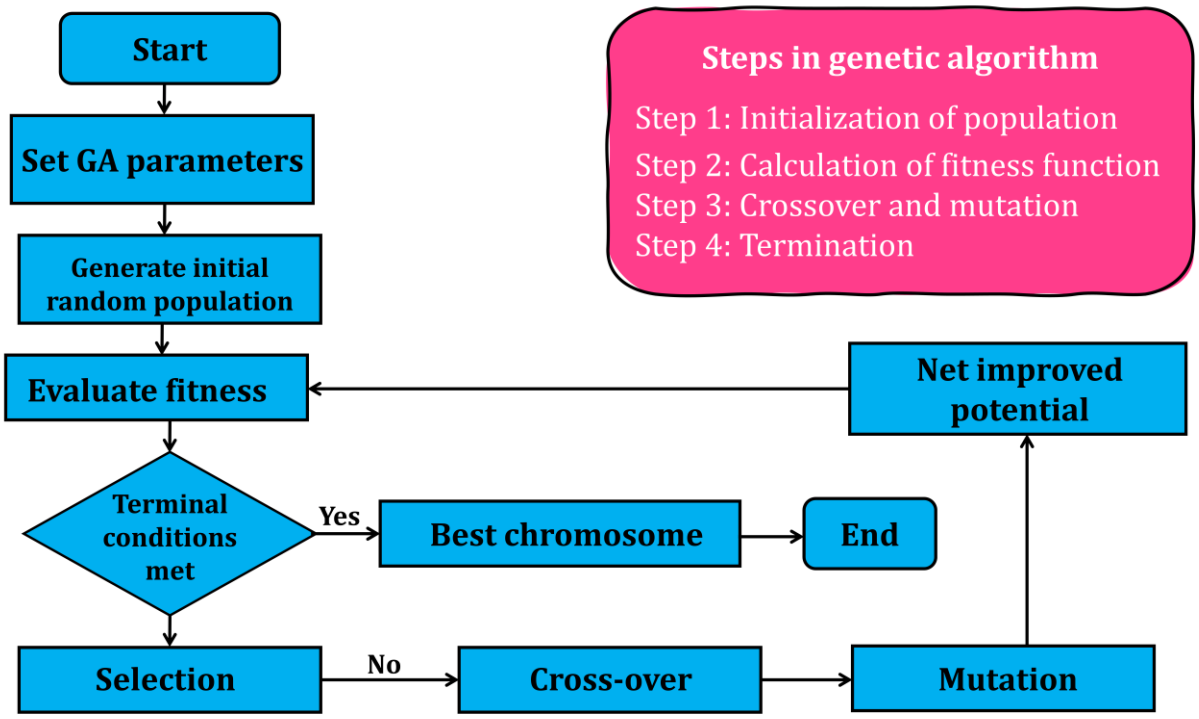

Fig. 2.7: Flow chart for Genetic Algorithm in common practice [2, 97].

The following is a synopsis of the several actions taken in GA [2]:

Step 1: *Initialization of Population*

The population is initially made up of a group of people. Genes make up chromosomes, which are present throughout the general population. In GA, genes are a collection of components that result in chromosomes. The set of genes can be represented by an alphabet or binary representation (0 and 1). Gene transcription is the process of encoding genetic information.

Step 2: *Computation of fitness function*

The fitness function, also referred to as the evaluation function, measures the degree to which a certain solution resembles the optimal option. The function shows how competitive a gene is with other genes. The probability of an individual being chosen for reproduction is measured using a fitness function.

Step 3: *Selection making process*

The selection of the best candidates (genes) is aided by the filtering procedure. The genes that are best suited for survival are handed down to the next generation. In the GA population, which consists of two sets of individuals, parent genes are utilized to assess an individual's fitness. The individuals with the highest significant fitness values have a higher probability of having the mutation.

Step 4: *Implementation of crossover and mutation*

Crossover: Choosing the best candidates ensures that the right individuals are chosen (genes). Strong genes are inherited by the generation that follows. All along the way, the fitness ratings of the two-parent genes are also evaluated. It is more likely that the most fit individuals will be chosen for procreation. Three different types of breeding combinations are made possible by the genetic algorithm. There are three types of these crossovers: uniform, two-point, and single-point crossovers. In a single crossover, the parent chromosome string is examined to determine a favorable crossing point. Following that, the two-parent organisms receive all the organism's information. Strings are distinguished by the existence of positional bias. In a two-point crossover, genetic material can move across two randomly chosen locations on each chromosome. A random gene is chosen from the chromosomes of each parent using the uniform crossover approach. Take the coin toss method, for instance, as a contrast.

Mutation: In genetic algorithms, the accumulated genetic variety is preserved by the genetic operator known as the mutation. This might be thought of as a biological mutation in an analogy. The genes on a chromosome may alter in some way as a result of a genetic mutation. A solution may indicate that it has undergone a complete transformation when it undergoes mutation. GA might therefore be more effective at resolving issues. A user-defined chance of mutation can be used to control whether the natural mutation process is activated or inactive. The possibility needs to be reduced as much as is practical. If the search value is set too high, it will become a main, aimless hunt. By selecting a varied sample from the population, GAs use mutation to avoid local minima. Utilizing mutation operators also has the advantage of potentially delaying or stopping the convergence of the global optimum to the chromosomal population. GA selects a sample group with a bias toward the fittest rather than only the fittest members of their group when choosing the next generation.

Step 5: *Termination process*

If the following generation differs greatly from the previous one, then the next generation may have started to converge. The procedure is performed as many as required until the desired convergence is obtained. In this approach, a population size of 200 and a maximum of 500 iterations are used. It is widely understood that increasing the total number of fitness function evaluations, which is determined by the product of population size and maximum iterations, generally enhances the likelihood of the algorithm finding superior solutions. Conversely, reducing these values typically diminishes this likelihood. The chosen crossover and mutation rates of 0.8 and 0.2, respectively, have been selected based on their superior performance compared to other rate combinations. Ref. [98], which offers a thorough working explanation of GA, has more information about the process.

2.7 Summary

This chapter delves into gas pipeline modeling, focusing on a comprehensive mathematical framework for effective pipeline management. It begins with the essential equations governing gas flow, including the continuity, momentum, and energy equations, providing a thorough explanation of each. This chapter also validate the pipeline equation with another paper. Constraints such as pressure limits, flow rate restrictions etc. are addressed to ensure system safety and performance. The objective function is defined to optimize operational performance, typically aiming to minimize fuel consumption while meeting demand. Various optimization methods, such as linear programming and nonlinear optimization techniques, are explored to solve the objective function efficiently. By integrating these elements, the chapter provides a detailed overview of how to model and optimize gas pipeline systems for enhanced performance.

Chapter 3

Gas pipeline network model

This chapter examines natural gas transmission pipeline systems, focusing on simple and multi-delivery node networks. Utilizing critical input data, we validate the model develop in Chapter 2 by referencing methodologies and results from two published papers on gas network optimization and reliability analysis, ensuring comprehensive evaluation and accuracy. The overall framework of the study is shown in **Fig. 3.1**.

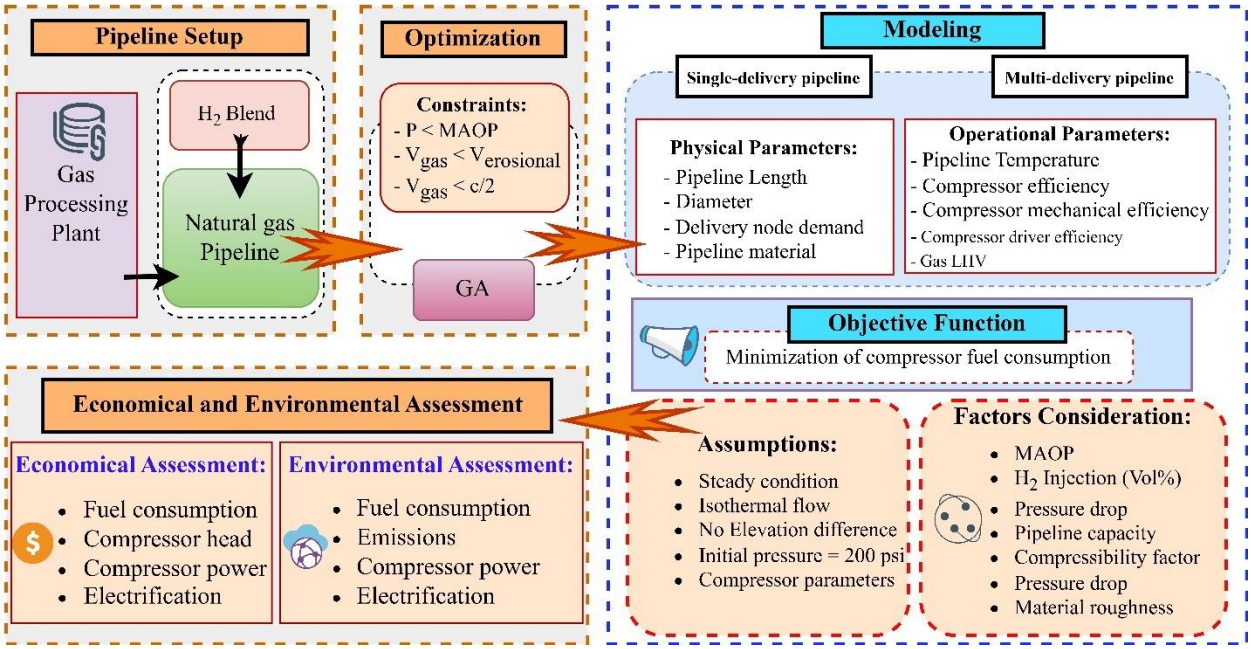

Fig. 3.1: Schematic illustration of the framework for the present study.

3.1 Study Area

One of the biggest natural gas infrastructures in North America is in Alberta. Canada is the fourth-largest producer of natural gas in the world, with 71% of the country's supply coming from the western province of Alberta [99]. Alberta uses about 49% of its natural gas production locally. The residential and commercial sectors in Alberta make up 17%. The industrial, transportation, and electricity production sectors use the remaining 83% of natural gas that is consumed in Alberta [100]. In 2022, Alberta's marketable natural gas output reached its greatest levels since 2010 with an average daily production of 309.1 million cubic meters per day or 11 billion cubic feet per day (Bcf/d). This growth indicates an annual growth rate of 6.7%. It is anticipated that commercial

natural gas output will increase by 10% to 341.5 106 m^3/d (12.1 Bcf/d) by 2032 [101]. Additionally, about 4 million tons (Mt) of hydrogen are produced in Canada each year, or 5–6% of the world's total, with Alberta producing the majority of it mostly through heavy oil upgrading and ammonia manufacturing [99].

The study considers natural gas transmission from Alberta to British Columbia (BC). The length of the main transmission line between Alberta to BC is assumed to be 800 km, in the present study, as shown in **Fig 3.2**. In the study, eight compressor stations and six gas delivery points are considered. Of the total gas delivery, 20% is directed to an area near Kimberley, 20% to Kelowna, and the remaining 60% is distributed among Vancouver, Surrey, and an area near Langley, BC.

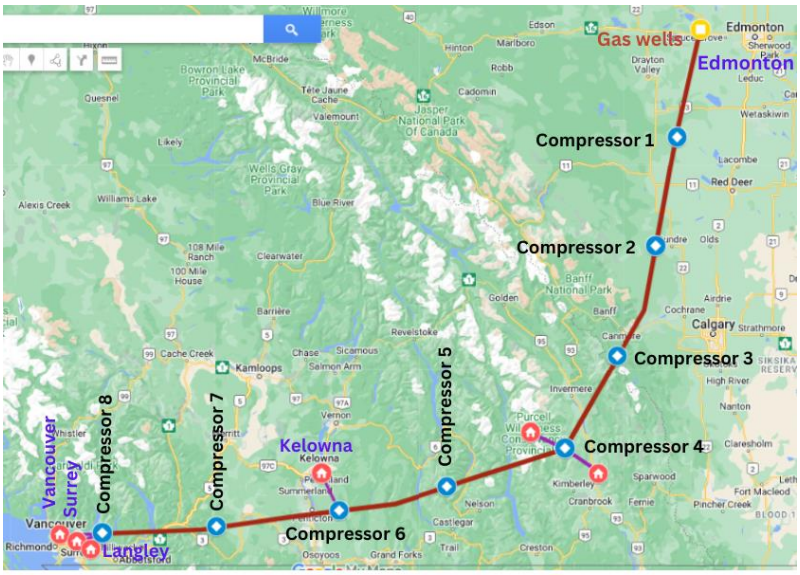

Fig. 3.2: Selected area for gas transmission in the google map.

3.2 Simple delivery node gas transmission network

Natural gas is collected from individual wells and transferred by gas collection systems to gas processing plants. There, it is purified for home use by eliminating natural gas liquids and other contaminants including butane, propane, and ethane. Natural gas is collected in progressively bigger pipelines as it exits the processing facility. These pipelines eventually connect to high-pressure transmission pipelines, which transport the gas to significant markets and regions with strong consumer demand.

A simple gas transmission system with an 800 km pipeline length is considered for this study, as shown in **Fig. 3.3**. Eight compressor stations are considered along this pipeline where all are single

stage compressors, except the first compressor. The distance between adjacent compressors is 100 km. There are eight pipeline arcs (G1-G8) in the transmission line with sixteen nodes. Initially gas comes from the gas processing plant at 1.38 MPa (200 psi) bar to the first compressor. After that the gas is compressed at the first compressor and goes forward to the other compressors towards delivery node (node 16).

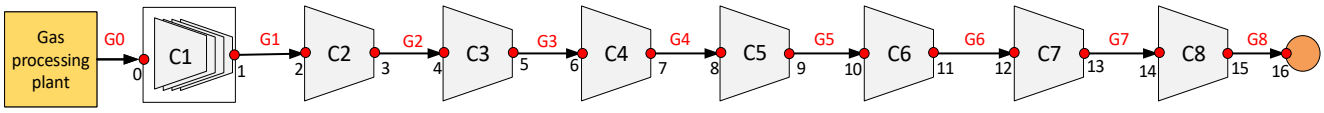

Fig. 3.3: Simple transmission line with single delivery point.

The diameter of the pipeline as shown in **Fig. 3.3** is considered as 0.9 m and the pipeline operating pressure is always lower than the maximum allowable operating pressure (MAOP), which is 8.6 MPa for 0.9 m pipeline, and the delivery pressure at node 16 is equal or greater than 1.38 MPa.

3.3 Model validation

In this section, data from two published papers have been compared with data generated by the present model. Khan et al. [84] considered a pipeline of 1500 km for H_2 transportation and considered compressor station every 500 km, 300 km, and 100 km distance. The schematic pipeline diagram for the three scenarios is showed in **Fig. 3.4**. The initial pressure to the initial compressor from the gas processing plant is 2 MPa and the initial pressure to the first compressor is 7 MPa. The values used for the modeling are presented in **Table 3.1**. **Equation (2.33)** [2] is used for the validation considering an additional parameter for elevation of the pipeline.

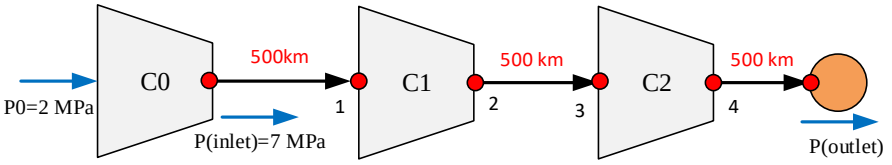

(a)

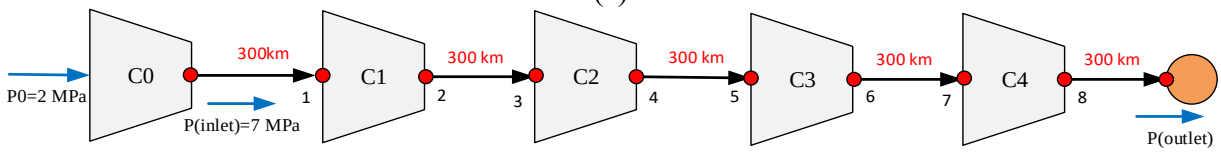

(b)

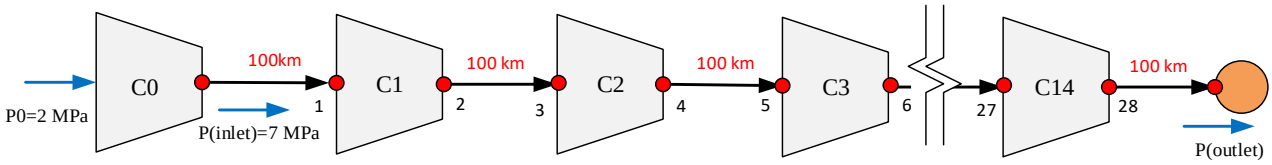

(c)

Fig. 3.4: 1500 km pipeline system for compressor distance of (a) 500 km, (b) 300 km, and (c) 100 km.

Table 3.1: Parameters and their values used in the validation [84].

Parameter	Value	Parameter	Value
Base pressure, P_b (kPa)	101	Compressor distance (km)	500, 300, and 100
Base temperature (K)	288.706	Pipe roughness (mm)	0.0178
Inlet pressure, P_1 (MPa)	7	Outlet gas velocity (m/s)	35
Full pipeline length (km)	1500	η_{isen} (%)	80
Compression ratio	2.1	Z	1.031
H_2 gas density (kg/m^3)	0.08375	Molar mass, M (g/mol)	2.02 (assumed)
Elevation difference (m)	100		

Fig. 3.5 depicts the H_2 capacity (t_{H_2}/day) of the pipeline for the corresponding nominal pipe size (NPS) for three different compressor station distances, where **Fig. 3.5 (a)** shows the reference paper and **Fig 3.5 (b)** shows the results from the present study using the same information. In the figure, H_2 pipeline capacity is shown for the pipe diameters of 10, 14, 18, 24, 36, 42, and 48 inches (0.25 m, 0.36 m, 0.46 m, 0.7 m, 0.91 m, 1.07 m, 1.22 m) and considering 500 km, 300 km, and 100 km compressor distances. However, for the advantage of the calculation, pipe size 10, 20, 30, 40, and 50 inches are considered for the present study. It is noticeable that the present study follows the similar trends and values as the reference paper. The little difference between these two figures might be because of the molar mass which is assumed in the present study.

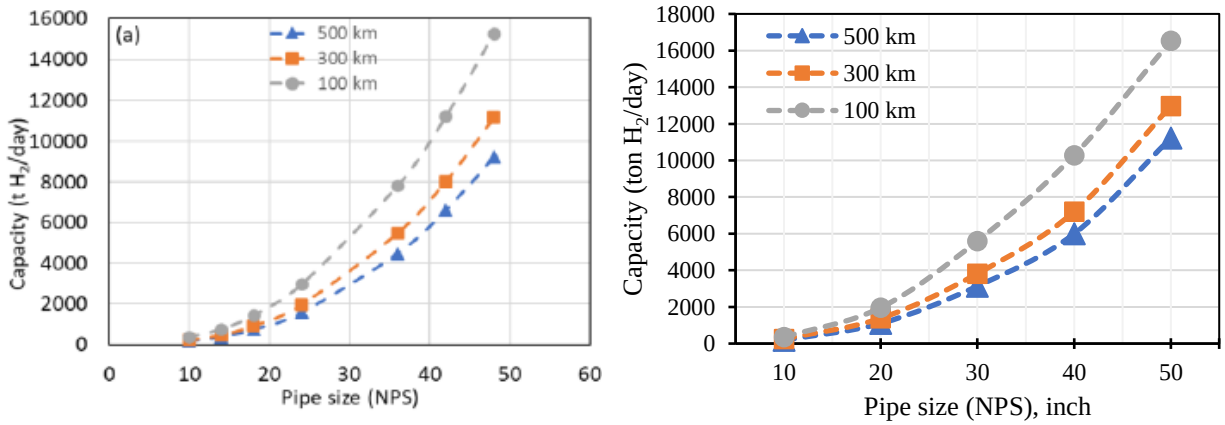

(a) (b)

Fig. 3.5: Pipeline H_2 capacity (t_{H_2}/day) versus pipe size (NPS) as a function of distance between compressor stations for (a) reference paper, and (b) present study.

Fig. 3.6 presents the outlet pipeline pressures (bar) for different pipe sizes, considering 500 km, 300 km, and 100 km compressor distances for the current study (b), and the reference study (a). The results of the current study show similar trends and values as in the reference study. From the **Fig. 3.6 (a),** the outlet pressures for pipe sizes 10-inch, 30 inch, and 30 inch are around 14, 26.5, and 32.5 bar respectively for 500 km compressor distance, whereas in the present study it is 14.4, 26.9, and 32.8 bar correspondingly as shown in **Fig. 3.6 (b)**. Similarly, the results are also close to the reference paper for 300 km and 100 km compressor distances.

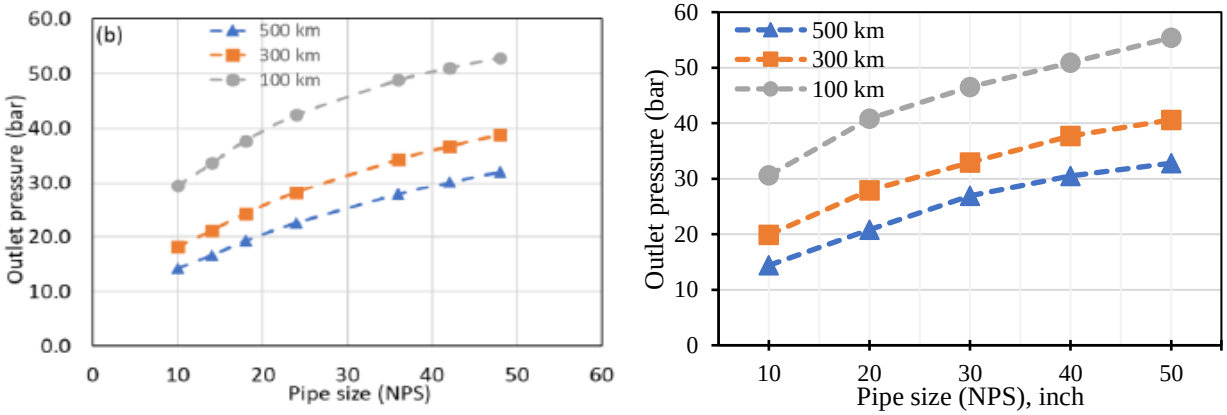

Fig. 3.6: Pipeline outlet pressure (bar) versus nominal pipe size (inch) as a function of compressor station distance for (a) reference paper, and (b) present study.

The model developed in the current study is also validates against a study of a H_2 pipeline network [102]. In this study, the pipeline is simulated using Aspen Plus with an H_2 transmission pipeline, and multiple enroute stations. The input station compresses the hydrogen gas to the design pressure before it is released from the alkaline electrolyzer. Next, as depicted in **Fig. 3.7**, it is transported via the hydrogen transmission pipelines.

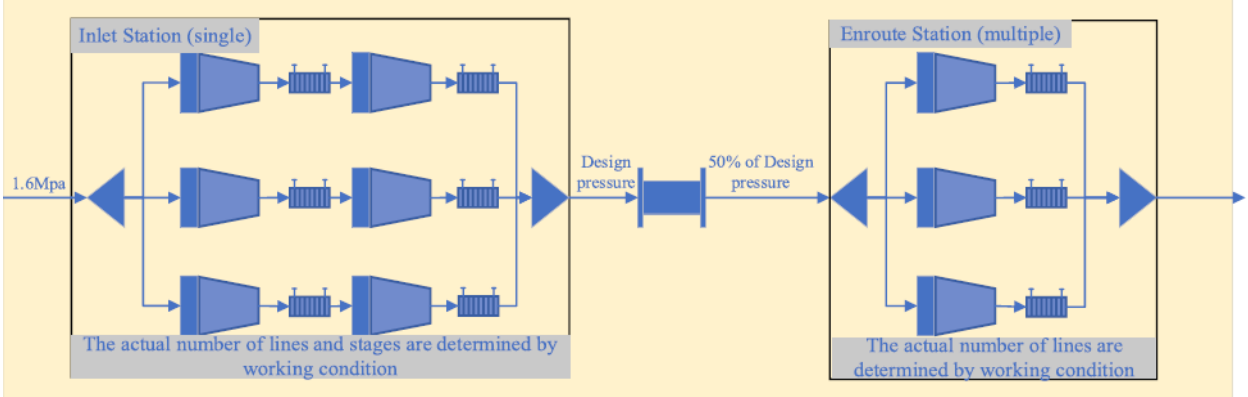

Fig. 3.7: Diagrammatic representation of the Aspen Plus process model from the reference paper [102].

The simplified schematic diagram is depicted in **Fig. 3.8** for 4 MPa inlet pressure to the enroute stations where five enroute stations are considered and the distance between two enroute compressor stations is 300 km.

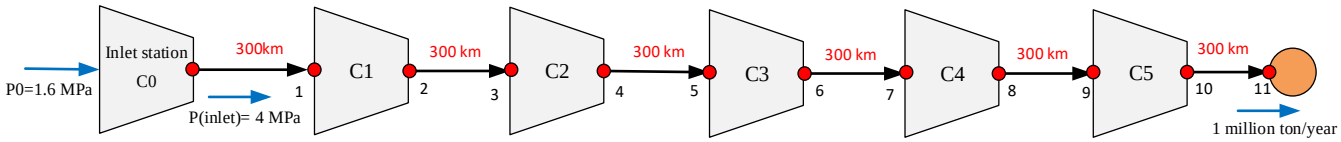

Fig. 3.8: Simplified schematic diagram of the considered model. The initial pressure is 1.6 MPa from the electrolyzer and the inlet pressure to the enroute stations are 4-10 MPa.

The information used for this validation is presented in **Table 3.2**. The transmission distance is 1800 km for gas transmission rate 28.80 kg/s considering diameter range 500 to 900 mm. The base pressure and molar mass are assumed in the present study as it is not mentioned in the reference paper. The inlet pressure is 1.6 MPa after which the pressure is raised to 4-10 MPa by the inlet compressor. Then the gas flows into the transmission line and through the enroute stations. A compression ratio of 2.0 is considered in all cases.

Table 3.2: Information used for the validation of Yu et al. [102] reference paper.

Parameter	Value	Parameter	Value
Base pressure, P_b (kPa)	101.352 (assumed)	Nominal diamter (DN) (mm)	500 to 900
Base temperature (K)	293.15	η_i	0.8
Transmission distance (km)	1800	Mechanical efficiency	0.96
Molar mass, M (g/mol)	2.02 (assumed)	Gas flow rate (million ton/year)	1
Compression ratio	2	Gas flow rate (kg/s)	28.80
Pipe roughness (mm)	0.04		

Fig. 3.9 (a) and **Fig. 3.9 (b)** show the compressor power for each station (kW) (left vertical axis) and number of enroute stations (right vertical axis) versus design pressure after compression of inlet station for reference paper and present study. For design pressure 4 MPa, the compressor power for inlet station and enroute stations are 3.98×10^4 kW and 2.10×10^5 kW respectively where the enroute station is composed of five compressors. Similarly, the compressor power for inlet station and enroute stations for 6 MPa, 8 MPa, and 10 MPa design pressures are 7.48×10^4 and 1.37×10^5, 8.26×10^4 and 2.02×10^5, and 9.43×10^4 and 2.56×10^5 respectively considering 4, 5, and 6 enroute stations. All the results in the present study follow the similar trends and almost same to the reference paper.

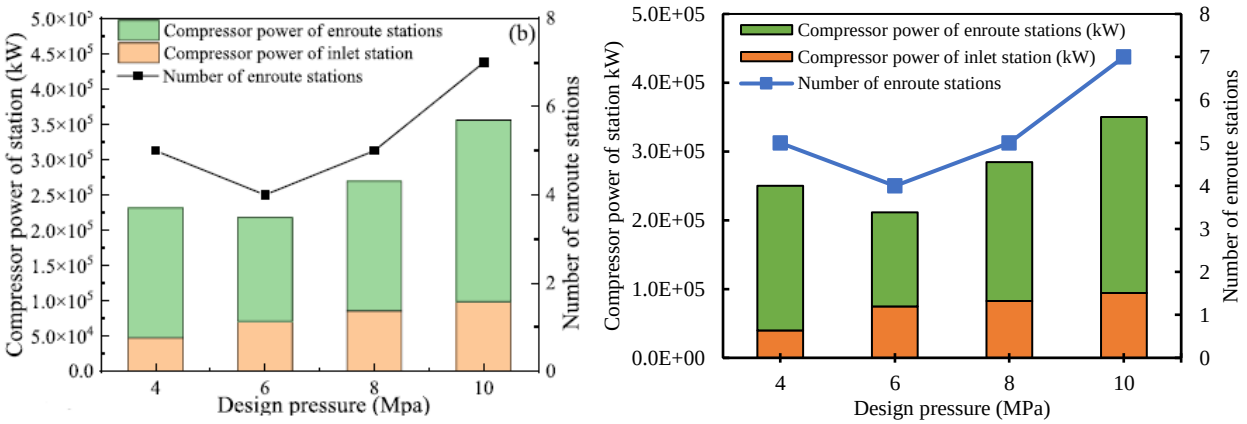

(a) (b)

Fig. 3.9: Compressor power station (kW) and number of enroute stations versus design pressure (MPa) for (a) reference paper, and (b) present study.

Fig. 3.10 shows the pipe nominal diameter corresponding with the annual gas transmission amount (Mtons/year) for 4 MPa, 6 MPa, 8 MPa, and 10 MPa inlet pressure in case of (a) reference paper, and (b) present study. The results obtained from the present study show similar trends and values as in the reference paper. The small difference in the results is because of some difficulties in the study. The major difficulties were due to the lack of enough information about the pipeline length and number of enroute stations in the transmission pipeline. Therefore, for the simplicity of the simulation single compressor is assumed and 300 km pipeline length is assumed.

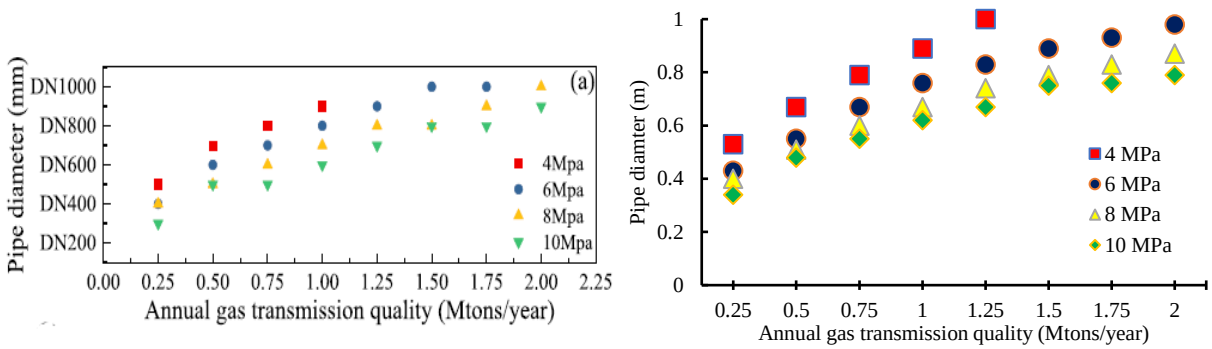

(a) (b)

Fig. 3.10: Pipe nominal diameter corresponding with the annual gas transmission amount (Mtons/year) for 4 MPa, 6 MPa, 8 MPa, and 10 MPa inlet pressure in case of (a) reference paper, and (b) present study.

3.4 Multi delivery node transmission network

A multi-delivery point pipeline enables the distribution of natural gas to multiple end-users spread over a large geographic area. This ensures that various regions, industries, and residential areas receive a reliable gas supply. Different delivery points allow for tailored supply management, catering to varying demand levels at each location. This flexibility helps in balancing the supply according to regional consumption patterns.

An 800 km natural gas transmission network with multi-delivery points is designed to ensure efficient gas delivery while minimizing compressor fuel consumption. Starting with an initial pressure of 1.38 MPa from the gas processing plant, the gas travels through a pipeline punctuated by eight strategically placed compressor stations, each positioned 100 km apart. These compressor stations are crucial in maintaining the necessary pressure levels to counteract the natural pressure drops that occur over long distances, ensuring a steady flow of gas. The network also includes six delivery nodes, situated at various points along the pipeline to distribute the gas effectively.

A schematic diagram is shown in **Fig. 3.11** and the lengths (km) and diameters (m) of the pipeline arcs (G1-G13) are presented in **Table 3.3**. The first compressor station is composed of a series of compressors to boost the pressure of the gas from gas processing plant. The diameter of the pipeline arc is 0.9 m, and the length of the pipeline is 100 km with full load capacity in the pipeline (G1-G4). At node 9, 10% gas is delivered at each point of 10 and 11. The remaining 80%

of the delivery gas is transported though the main pipeline. Similarly, 20% of the gas is delivered at node 15 (delivery node 3).Furthermore, remaining 60% of the gas is from node 18 to nodes 19, 29, and 21 (delivery nodes 4,5, and 6).

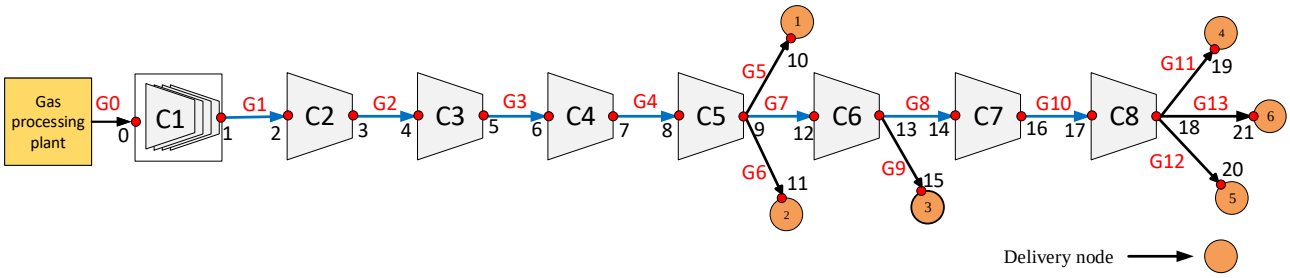

Fig. 3.11: Gas transmission pipeline network of 800 km length with multiple delivery points.

Table 3.3: Pipeline arc (G1-G13) length and diameter of an 800 km gas transmission pipeline network.

Pipeline Arc	Length, km	Diameter, m
G1	100	0.9
G2	100	0.9
G3	100	0.9
G4	100	0.9
G5	30	0.254
G6	40	0.254
G7	100	0.76
G8	20	0.254
G9	100	0.66
G10	100	0.66
G11	10	0.3
G12	15	0.3
G13	20	0.3

The following mass balances are considered in the optimization process:

$$m_9 = m_{10} + m_{11} + m_{12}$$

$$m_{13} = m_{14} + m_{15}$$

$$m_{18} = m_{19} + m_{20} + m_{21}$$

The mass flow rate at node 9 is equal to the sum of the mass flows at nodes 10, 11, and 12. The total mass flow at nodes 14 and 15 is equal to the mass flow rate at node 13. Additionally, the flow rate at node 18 is equal to the sum of the mass flow rates at nodes 19, 20, and 21. The total mass flow rate is designed to deliver 8 GW of power. Extra fuel (m_f) is accounted for throughout the pipeline to be consumed by the compressor stations.

Key input data for the pipeline model are stated in **Table 3.4**. The gas temperature in the pipeline is assumed to be 283 K, and the isentropic exponent is 1.3. In the present study, the compressor isentropic efficiency is assumed to be 0.72. The mechanical efficiency and compressor drive efficiency are considered to be 0.9 and 0.35, respectively. The molar mass of the NG and H_2 are 16.5 g/mol and 2.02 g/mol, respectively. The lower heating value (LHV) of NG and H_2 are 48.83 MJ/kg and 120 MJ/kg, respectively. The critical temperature and pressure of NG are 190.9 K and 4.58×10^6 Pa, respectively, while for H_2, they are 33.2 K and 1.31×10^6 Pa. The current study considers steel pipeline with roughness factor 50μm.

Table 3.4: Key input data for the pipeline model [2, 87].

Parameter	Value	Parameter	Value
Pipeline gas temperature, T (K)	283	Molar mass of NG (g/mol)	16.5
Universal gas constant, R (J/mol.K)	8.314	Molar mass of H_2 (g/mol)	2.02
Isentropic exponent, k	1.3	Lower heating value of NG (MJ/kg)	48.83
Compressor isentropic efficiency	0.72	Lower heating value of H_2 (MJ/kg)	120
Compressor mechanical efficiency	0.9	Critical temperature of NG (K)	190.9
Compressor driver efficiency	0.35	Critical temperature of H_2 (K)	33.2
Steel pipe roughness, ε (μm)	50	Critical pressure of NG (Pa)	4.58×10^6
Density of NG at standard condition (kg/m^3)	0.712	Critical pressure of H_2 (Pa)	1.31×10^6
Density of H_2 at standard condition (kg/m^3)	0.0898		

3.5 Summary

This chapter focuses on the detailed examination of a gas transmission pipeline system. It begins with an exploration of the study location, highlighting the key features and geographical significance of the pipeline route. The chapter then delves into the modeling of the gas supply pipeline, encompassing both simple and multi-delivery node configurations to address different supply scenarios. Subsequently, the chapter validates the current model against findings from two previously published papers, demonstrating the model's accuracy and reliability. Finally, a thorough analysis of all essential input parameters for the modeling is presented, ensuring that all critical factors influencing the pipeline system are considered and accounted for. This comprehensive approach provides a solid foundation for the effective modeling and optimization of gas supply pipelines.

Chapter 4

Result and discussion

4.1 Introduction

The integration of hydrogen into natural gas transmission systems represents a critical step towards a more sustainable and decarbonized energy infrastructure. This chapter presents the outcomes of the simulation models developed to assess the implications of hydrogen injection into natural gas pipelines. The results are structured to provide a comprehensive analysis, starting with the baseline performance of the natural gas transmission system without hydrogen admixture. Following this, the effects of various concentrations of hydrogen on key parameters such as pressure drop, fuel consumption, and energy density are examined. Finally, an existing natural gas transmission pipeline, Coastal GasLink Pipeline Ltd., is optimized using the current model, and the effects of electrifying the compressor stations on fuel costs and emissions are analyzed.

4.2 Single-delivery transmission pipeline

Fig. 4.1 shows the maximum operating pressure (MPa) in the transmission pipeline for different transmission lengths (km) considering NG (100% NG), 10% H_2 (90% NG-10% H_2), 20% H_2 (80% NG-20% H_2) and 100% H_2 gas compositions (vol%). The maximum operating gas pressure for single pipeline (100 km) with single compressor is 3.23 MPa, 3.45 MPa, 3.72 MPa, and 4.22 MPa for NG, 10% H_2, 20% H_2, and 100% H_2 gas compositions, respectively to minimize compressor fuel consumption. The maximum operating pressure increases with increasing pipeline length. Above 500 km pipeline length, the rate of maximum pressure increase is not as significant as for shorter pipelines. From the figure, it can also be seen that the maximum operating pressure increases with hydrogen injection. The highest maximum pressure is obtained for 100% H_2 gas composition followed by 20% H_2, 10% H_2, and then 100% NG gas composition.

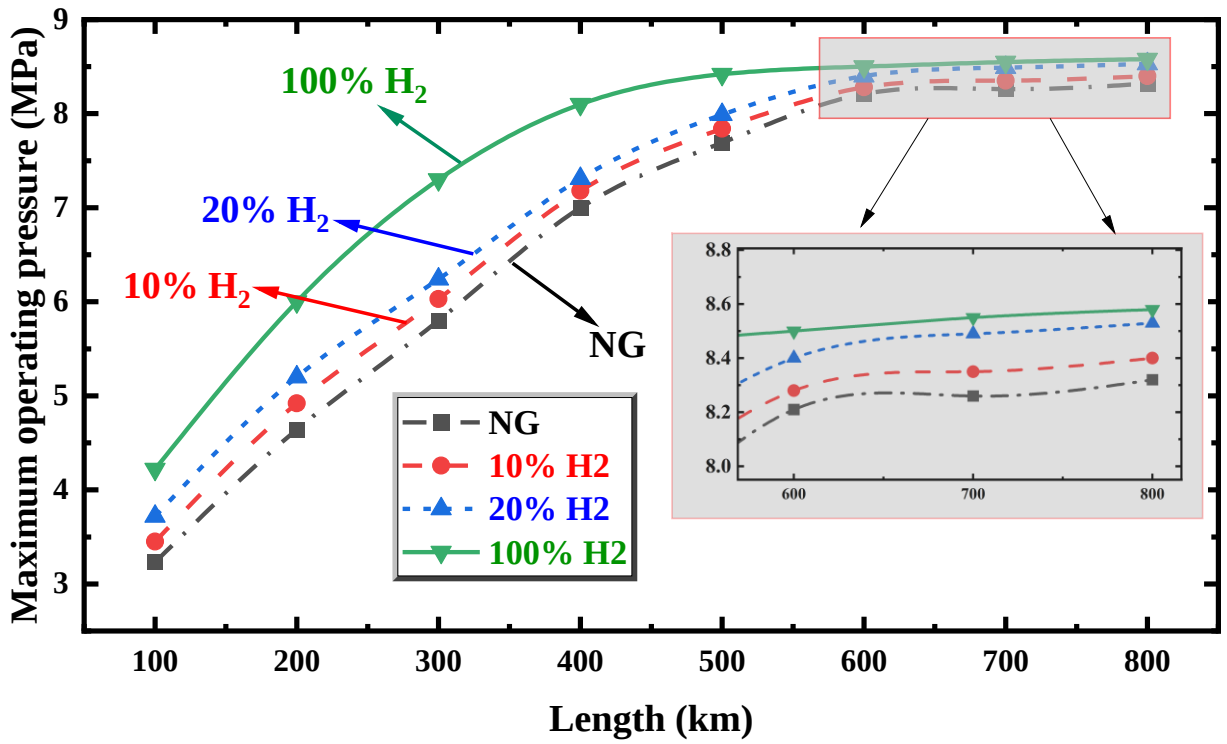

Fig. 4.1: Maximum operating pressure (MPa) in the transmission pipeline for different pipeline length (km).

The minimum operating pressure (MPa) for pipelines having a range of transmission lengths (km) for different gas compositions are shown in **Fig. 4.2**. These figures show that the minimum is obtained for 100% H_2 transmission followed by 20% H_2, 10% H_2 injection, and NG. The pressure drop of a gas with a lower molar mass tends to be higher due to several interconnected factors primarily governed by the principles of fluid dynamics and gas properties.

According to the continuity equation for incompressible fluids, $Q = AV$, where Q is the volumetric flow rate, A is the cross-sectional area, and V is the velocity, for a constant Q, a lighter gas will have a higher velocity. Higher velocity leads to increased frictional losses and turbulence, both of which contribute to a greater pressure drop. Moreover, lower density for lighter gases, combined with higher velocity, increases the Reynolds number, making the flow more turbulent. Turbulent flow causes higher frictional losses, leading to a greater pressure drop. Gases are compressible fluids, and their behavior under pressure can vary. For lighter gases, the compressibility factor (Z) can vary, especially at high velocities and pressures, affecting the overall pressure drop calculations. As the pressure drop for a single pipeline is higher with lower molar

mass of a gas, therefore the pressure drop for NG is lower compared to the other gas compositions. For single delivery gas transmission pipeline, the lower operating pressure increases with the increasing transmission length for all the gases. In case of 800 km transmission pipeline, the minimum operating pressure for NG in the last node of the pipeline is 5.92 MPa, whereas it is 4.9 MPa, 3.67 MPa, and 2.08 MPa for the 10% H_2, 20% H_2, and 100% H_2 gas compositions, correspondingly.

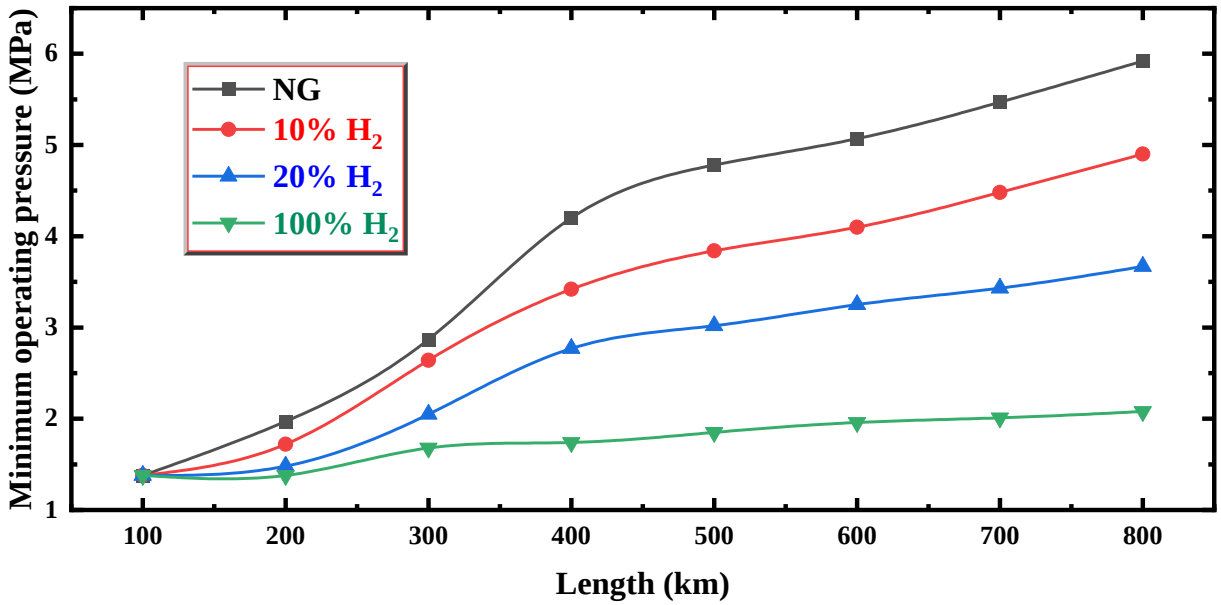

Fig. 4.2: Lower operating pressure (MPa) versus single delivery pipeline transmission length for different gas compositions.

Fig. 4.3 shows the fuel consumption percentage of the compressor relative to the total delivered fuel to the delivery node, considering a constant power delivery of 8 GW for three different gas compositions over varying pipeline lengths. The gas compositions include NG, a mixture of 10% hydrogen and 90% natural gas (10% H_2), and a mixture of 20% hydrogen and 80% natural gas (20% H_2). The NG fuel consumption line starts at about 1.42% for 100 km and gradually increases to 2.98% at 800 km. Moreover, 10% H_2-fuel consumption line starts slightly higher than NG at 1.6% for 100 km and increases to about 3.73% at 800 km. Furthermore, 20% H_2-fuel consumption line begins the highest among the three at around 1.85% for 100 km and rises to approximately 4.43% at 800 km.

For all pipeline lengths, the fuel consumption percentage increases with the amount of hydrogen mixed with natural gas. The rate of increase in fuel consumption with pipeline length is

higher for mixtures containing hydrogen compared to pure natural gas. At longer distances, the difference in fuel consumption between the gas compositions becomes more pronounced. The higher the hydrogen content, the greater the fuel consumption for the same pipeline length, indicating increased energy requirements for transmission.

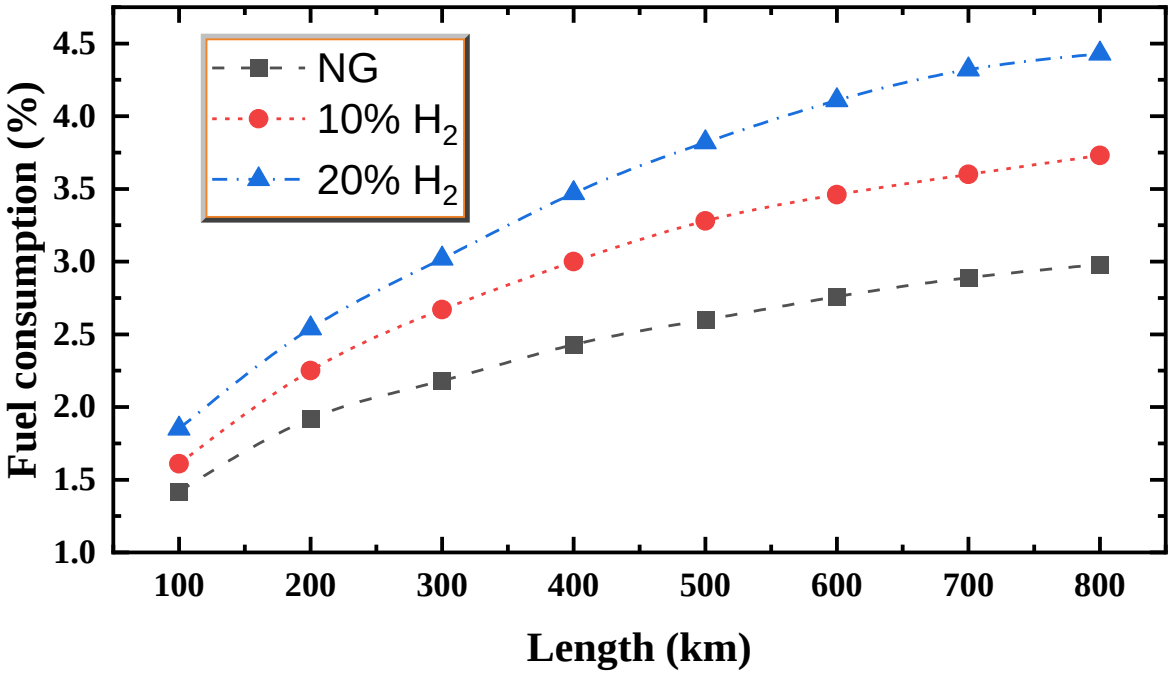

Fig. 4.3: Fuel consumption (%) variation at different pipeline transmission length (km) for different gas compositions to deliver 8 GW power.

Fig. 4.4 depicts the operating pressure (MPa) along an 800 km pipeline with eight compressors, corresponding to 16 pipeline nodes, for different gas compositions: NG, 10% H_2, 20% H_2, and 100% H_2. The delivery power for all the gases is 8 GW. The operating pressure generally decreases as the hydrogen content increases in the gas mixture. Initially at 1st node, the operating pressure is lowest for NG, and at the delivery end it is maximum because of the of the lower pressure drop compared to other gases. The pressure fluctuations and drops become more pronounced with higher hydrogen content, indicating a higher pressure drop along the pipeline for hydrogen-rich mixtures. All the cases, the minimum pressure follows the constraint of equal or greater than 1.38 MPa (around 200 Psi).

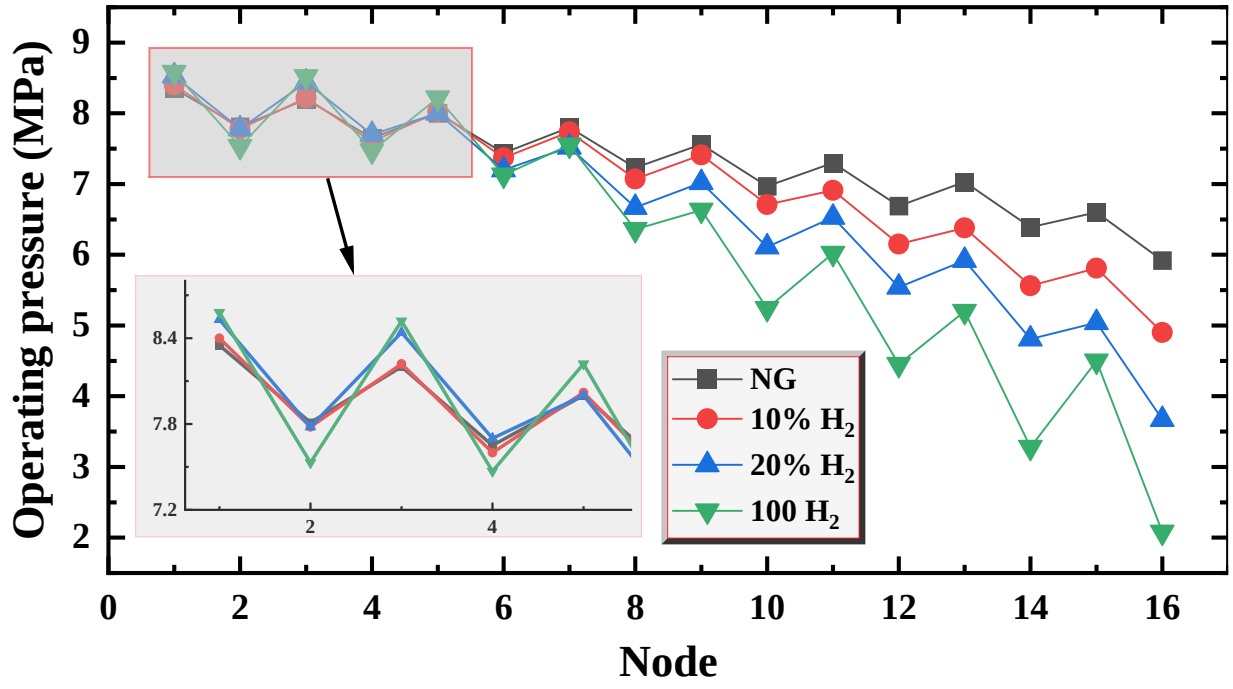

Fig. 4.4: Operating pressure (MPa) of the pipeline throughout at different nodes to deliver 8 GW power to a single delivery point.

The maximum delivered power (GW) and compressor fuel consumption (%) corresponding to variations in Maximum Allowable Operating Pressure (MAOP) for three different gas compositions: NG, 20% H_2, and 100% H_2 are shown in **Fig. 4.5**. In the case of NG, delivered power remains consistently at 8 GW for MAOP values from 8.6 MPa to 5 MPa . Delivered power then decreases with decreasing MAOP and is 2.6 GW at 2 MPa. Like NG, delivered power for 20% H_2 gas mixture is 8 GW up to 5 MPa MAOP and decreases to 2.2 GW at 2 MPa. In the case of 100% H_2, delivered power is 8 GW for higher MAOP (8.6 MPa to 6 MPa) but drops below 8 GW as MAOP decreases, dropping to about 1.6 GW for an MAOP of 2 MPa.

Fuel consumption increases as MAOP decreases for all gas compositions with the same delivered power. However, the rate of increase is much steeper for 100% H_2 compared to NG and 20% H_2. From the figure, fuel consumption (%) increases gradually for 8.6 MPa to 5 MPa of MAOP whenever the delivered power is 8 GW and the fuel consumption for 20% H_2 gas mixture is always higher than NG for all values of MAOP. After 5 MAOP, the fuel consumption decreases with the decreasing MAOP as the delivered power also decreases. The minimum fuel consumption for NG and 20% H_2 is 2.96% and 4.3% at MAOP of 2 MPa where the delivered power is 2.6 GW

and 2.2 GW. The fuel consumption is maximum (21.4%) at 6 MPa, and then it gradually decreased to 14.6% for 2 MPa. Overall, the fuel consumption gradually increases with the decreasing MAOP for delivering constant power. Moreover, if the delivered power decreases, then the fuel consumption also decreases with decreasing MAOP. Transitioning to hydrogen-rich mixtures requires careful consideration of MAOP to balance delivered power and fuel consumption, potentially requiring infrastructure upgrades to handle the higher fuel consumption and maintain efficiency.

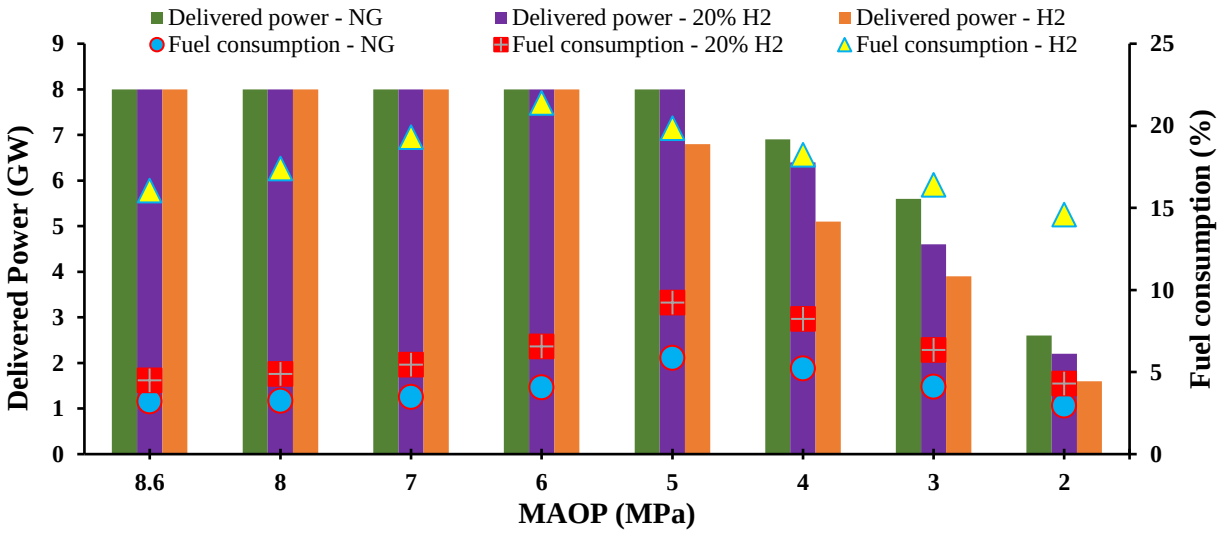

Fig. 4.5: Maximum delivered power (GW) and fuel consumption (%) corresponding to MAOP (MPa) variations for NG, 20% H_2 (vol%), and 100% H_2 gases.

4.3 Pipeline for transmission with multiple delivery points

Fig. 4.6 demonstrates the Pareto front of fuel consumption optimization in a natural gas transmission system using a GA. The rapid initial reduction in fuel consumption followed by convergence illustrates the GA's capability to efficiently explore and exploit the solution space to achieve near-optimal operational settings for the transmission system. The operating pressure for an 800 km long multi-delivery pipeline at different nodes, except delivery nodes, are shown in **Fig. 4.7**. Initially the outlet pressure from the first compressor is always higher than at other nodes. In all cases, the operating pressure maintains the MAOP of the pipeline. The upstream pressure of a pipeline for 100% H_2 is always higher than other gases, followed by 20% H_2, 10% H_2, and NG. Moreover, the downstream pressure of the pipeline is lower in the case of 100% H_2, indicating a larger pressure drop compared to other gases. At node 9, after compressor 9, 20% of the gas is

delivered to nodes 10 and 11, and the remaining 80% is transmitted through the main line. Similarly, at node 13, 20% of the gas is delivered to node 15. As a result, the upstream and downstream pressures both decrease after node 9. Finally, the remaining 60% of the gas is delivered from node 18 to nodes 19, 20, and 21, with 20% delivered at each point. In this scenario, the NG operating pressure is lower at node 18 than for other gases, as a lower pressure drop is encountered for NG and the delivery pressure is constrained to be equal to or greater than 1.38 MPa.

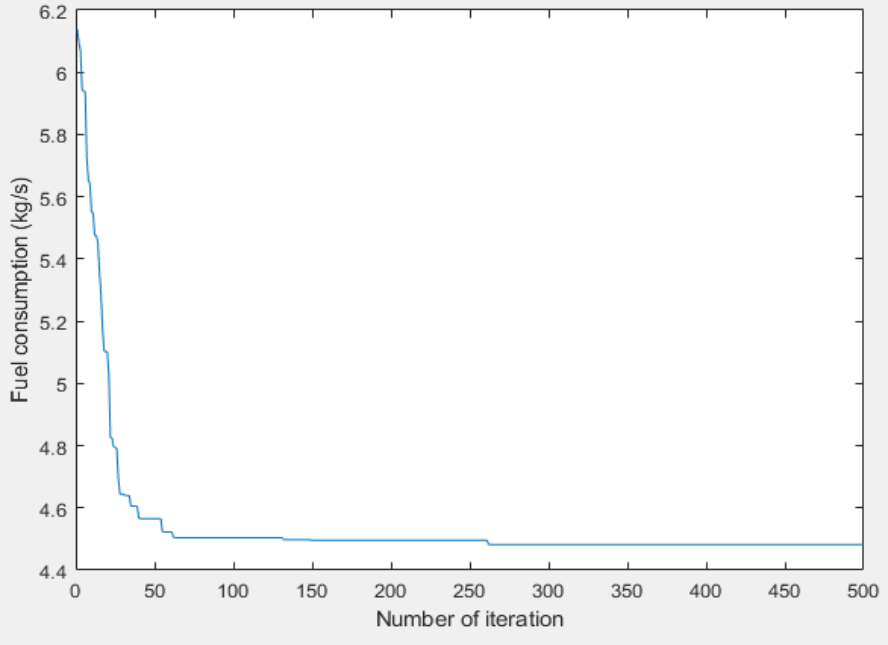

Fig. 4.6: Convergence curve to optimize fuel consumption of multi-delivery points natural gas pipeline.

Pipeline pressure drop is higher for gases with lower molar mass due to their higher velocity and reduced density when flowing through the pipeline. Hydrogen, with a molar mass significantly lower than that of natural gas, experiences a greater pressure drop over the same distance. This occurs because, for a given flow rate, lighter gases like hydrogen require higher velocities to maintain the same mass flow rate as heavier gases. These higher velocities result in increased frictional forces and turbulence within the pipeline, leading to greater energy losses and, consequently, a higher pressure drop. This phenomenon necessitates careful pressure management and compressor placement in pipelines transporting low molar mass gases to ensure efficient and safe operation. The pressure drops for different gas compositions are compared in **Fig. 4.8**,

considering the pressure drop at the first pipeline arc (G1). The pressure drop for NG is 6.9%, while it is 7.1%, 7.5%, 7.9%, and 8.3% for 5% H_2, 10% H_2, 15% H_2, and 20% H_2, respectively. In all cases, a constant power delivery of 8 GW is considered.

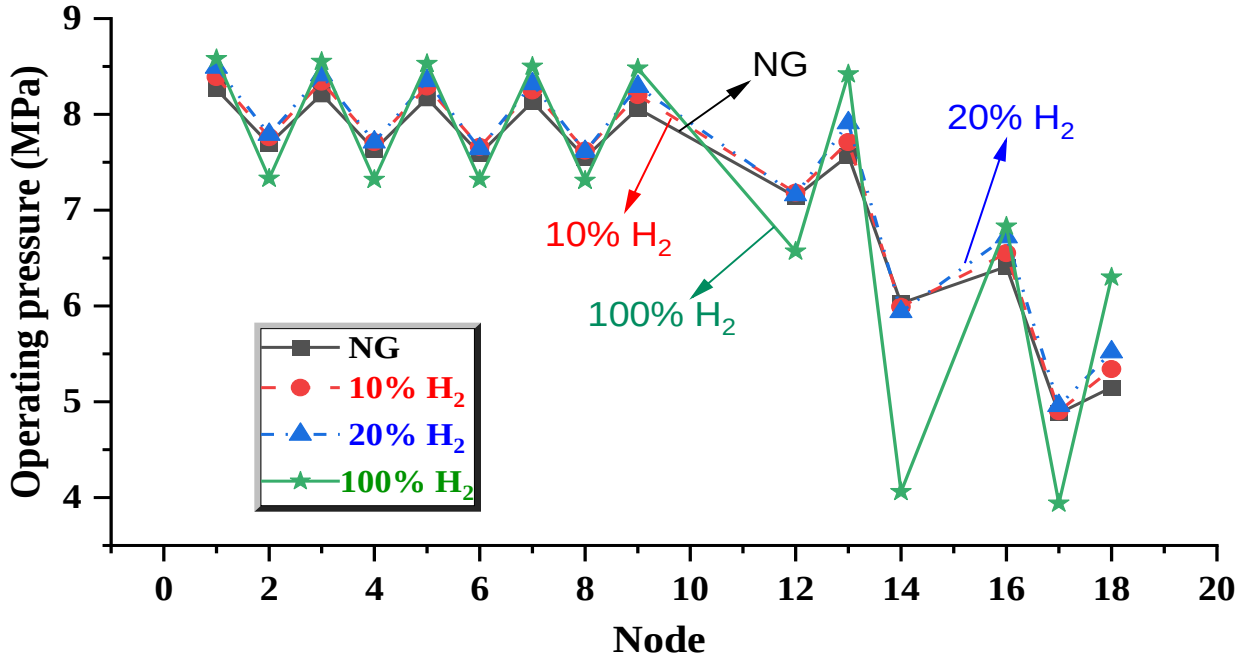

Fig. 4.7: Pipeline operating pressure (MPa) corresponding to the pipeline node to deliver 8 GW power for different gas compositions.

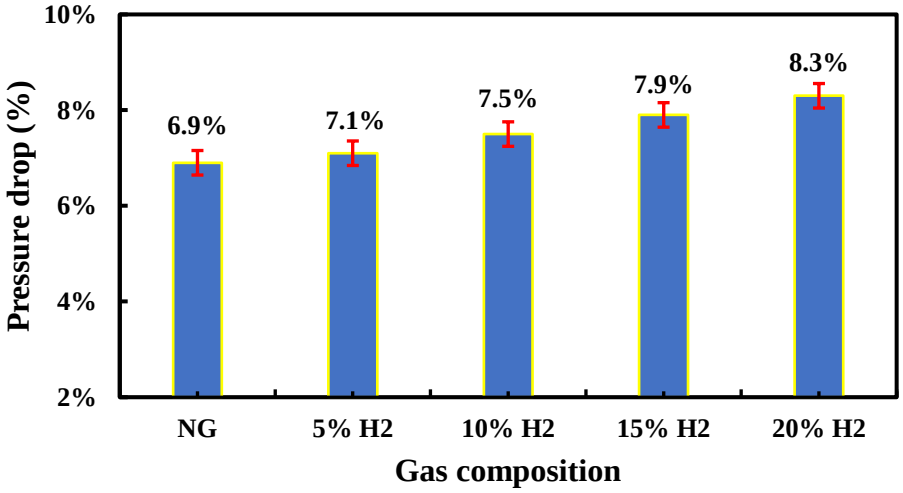

Fig. 4.8: Pressure drop comparison for different gas compositions at the first pipeline arc (G1).

The compressibility factor (Z) is higher for lower molar mass gases in a pipeline transmission system operating at high pressure because lighter gases, such as hydrogen, deviate more

significantly from ideal gas behavior under these conditions. The compressibility factor accounts for the non-ideal interactions between gas molecules, which become more pronounced at high pressures. For gases with lower molar mass, the intermolecular forces and the volume occupied by the gas molecules themselves have a greater relative impact. This leads to a higher Z value, indicating a larger deviation from ideal gas laws. Consequently, the gas occupies more volume than predicted by the ideal gas equation, affecting the flow dynamics and efficiency of the pipeline system.

Understanding and accounting for these deviations is crucial for accurate pressure and flow rate management in high-pressure pipeline operations. As shown in **Fig. 4.9**, the compressibility for NG is 0.79 at the first pipeline arc, while it is 0.82, 0.84, 0.86, 0.88, and 1.06 for 5% H_2, 10% H_2, 15% H_2, 20% H_2, and 100% H_2, respectively. The value of Z generally decreases with lower pressure in a pipeline gas transmission system. At lower pressures, gases behave more ideally, meaning their behavior more closely follows the ideal gas law, where the compressibility factor approaches 1. As pressure decreases, the intermolecular forces and the volume occupied by the gas molecules themselves have less impact on the gas overall behavior of the gas, leading to a compressibility factor closer to unity. Conversely, at higher pressures, the deviations from ideal gas behavior become more significant, resulting in a higher compressibility factor. Therefore, as pressure drops in a pipeline, the compressibility factor typically decreases. In the present study, the value of Z also increases with the decrease in operating pressure which are not shown in the figure.

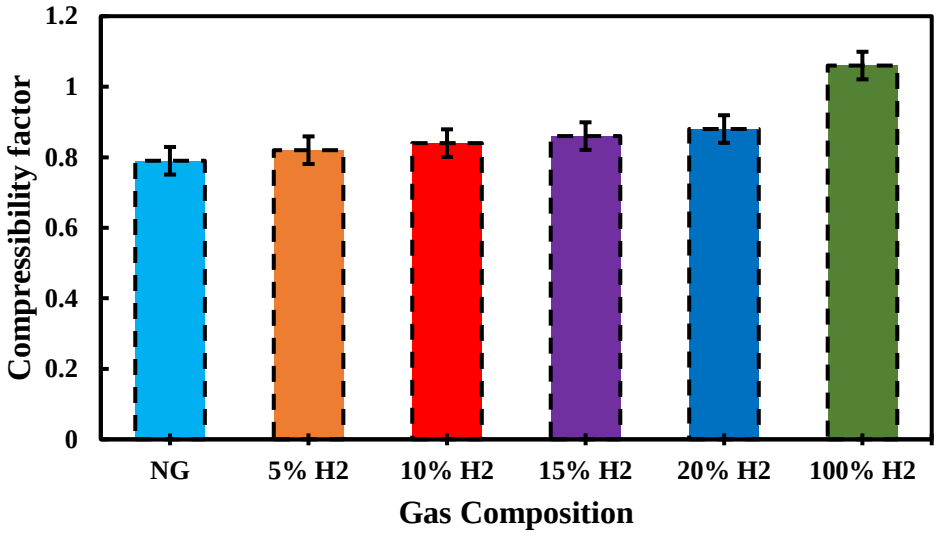

Fig. 4.9: Compressibility factor for different gas compositions at first pipeline arc (G1).

The gas consumption by the compressors, which is the objective function in the present study, for the 800 km transmission pipeline with eight compressor stations is shown in **Fig. 4.10**. Compressor gas consumption (%) in a pipeline is higher for lower molar mass gases due to their lower density and higher flow velocities required to achieve the same mass flow rate as heavier gases. Lighter gases like hydrogen require more energy to compress because their molecules are more spread out, increasing the volume that needs to be compressed. This increased volume translates to higher compression work and, consequently, higher energy consumption by the compressors. Additionally, the higher flow velocities of low molar mass gases create more frictional resistance within the pipeline, necessitating more frequent and powerful compression to maintain the desired pressure and flow rate. As a result, the percentage of gas consumed by the compressors is higher for gases with lower molar mass, impacting the overall efficiency of the pipeline transmission system.

Therefore, in the present study, NG consumes 2.7% of the delivered gas to maintain 8 GW power delivery, while it consumes more fuel with the H_2 injection quantity. The compressor stations consume 3%, 3.2%, 3.5%. 3.8%, and 19.9% of the delivered gas to supply 8 GW power in case of 5% H_2, 10% H_2, 15% H_2, 20% H_2, and 100% H_2, respectively. In all cases, maximum amount of fuel is consumed at first compressor station as it increases the pressure of the gas from gas processing plant (1.38 MPa) to a high pressure. For NG, the first compressor station consumes around 85% of the total fuel consumption, where the rest of the fuel (15%) is consumed by other

enroute compressor stations. Similarly, the first compressor station consumes around 84.5%, 83.3%, 81.9%, 80.7%, and 64.4% of the delivered fuel in case of 5% H_2, 10% H_2, 15% H_2, 20% H_2, and 100% H_2, respectively.

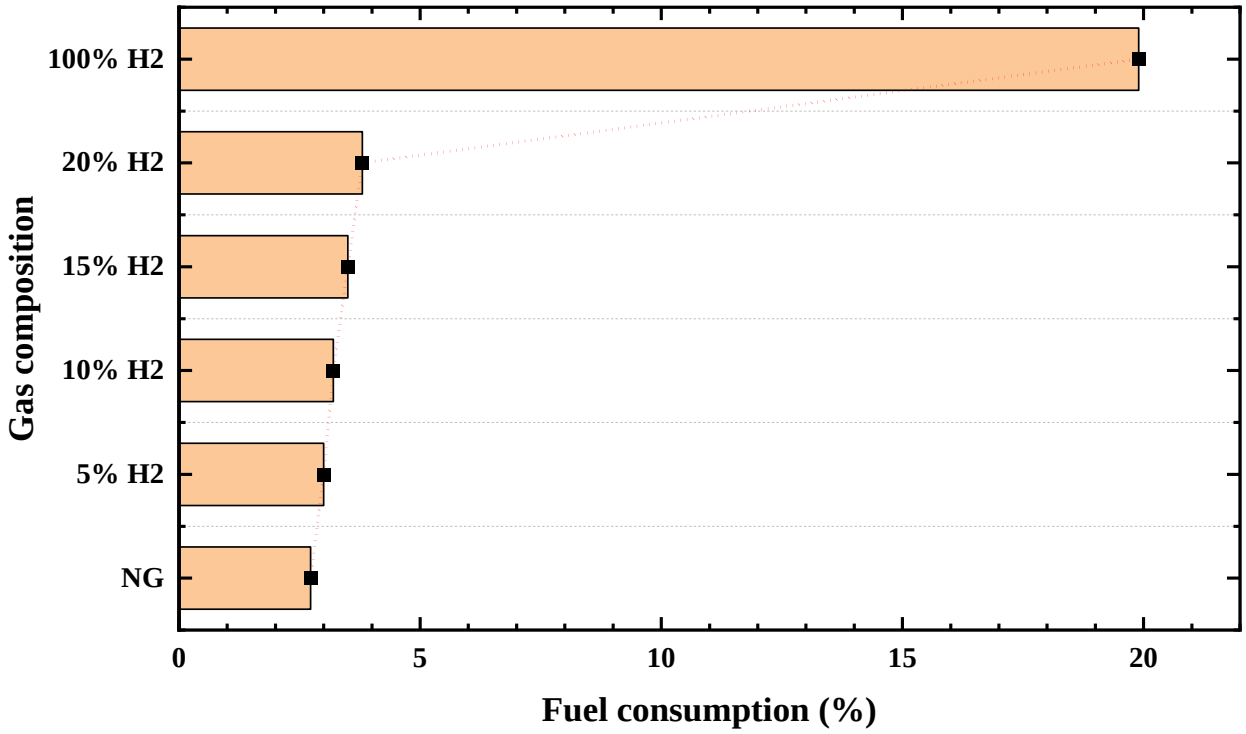

Fig. 4.10: Compressor gas consumption ($\frac{m_f}{m_d}\%$) for different gas compositions to deliver 8 GW power in an 800 km pipeline.

Initially, the supplied power through the pipeline is always higher than the required delivery power because a portion of the power is consumed by the compressors. **Fig. 4.11** depicts the power consumption (%) by the compressors as a function of the delivered power (GW) for various gas compositions, including NG and mixtures with different percentages of H_2. A clear trend emerges from the data: as the proportion of hydrogen in the gas mixture increases, the power consumption by the compressors also rises. This can be attributed to several factors related to the physical properties of hydrogen compared to natural gas. Hydrogen has a significantly lower molar mass than natural gas, resulting in lower density. To transport a given mass flow rate of hydrogen through the pipeline, the gas must move at a higher velocity than natural gas. This increased velocity leads to higher frictional losses within the pipeline, necessitating more frequent and powerful compression to maintain the desired flow rate and pressure. Consequently, the compressors consume more energy, which is reflected in the higher power consumption

percentages for gas mixtures with higher hydrogen content. At the lowest delivered power (6 GW), the power consumption for natural gas is approximately 2.25%, the lowest among all the gas compositions. As the hydrogen content increases, the power consumption rises incrementally. For instance, at 6 GW delivered power, the power consumption is slightly higher for 10% H_2 compared to pure NG, and it continues to increase for 20% H_2, 30% H_2, 40% H_2, and peaks at 50% H_2. This upward trend is consistent across the range of delivered power values shown in the graph. The data points for 50% H_2 exhibit the steepest increase in power consumption, starting around 5.8% at 6 GW and rising sharply as delivered power increases. This indicates that compressors must work significantly harder to handle the higher hydrogen content, which demands more energy due to the lower efficiency in compressing lighter gases. The rapid increase in power consumption for higher hydrogen mixtures highlights the substantial impact of hydrogen's physical properties on pipeline transmission efficiency.

From the figure, it is also noticeable that a maximum of 13 GW can be delivered with the while consuming 6.13% of the delivered power. Similarly, the maximum possible delivered power for 10%, 20%, 30%, 40%, and 50% is 12.36 GW, 11.99 GW, 11.36 GW, 11.25 GW, and 10.88 GW, respectively, while it consumes 7.32%, 8.76%, 10.23%, 12.11%, and 14.5% of the delivered power. Overall, the graph underscores the challenges associated with integrating higher proportions of hydrogen into existing natural gas pipeline systems. While hydrogen offers numerous benefits, such as reduced carbon emissions, its physical characteristics require more energy-intensive compression processes. This results in higher operational costs and energy consumption, which must be considered when designing and optimizing pipeline systems for hydrogen transport. The maximum amount of power delivery and corresponding mass flow rate for different gas compositions are presented in **Table 4.1**.

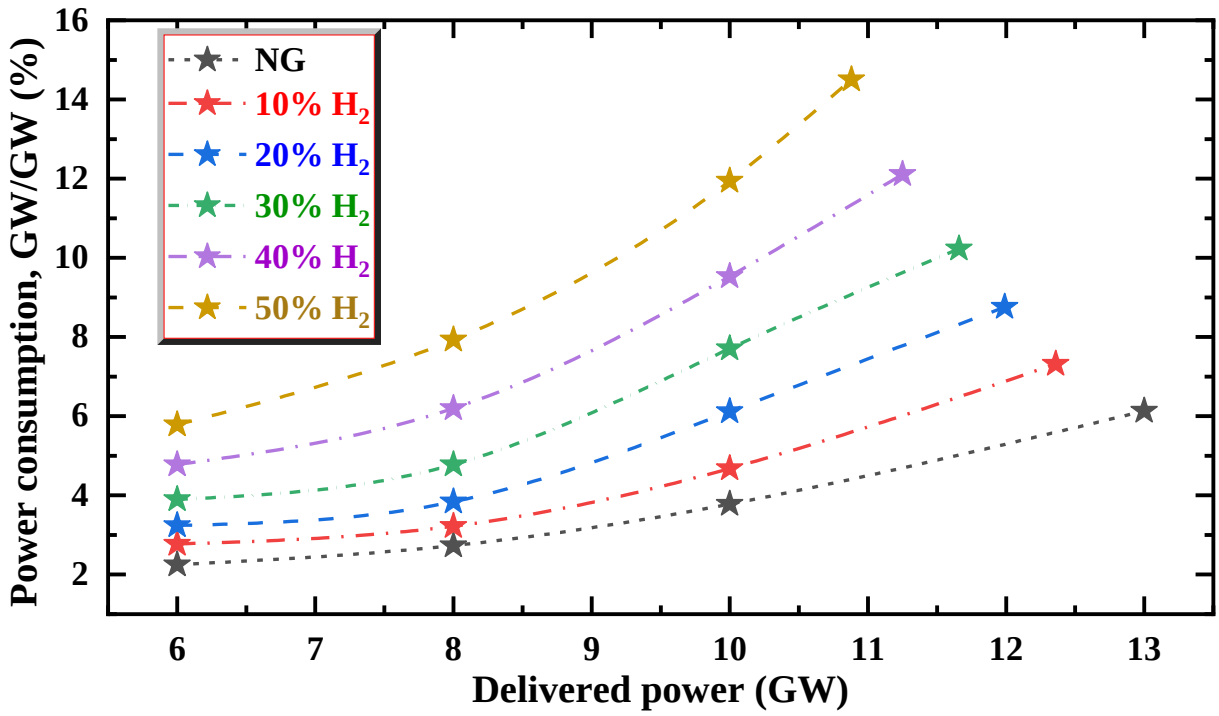

Fig. 4.11: Power consumption (%) by the compressors with the variation of delivered power (GW).

Table 4.1: Maximum possible supply power and mass flow rate (kg/s) with the considered pipeline for different compositions.

Gas Type	Max possible gas supply (kg/s)	Max possible power supply (GW)
NG	248.2	13.0
5% H_2 – 95% NG	242.3	12.8
10% H_2 – 90% NG	236.0	12.4
15% H_2 – 85% NG	228.6	12.2
20% H_2 – 80% NG	222.1	12.0
30% H_2 – 70% NG	209.3	11.7
40% H_2 – 60% NG	195.1	11.3
50% H_2 – 50% NG	181.9	10.9
100% H_2	81.5	9.9

Fig. 4.12 illustrates the relationship between delivered power (GW) and fuel consumption (%) across different MAOP for NG, 20% H_2, and 100% H_2. As MAOP decreases from 8.6 MPa to 3 MPa, several trends emerge in both delivered power and fuel consumption. For delivered power, NG consistently shows higher delivered power compared to the other compositions, indicating its efficiency in maintaining power delivery at various MAOP levels. The 20% H_2 follows closely behind NG in delivered power, reflecting the impact of hydrogen on reducing overall delivery efficiency but still maintaining a relatively high level of performance. 100% H_2 exhibits the lowest

delivered power across all MAOP levels, highlighting the challenges of transporting hydrogen efficiently through pipelines. The delivered power remains constant at 8 GW for MAOP values from 8.6 MPa to 6 MPa. After that, the delivered power decreases as the MAOP decreases. For the 20% H_2 mixture, an 8 GW power delivery is only possible at 8.6 MPa; it then gradually decreases with the reduction in MAOP. Similarly, for 100% H_2, an 8 GW power delivery is only achievable at 8.6 MPa, and it subsequently decreases, with the delivered power being significantly lower compared to other gases.

In terms of fuel consumption, there is a clear distinction between the different gas compositions. 100% H_2 consistently shows the highest fuel consumption percentages across all MAOP levels. This indicates that a significant portion of the supplied power is consumed by the compressors, owing to hydrogen's lower molar mass and higher compression requirements. The 20% H_2-80% NG mixture shows intermediate fuel consumption levels, higher than NG but lower than pure hydrogen, reflecting the added energy demands of incorporating hydrogen into the gas mix. NG has the lowest fuel consumption percentages, demonstrating its efficiency in terms of compressor energy requirements. The fuel consumption increases with lower MAOP for a constant power delivery, and after that the fuel consumption reduces with the reduction of the delivery power. For NG, the fuel consumption increases from 2.73% at 8.6 MPa MAOP to 3.18% at 7 MPa to deliver a constant power of 8 GW. Afterward, the fuel consumption decreases as the delivered power reduces with the decrease in MAOP. For the 20% H_2 mixture, the maximum fuel consumption is 3.88% at 8.6 MPa MAOP with an 8 GW power supply; it then decreases with the reduction in MAOP and power delivery. Similarly, for 100% H_2, the maximum fuel consumption is 19.38% at 8.6 MPa MAOP with an 8 GW power supply, and it subsequently reduces as the MAOP and power delivery capacity decrease.

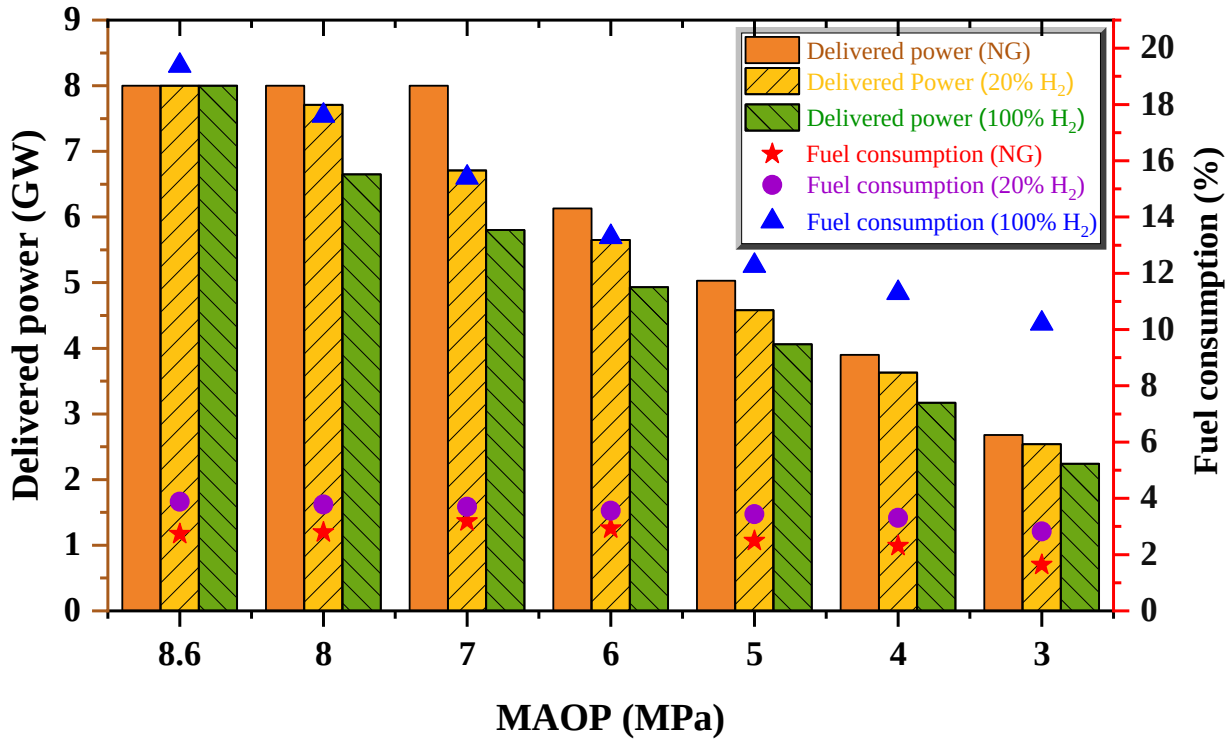

Fig. 4.12: Delivered power (GW) and fuel consumption (%) with the variation of MAOP (MPa).

Fig. 4.13 illustrates the effect of pipeline material roughness on fuel consumption in a multi-delivery point natural gas transmission system. The x-axis represents the roughness of the pipeline's internal surface, measured in micrometers (μm), ranging from 20 to 180 μm. The y-axis shows fuel consumption as a percentage, with values ranging from 2.58% to 3.04%. The data points indicate a clear positive correlation between material roughness and fuel consumption. As the roughness increases, the fuel consumption also rises, indicating that rougher surfaces create more resistance to gas flow, which in turn requires more fuel to maintain the same flow rate. This trend is most pronounced at lower roughness levels, where small increases in roughness lead to significant increases in fuel consumption. Beyond 80 μm, the curve flattens, suggesting that the rate of increase in fuel consumption slows as roughness continues to rise. The figure underscores the importance of minimizing pipeline roughness to optimize fuel efficiency, reduce operational costs, and lower the environmental impact associated with fuel use in natural gas transmission systems.

Fig. 4.14 illustrates the percentage reduction in CO_2 emissions from compressor fuel consumption achieved by injecting hydrogen into a natural gas transmission pipeline at various blending ratios. The x-axis represents the percentage of hydrogen injected into the natural gas,

ranging from 5% to 20%. The y-axis shows the corresponding reduction in CO_2 emissions in percentage terms. The data points plotted on the graph indicate a clear positive relationship between the amount of hydrogen injected and the reduction in CO_2 emissions. At 5% H_2 injection, the CO_2 emission reduction is approximately 1.85%, while the percentage of reduction is 3.54%, 5.27%, and 7.25% with the hydrogen injection of 10%, 15%, and 20%. This graph visually confirms that blending hydrogen into natural gas can effectively reduce CO_2 emissions, with greater reductions achieved at higher hydrogen blending ratios. In the study, no additional safety factors are considered for the injection of hydrogen into pipeline.

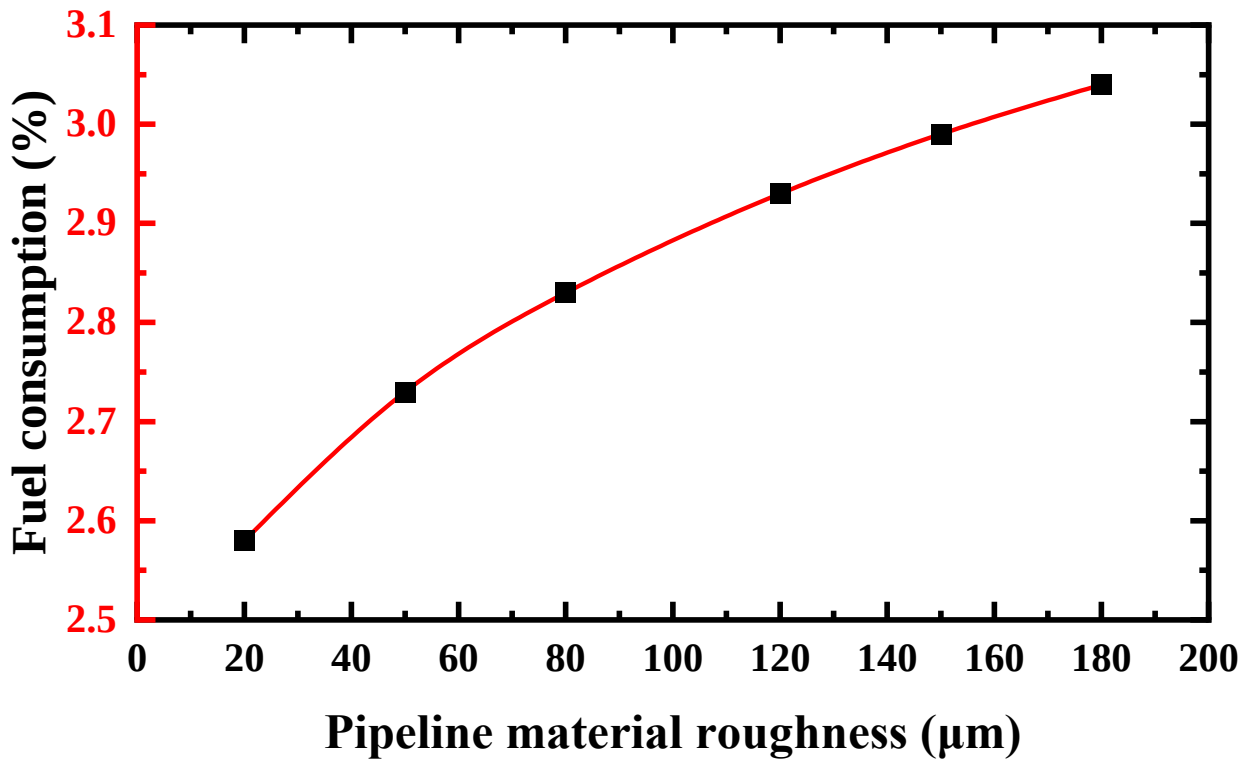

Fig. 4.13: Effect of pipeline material roughness (µm) on the fuel consumption of a multi-delivery points natural gas transmission pipeline.

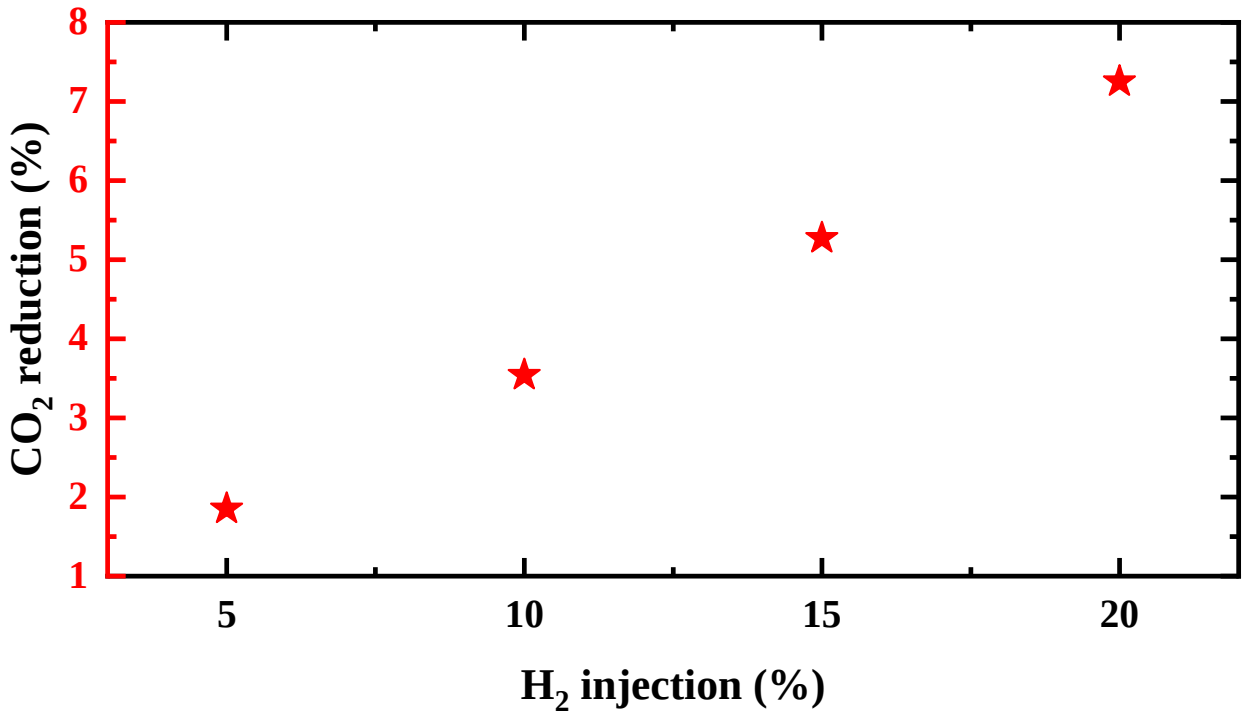

Fig. 4.14: CO_2 emission reduction (%) from compressor fuel consumption with the injection of H_2 into natural gas transmission pipeline.

4.4 Electrification of the compressor

Electrification of compressor stations in natural gas transmission pipeline systems involves replacing gas turbines with electric motors to power the compressors. There are several compelling reasons for this transition:

- *Emission Reduction:* Natural gas turbines produce significant CO_2 and other greenhouse gases. Electrification, especially when paired with renewable energy sources, can drastically reduce or even eliminate these emissions. This helps in meeting stringent environmental regulations and corporate sustainability goals.
- *Energy Efficiency:* Electric motors are generally more efficient than gas turbines in converting energy into mechanical work. This efficiency reduces overall energy consumption, potentially lowering operational costs despite higher initial power costs.
- *Operational Benefits:* Electric motors typically require less maintenance compared to gas turbines, which are complex mechanical systems with more frequent maintenance needs and higher downtime. This leads to lower maintenance costs and increased reliability. Electric compressors can be more easily controlled and adjusted, providing greater

flexibility in pipeline operations. This allows for more precise management of gas flow and pressure.

- *Energy Source Diversification:* Electrification allows compressor stations to tap into a broader mix of energy sources, including renewable energy such as wind, solar, and hydropower. This diversification reduces reliance on fossil fuels and enhances energy security.
- *Regulatory Compliance:* Many regions are tightening regulations on greenhouse gas emissions. Electrifying compressor stations can help companies comply with these regulations and avoid penalties. Companies and countries aiming for net-zero carbon emissions see electrification as a critical step toward achieving these targets.
- *Noise Reduction:* Electric motors typically operate more quietly than gas turbines, which can be a significant advantage in areas where noise pollution is a concern.
- *Market and Economic Factors:* As the cost of electricity from renewable sources continues to decrease, the long-term economics of using electric motors can become more favorable compared to natural gas turbines, which are subject to fuel price volatility. Moreover, although the initial capital cost for installing electric motors might be higher, the long-term operational savings from reduced fuel and maintenance costs can make it economically advantageous.
- *Technological Advancements:* Additionally, continuous improvements in electric motor technology, including higher efficiencies and better performance under varying loads, make electrification a more viable and attractive option.

Fig. 4.15 demonstrates the impact on emissions and costs associated with different levels of electrification for compressors in a natural gas transmission pipeline across four cases. In this case, all the parameters considered is stated in **Table 4.2**.

Table 4.2: Parameters considered for electrification effect on the cost and emissions [103, 104].

Parameter	Value	Parameter	Value
Motor efficiency	0.9	BC emission factor, kg CO_2/m^3	2.162
BC Electricity cost, $/kWh	0.0835	Density of NG, kg/m^3	0.712
Operating hours, hr./year	8,760	Emission intensity, kg CO_2/kg NG	3.04
Natural gas price, $/GJ	2.23	BC electricity emission factor, gCO_2e/kWh	15

In Case 1, where all compressors use natural gas, emissions from compressor fuel consumption are highest at around 430 kilotons of CO_2 per year, with negligible compressor power supply costs (15.39 M$/year). Case 2 shows a significant reduction in emissions to 371 kilotons of CO_2 per year (13.7% reduction than case 1) when the first compressor continues to use natural gas and the others switch to electricity, but the power supply costs rise to around 40 million dollars annually (155.8% raise than case 1). In Case 3, where the first compressor uses electricity and the others use natural gas, emissions further drop to 90.6 kilotons of CO_2 per year, with power supply costs increasing to 154 million dollars per year. Case 4, with all compressors using electricity by replacing turbine with electric motor, results in the lowest emissions, close to zero (31.9 $ktCO_2$/year), but the highest power supply cost at 178 million dollars per year. This indicates a clear trade-off between reducing emissions and increasing power supply costs when transitioning from natural gas to electricity for compressor operation.

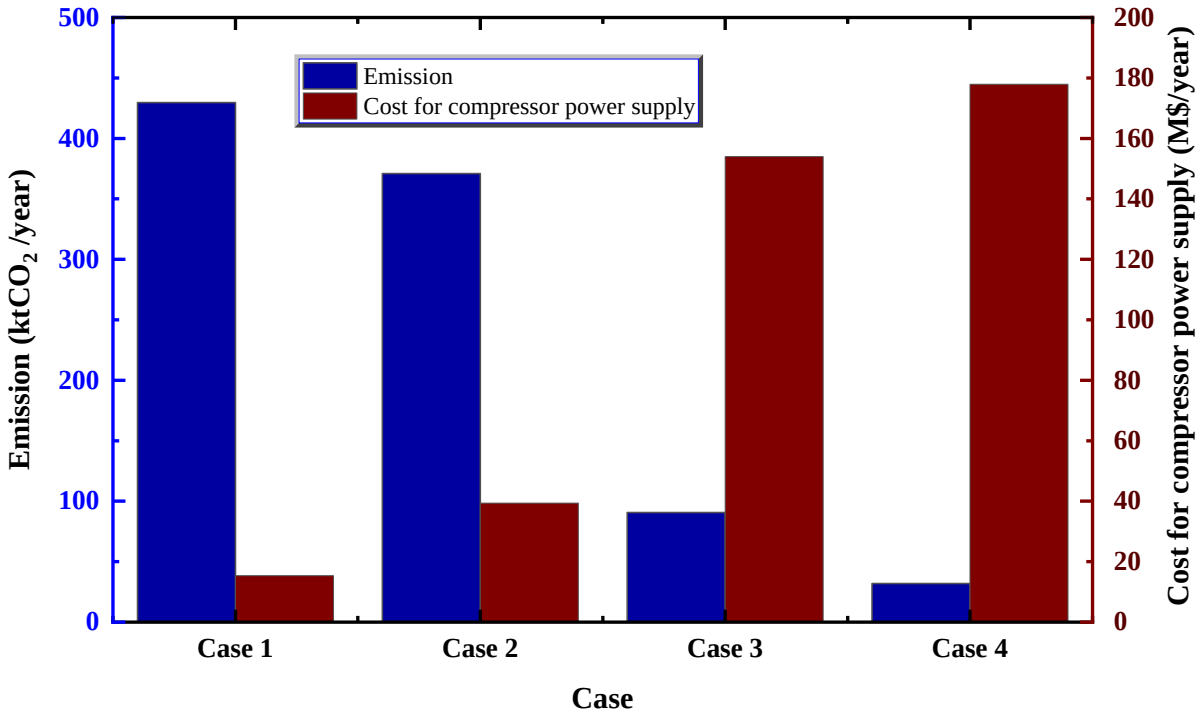

Fig. 4.15: Effect of electrification levels on the compressor power supply cost (M$/year) and emission ($ktCO_2$/year) for four cases.

4.5 Case Study: Coastal GasLink Pipeline Ltd.

An existing natural gas transmission pipeline is optimized in the present study. Coastal GasLink Pipeline Ltd. is at the forefront of a significant energy infrastructure project aimed at transporting

natural gas from northeastern British Columbia to the LNG Canada export facility in Kitimat, BC as shown in **Fig. 4.16**. The pipeline spans approximately 670 kilometers and features a substantial diameter of 1.219 meters. Designed to meet a variable daily demand ranging from 56 to 85 million cubic meters, the project underscores the need for efficient and scalable natural gas transportation. To maintain optimal flow and pressure across this extensive network, the pipeline will incorporate up to eight compressor stations strategically located along the route. This infrastructure not only enhances energy export capabilities but also plays a pivotal role in supporting economic growth and energy security in the region, making it an intriguing case for optimization modeling and analysis.

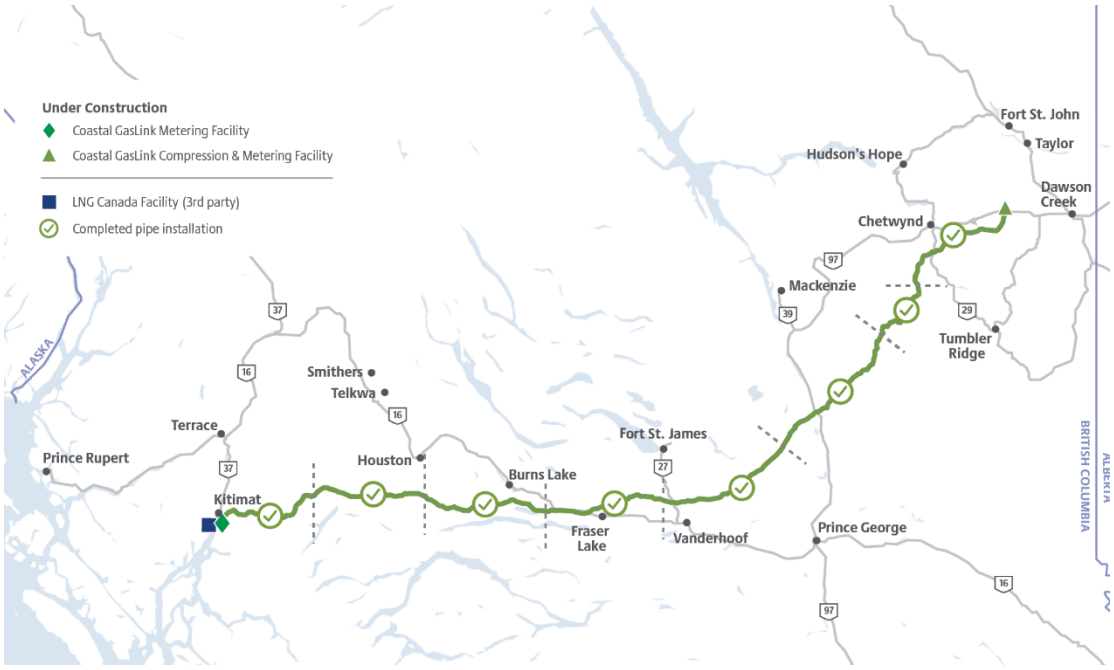

Fig. 4.16: Coastal GasLink transmission pipeline [105].

The graph in **Fig. 4.17** illustrates the relationship between the MAOP and two key performance metrics: the delivered mass flow rate (measured in kg/s) and fuel consumption (measured in percentage) for the Coastal GasLink Pipeline Ltd. case study. The MAOP values, ranging from 2 MPa to 8.2 MPa, are plotted along the x-axis, while the delivered mass flow rate is represented on the left y-axis, and fuel consumption is shown by the red line on the right y-axis.

As MAOP decreases from 8.2 MPa to 2 MPa, the delivered mass flow rate initially shows a constant value of 431.3 kg/s until 4 MPa, beyond which it is not possible to supply same mass

flow rate because of the low-pressure boundary constraint ($p \geq 1.38$ MPa). This indicates that higher pressures enable a greater volume of natural gas to be transported through the pipeline, maximizing its delivery capacity. On the other hand, fuel consumption exhibits a different trend: it starts low, rises sharply to a peak (8.97%) around 4 MPa, and then gradually decreases as MAOP continues to decrease. Overall, fuel consumption increases with an increase in MAOP for the same mass transfer capacity, but it decreases with a decrease in capacity, even when MAOP is low. The interplay between these factors highlights the importance of optimizing MAOP to balance high mass flow rates with acceptable fuel consumption levels, ensuring both economic and operational efficiency in pipeline management.

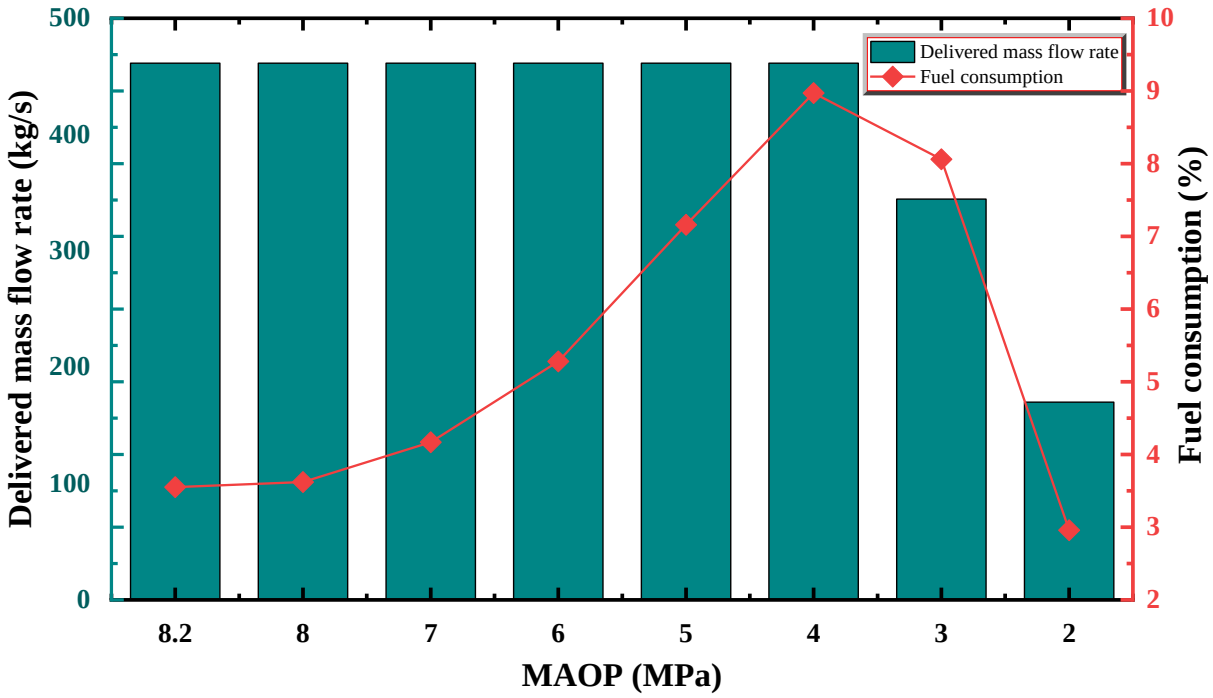

Fig. 4.17: Effect of MAOP on the delivered mass flow rate (kg/s) and fuel consumption (%) in a case study of Coastal GasLink Pipeline Ltd.

The graph in **Fig. 4.18** illustrates the impact of different energy configurations on emissions and the cost of compressor power supply for the Coastal GasLink Pipeline Ltd. under four distinct cases. In Case 1, where all compressors consume NG, emissions from compressor fuel consumption are the highest, around 1570 $ktCO_2$ per year, but the compressor power supply cost is the lowest at around 56 M$/year. In Case 2, with the first compressor using NG and the rest using electricity, emissions decrease to approximately 1066 $ktCO_2$ per year, while the cost rises to about 262 M$/year. In Case 3, where the first compressor is powered by electricity and the

remaining ones by NG, emissions further reduce to around 620 $ktCO_2$ per year, and the power supply cost is about 444 M$/year. In case 4, where all compressors use electricity, shows the lowest emissions, near 116 $ktCO_2$ per year, but incurs the highest power supply cost to compressor, around 650 M$/year. Overall, although electrification of compressors delivers low emissions, but it requires more cost than conventional NG fueled turbine-compressor system. The figure highlights the trade-off between reducing emissions through increased electrification of compressors and the associated rise in power supply costs.

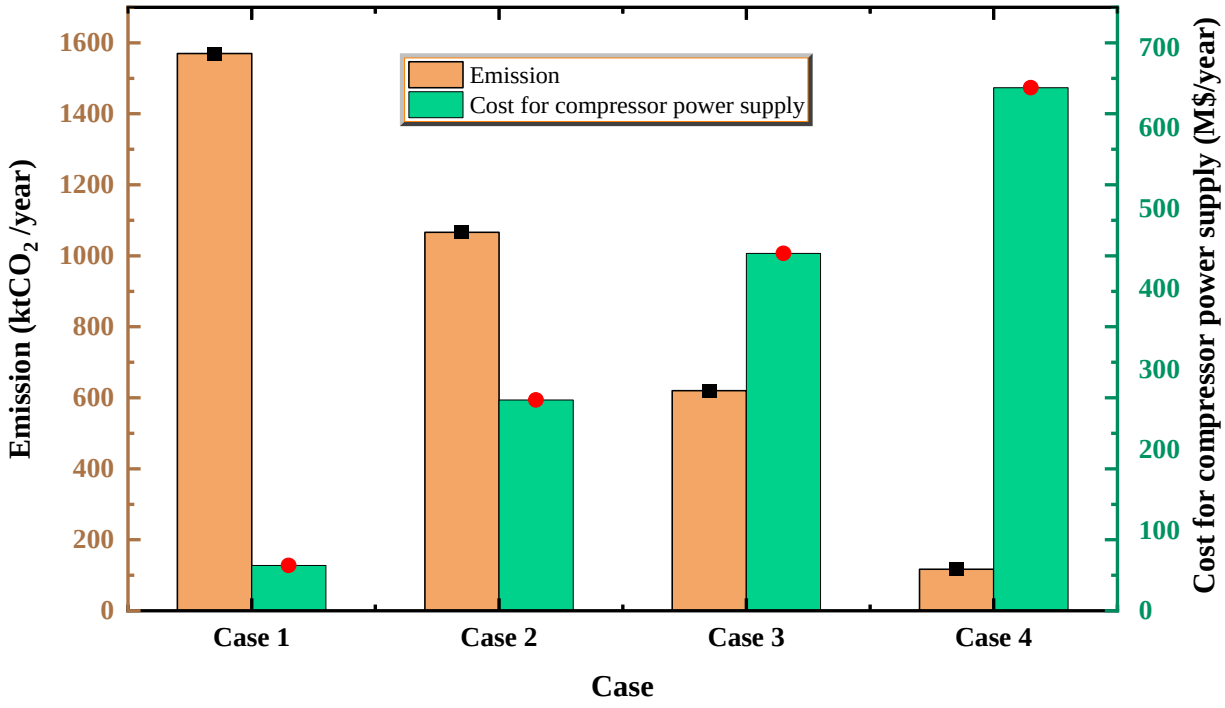

Fig. 4.18: Emission ($ktCO_2$/year) and cost for compressor power supply (M$/year) for different electrification levels.

4.6 Summary

This chapter provides an in-depth analysis of optimizing pipeline operations, with a specific focus on the Coastal GasLink Pipeline Ltd. We explored the effects of operating pressure on compressor fuel consumption, identifying strategies to minimize it. The study examined the maximum power delivery possible with the existing pipeline and the influence of the MAOP on both power delivery and fuel consumption. It also addressed the impact of hydrogen injection on performance, highlighting potential environmental and operational benefits. Furthermore, the chapter investigated the effects of electrifying compressors, showing significant potential for reducing emissions and impact on costs. The chapter concluded with a case study demonstrating how these

optimizations, especially electrification, could significantly enhance system performance and sustainability.

Chapter 5

Conclusion and Recommendations

5.1 Conclusion

In conclusion, optimizing natural gas pipelines using MATLAB and genetic algorithms provides a powerful and efficient solution for reducing compressor fuel consumption. The genetic algorithm's capability to handle complex, nonlinear optimization problems makes it ideally suited for this application, enabling the exploration of numerous potential solutions, and identifying the most effective strategies for fuel savings. By defining the objective function to minimize fuel consumption, it ensures that the optimization aligns with both economic and environmental goals, leading to cost reductions and lower greenhouse gas emissions. MATLAB's robust computational framework facilitates detailed modeling and simulation of pipeline systems, allowing for accurate and practical solutions that consider real-world constraints and variables. The results demonstrate that this approach not only achieves significant fuel efficiency but also enhances overall pipeline performance. This optimization strategy, therefore, represents a significant advancement in pipeline management, promoting more sustainable and cost-effective operations in the natural gas industry. In the present study, a single delivery, and a multi-delivery pipeline of 800 km length from Alberta to BC, Canada is optimized. From the optimization process following major contributions are remarkable:

- The study uses single and multi-delivery natural gas pipelines for the modeling and optimization, reducing compressor fuel consumption and demonstrating a powerful method for achieving sustainable and environmentally friendly pipeline management.
- For an 800 km pipeline, the fuel consumption for delivering 8 GW of power is 2.98% for single delivery considering natural gas transmission.
- For a multi-delivery pipeline with six delivery points delivering the same 8 GW of power, around 2.7% fuel is consumed, considering natural gas transmission.
- Introducing hydrogen into the natural gas mixture increases fuel consumption proportionally, with 5-20 vol% hydrogen injections resulting in fuel consumptions of 3-3.8% for multi-delivery pipelines. Introducing hydrogen into the natural gas mixture increases fuel consumption proportionally, with 5-20 vol% hydrogen injections resulting

in 3-3.8% fuel consumption for multi-delivery pipelines, while pure hydrogen (100% H_2) injection leads to a significant increase in fuel consumption up to 19.9%.

- The maximum operating pressure in the pipeline increases with higher hydrogen injection, primarily due to hydrogen's lower density and higher diffusivity compared to natural gas, which necessitates higher pressures to maintain the same energy flow rates. For multi-delivery pipeline, the maximum operating pressure in this study for NG, 10% H_2, 20% H_2, and 100% H_2 is 8.26 MPa, 8.39 MPa, 8.49 MPa, and 8.59 MPa, respectively, while MAOP is 8.6 MPa.
- For a fixed rate of energy delivery, pipeline pressure drop is higher for gases with lower molar mass due to their higher velocity and reduced density.
- Maximum 13 GW power delivery is possible with the natural gas pipeline with the existing pipeline considering multi-delivery points, while it is 12.36 GW, 12 GW, 11.66 GW, 11.25 GW, and 10.88 GW for 10% H_2, 20% H_2, 30% H_2, 40% H_2, and 50% H_2, respectively. Therefore, the more hydrogen injection, the less power can be delivered through the pipeline.
- Fuel consumption increases gradually with the decrease in MAOP to deliver same amount of power for all the gas compositions. If the delivery capacity decreases, then the fuel consumption also decreases, even when the MAOP is low. For single delivery pipeline, fuel consumption has been increased from 3.21% to 5.86% for the decreasing MAOP of 8.6 to 5 MPa for 8 GW power supply. Beyond 5 MPa, power delivery capacity has decreased with the decreased in MAOP, and therefore the fuel consumption also decreased. In case of multi-delivery pipeline, fuel consumption jumped from 2.73% to 3.18% for decrease in MAOP 8.6 MPa to 7 MPa considering NG. After that power delivery capacity decreases with the decrease in MAOP, and it is 1.64% with the MAOP of 3 MPa to deliver 2.68 GW power.

- Minimizing pipeline roughness is crucial for optimizing fuel efficiency, as increased roughness significantly raises fuel consumption due to higher flow resistance, especially at lower roughness levels. The fuel consumption is decreased from 2.73% to 2.58%, while pipeline roughness deceases 50μm to 20μm.

- The study shows that blending hydrogen with fuel significantly reduces CO_2 emissions from compressor fuel consumption. Specifically, there is a reduction of 1.85% to 7.25% when hydrogen is injected at concentrations of 5% to 20% by volume.
- The study reveals that transitioning compressor operations in a natural gas pipeline to electricity significantly reduces CO_2 emissions from compressor fuel consumption but increases compressor power supply costs. Emissions decrease from 430 $ktCO_2$/year (natural gas, $15.39M/year) to 31.9 $ktCO_2$/year (full electrification, $178M/year), highlighting the trade-off between emissions reduction and rising power supply costs.

The findings presented here are crucial for stakeholders in the energy sector, policymakers, and researchers, offering insights into the feasibility, benefits, and challenges of transitioning towards a hydrogen-enriched natural gas network. The integration of these results with existing literature highlights both the advancements made and the gaps that need to be addressed in future studies.

Future Recommendations

Beyond the results discussed, this thesis paper points to the scope for future work as summarized below:

- Employment of multi-objective optimization algorithms to simultaneously minimize compressor fuel consumption, pipeline operational cost, and maximize the hydrogen blend in natural gas, balancing economic, operational, and environmental goals.
- Exploration of the feasibility of integrating renewable energy sources, such as solar and wind, to power compressor stations and other critical infrastructure, reducing dependence on traditional fuels and further minimizing overall fuel consumption and emissions.
- The present study does not focus on the source of the injected hydrogen, which can be produced using water electrolysis and renewable energy sources.
- Create and refine safety protocols to manage the risks associated with hydrogen blending, including leak detection, corrosion effect, response strategies, and regular maintenance, ensuring the safe operation of pipelines with minimal fuel wastage.
- The integration of renewable natural gas (RNG) can be studied into existing transmission systems, focusing on blending ratios, pipeline compatibility, and the impact on system performance and emissions. Research should explore the potential for RNG to supplement or replace traditional natural gas supplies.

- The integration of smart technologies, such as advanced sensors, Internet of Things (IoT) devices, and machine learning algorithms should be explored, to monitor and optimize pipeline operations in real-time. This includes predictive maintenance, leak detection, and efficiency improvements.
- The potential impacts of climate change on pipeline operations can be investigated, including changes in temperature, weather patterns, and natural disasters. Research should focus on adaptive strategies to ensure the resilience and reliability of natural gas transmission systems.
- Investigation of methods to reduce greenhouse gas emissions from natural gas transmission systems, including technologies for carbon capture and storage, methane leak detection, and the use of low-emission fuels for compressor stations.

By adopting these recommendations, the natural gas industry can significantly enhance the efficiency and sustainability of pipeline operations, effectively integrating hydrogen to reduce compressor fuel consumption, operation cost, and environmental impact.

Appendices

Appendix A

Formulation of the general form of equation

The one-dimensional momentum balance describing gas flow in a pipe is given in Equation (A.1) (Osiadacz, 1987):

$$\frac{\partial p}{\partial x}+\frac{f}{2D}\rho v^2 \pm g\rho\sin\alpha+\frac{\partial(\rho v^2)}{\partial x}+\frac{\partial(\rho v)}{\partial t}=0 \tag{A-1}$$

Given Equation (A-2), which describes the relationship between gas pressure and gas density, we can eliminate the density variable using Equations (A-3) and (A-4). It's important to note that the cross-sectional area of the pipe, A, remains constant, as do the gas's molecular weight, M, and the universal gas constant, R.

$$\rho=\frac{pM}{ZRT} \tag{A-2}$$

$$\frac{dp}{dx}+\frac{f}{2D}\frac{pM}{ZRT}\left(\frac{m}{\frac{pM}{ZRT}A}\right)^2 \pm g\frac{pM}{ZRT}\sin\alpha+\frac{\partial}{\partial x}\left(\frac{pM}{ZRT}\left(\frac{m}{\frac{pM}{ZRT}A}\right)^2\right)+\frac{\partial}{\partial x}\left(\frac{pM}{ZRT}\frac{m}{\frac{pM}{ZRT}A}\right)=0 \tag{A-3}$$

$$\frac{\partial p}{\partial t}+\frac{f}{2D}\frac{ZRT}{pMA^2}m^2 \pm g\frac{pM}{ZRT}\sin\alpha+\frac{R}{A^2M}\frac{\partial}{\partial t}\left(\frac{ZT}{p}m^2\right)+\frac{1}{A}\frac{\partial m}{\partial t}=0 \tag{A-4}$$

Since we have the following mathematically:

$$\frac{\partial}{\partial t}\left(\frac{ZT}{p}m^2\right)=2m\frac{ZT}{p}\frac{\partial m}{\partial t}+m^2\frac{\partial}{\partial x}\left(\frac{ZT}{p}\right) \tag{A-5}$$

Equation (A.4) is therefore developed as Equation (A-6), and Equation (A-7) follows.

$$\frac{\partial p}{\partial t}+\frac{f}{2D}\frac{ZRT}{pMA^2}m^2 \pm g\frac{pM}{ZRT}\sin\alpha+\frac{R}{A^2M}\frac{\partial}{\partial t}\left[2m\frac{ZT}{p}\frac{\partial m}{\partial x}+m^2\frac{\partial}{\partial x}\left(\frac{ZT}{p}\right)\right]+\frac{1}{A}\frac{\partial m}{\partial t}=0 \tag{A-6}$$

$$\frac{\partial p}{\partial t}+\frac{f}{2D}\frac{ZRT}{pMA^2}m^2 \pm g\frac{pM}{ZRT}\sin\alpha+\frac{2mR}{A^2M}\frac{ZT}{p}\frac{\partial m}{\partial t}+\frac{m^2}{A^2}\frac{R}{M}\frac{\partial}{\partial x}\left(\frac{ZT}{p}\right)+\frac{1}{A}\frac{\partial m}{\partial t}=0 \tag{A-7}$$

The aforementioned relationship is overly general for modeling isothermal gas flow. While the isothermal assumption is typically applied in gas pipeline simulations, it is important to note that in gas transmission lines, the gas temperature may drop significantly, sometimes falling below ambient temperature, due to substantial pressure drops.

Continuity equation simplification

Material balance for gas flow through a pipeline with a constant hydraulic cross-sectional area is typically expressed in differential form, as shown in Equation (A-8).

$$\frac{1}{A}\frac{\partial m}{\partial x}+\frac{\partial \rho}{\partial t}=0 \quad \text{(A-8)}$$

By substituting gas density from Equation (A-2) into the formulation as demonstrated in Equation (A-9), the continuity equation can then be straightforwardly derived and is represented by Equation (A-10).

$$\frac{1}{A}\frac{\partial m}{\partial x}+\frac{\partial}{\partial t}\left(\frac{pM}{ZRT}\right)=0 \quad \text{(A-9)}$$

$$\frac{1}{A}\frac{\partial m}{\partial x}+\frac{M}{R}\frac{\partial}{\partial t}\left(\frac{p}{ZT}\right)=0 \quad \text{(A-10)}$$

Gas pipeline transients can be simulated using Equation (A-10) in conjunction with Equation (A-7).

Continuity equation and equation of movement in steady state

In a steady state, the mass flow rate and gas density remain constant at every section of the pipe.

$$\frac{\partial m}{\partial t}=0 \quad \text{(A-11)}$$

$$\frac{\partial \rho}{\partial t}=0 \quad \text{(A-12)}$$

According to Equation (A-8), the gas mass flow rate is therefore constant along the pipeline's length:

$$\frac{1}{A}\frac{\partial m}{\partial x}=0 \Rightarrow m=\text{constant} \quad \text{(A-13)}$$

In a steady state, Equation (A-7) can be expressed as follows:

$$\frac{\partial p}{\partial t}+\frac{f}{2D}\frac{ZRT}{pMA^2}m^2 \pm g\frac{pM}{ZRT}\sin\alpha+\frac{m^2}{A^2}\frac{R}{M}\frac{\partial}{\partial x}\left(\frac{ZT}{p}\right)=0 \quad \text{(A-14)}$$

We aim to resolve the equation of motion under isothermal conditions by making two assumptions and then simplifying and solving Equation (A.14) algebraically:

1) Gas flowing through the pipe segment under isothermal conditions.
2) Constant compressibility factor.

The first assumption is widely applicable in many industrial scenarios, while the second is realistic for relatively short pipelines, for example. Using these assumptions, Equation (A-14) will be simplified, leading to Equations (A-15), (A-16), and (A-17) as demonstrated.

$$\frac{\partial p}{\partial t} + \frac{f}{2D}\frac{ZRT}{pMA^2}m^2 \pm g\frac{pM}{ZRT}\sin\alpha + \frac{m^2}{A^2}\frac{ZRT}{M}\frac{\partial}{\partial x}\left(\frac{1}{p}\right) = 0 \quad \text{(A-15)}$$

$$\frac{\partial p}{\partial t} + \frac{f}{2D}\frac{ZRT}{pMA^2}m^2 \pm g\frac{pM}{ZRT}\sin\alpha - \frac{m^2}{A^2}\frac{ZRT}{Mp^2}\frac{\partial p}{\partial x} = 0 \quad \text{(A-16)}$$

$$\left(1 - \frac{m^2}{A^2}\frac{ZRT}{Mp^2}\right)\frac{\partial p}{\partial x} + \frac{f}{2D}\frac{ZRT}{pMA^2}m^2 \pm g\frac{pM}{ZRT}\sin\alpha = 0 \quad \text{(A-17)}$$

We will solve the ordinary differential equation (A-17) for three scenarios: inclined, vertical, and horizontal pipelines. Given that $m = \rho v A$ and $A = \frac{\pi D^2}{4}$, Equation (A-17) can be rearranged into Equation (A-18) and subsequently transformed into Equation (A-19).

$$\frac{dp}{dx} = \frac{\frac{f}{2D}\frac{ZRT}{pMA^2}m^2 \pm g\frac{pM}{ZRT}\sin\alpha}{\frac{m^2}{A^2}\frac{ZRT}{Mp^2} - 1} \quad \text{(A-18)}$$

$$\frac{dp}{dx} = \frac{ap \pm bp^3}{c - p^2} \text{ where } a = \frac{f}{2D}\frac{ZRT}{pMA^2}m^2,\ b = g\frac{M}{ZRT}\sin\alpha,\ c = \frac{m^2}{A^2}\frac{ZRT}{M} \quad \text{(A-19)}$$

The polynomial development and integration operation between the pipe endpoints 1 and 2 are incorporated in the mathematical process to solve this latter parameterized problem as follows:

$$dx = \frac{c - p^2}{p(a \pm bp^2)}dp = \left(\frac{c/a}{p} - \frac{(1 \pm cb/a)p}{a \pm bp^2}\right)db = \left(\frac{c}{ap} - \frac{1 \pm cb/a}{\pm 2b}\frac{\pm 2bp}{a \pm bp^2}\right)dp \quad \text{(A-20)}$$

$$\int_1^2 dx = \int_1^2 \left(\frac{c}{ap} - \frac{1 \pm cb/a}{\pm 2b}\frac{\pm 2bp}{a \pm bp^2}\right)dp = \frac{c}{a}\int_1^2 \frac{dp}{p} - \frac{1 \pm cb/a}{\pm 2b}\int_1^2 \frac{\pm 2bp}{a \pm bp^2}dp \quad \text{(A-21)}$$

As demonstrated below, the result of this integration yields a quasi-explicit equation for calculating the pressure drop.

$$L = \frac{c}{a}\ln\left(\frac{p_2}{p_1}\right) - \frac{1 \pm cb/a}{\pm 2b}\ln\left(\frac{a \pm bp_2^2}{a \pm bp_1^2}\right) \quad \text{(A-22)}$$

By substituting the parameters, a, b, and c, this equation illustrates the influence of each parameter on the pressure drop across the pipe segment between points 1 and 2.

$$L = \frac{2D}{f}\ln\left(\frac{p_2}{p_1}\right) - \frac{fZRT \pm 2DgM\sin\alpha}{\pm 2bfgM\sin\alpha}\ln\left(\frac{f(ZRT)^2m^2 \pm 2DgM^2}{f(ZRT)^2m^2 \pm 2DgM^2}\frac{\sin\alpha A^2}{\sin\alpha A^2}\frac{p_2^2}{p_1^2}\right) \quad \text{(A-23)}$$

However, in the following circumstances where sin α = 1, this equation can be more simply expressed. It is not useful for horizontal pipes where sin α = 0.

Gas flow vertically upward:

$$L = \frac{2D}{f}\ln\left(\frac{p_2}{p_1}\right) - \left(\frac{ZRT}{2gM} + \frac{D}{f}\right)\ln\left(\frac{f(ZRT)^2m^2+2DgM^2}{f(ZRT)^2m^2+2DgM^2}\frac{A^2}{A^2}\frac{p_2^2}{p_1^2}\right) \quad \text{(A-24)}$$

Gas flow vertically downward:

$$L = \frac{2D}{f}\ln\left(\frac{p_2}{p_1}\right) + \left(\frac{ZRT}{2gM} - \frac{D}{f}\right)\ln\left(\frac{f(ZRT)^2m^2-2DgM^2}{f(ZRT)^2m^2-2DgM^2}\frac{A^2}{A^2}\frac{p_2^2}{p_1^2}\right) \quad \text{(A-25)}$$

Equation (2.18) should be used as the starting point for a horizontal pipe, and Equations (A-26) through (A-30) should follow:

$$\left(1 - \frac{m^2}{A^2}\frac{ZRT}{Mp^2}\right)\frac{dp}{dx} + \frac{f}{2D}\frac{ZRT}{pMA^2}m^2 = 0 \quad \text{(A-26)}$$

$$\left(p - \frac{m^2}{A^2}\frac{ZRT}{Mp}\right)\frac{dp}{dx} + \frac{f}{2D}\frac{ZRT}{pMA^2}m^2 = 0 \quad \text{(A-27)}$$

$$\int_1^2\left(\frac{m^2}{A^2}\frac{ZRT}{Mp} - p\right)dp = \int_1^2\frac{f}{2D}\frac{ZRT}{MA^2}m^2dx \quad \text{(A-28)}$$

$$\frac{m^2}{A^2}\frac{ZRT}{M}\ln(\frac{p_2}{p_1}) - \frac{1}{2}(p_2^2 - p_1^2) = \frac{f}{2D}\frac{ZRT}{MA^2}m^2L \quad \text{(A-29)}$$

$$(p_2^2 - p_1^2) - \frac{32m^2ZRT}{\pi^2D^4M}\ln\left(\frac{p_2}{p_1}\right) + \frac{16f}{\pi^2D^5}\frac{ZRT}{M}m^2L = 0 \quad \text{(A-30)}$$

This thesis uses equation (A-30) as its main formula to calculate pressure drop for a pipe segment that is restricted to locations 1 and 2.

Appendix B

Table B-1: Optimized results for NG of multi-delivery points NG pipeline.

Upstream pressure (MPa)	Downstream pressure (MPa)	Density (kg/m^3)	Mass flow rate (kg/s)	Z	Fuel consumption (kg/s)	Compressor head (kJ/kg)	Compressor required power (kW)
$p_1 = 8.26$	$p_2 = 7.69$	$\rho_1 = 70.68$	$m_0 = 169.17$	0.791	3.82	250.08	58758
$p_3 = 8.21$	$p_4 = 7.63$	$\rho_2 = 70.06$	$m_1 = 165.29$	0.793	0.111	7.85	1710.9
$p_5 = 8.17$	$p_6 = 7.59$	$\rho_3 = 69.61$	$m_2 = 165.11$	0.794	0.116	7.80	1789.3
$p_7 = 8.13$	$p_8 = 7.55$	$\rho_4 = 69.16$	$m_3 = 164.93$	0.795	0.117	7.80	1798.5
$p_9 = 8.06$	$p_{10} = 6.07$	$\rho_5 = 60.72$	$m_4 = 164.74$	0.815	0.117	7.66	1798.9
	$p_{11} = 6.62$	$\rho_6 = 63.66$	$m_5 = 16.38$	0.818	0.081	6.78	1241.5
	$p_{12} = 7.14$	$\rho_7 = 66.5$	$m_6 = 16.38$	0.801	0.063	7.03	964.8
$p_{13} = 7.57$	$p_{14} = 6.03$	$\rho_8 = 57.63$	$m_7 = 131.69$	0.823	0.056	6.36	869.9
	$p_{15} = 2.1$	$\rho_9 = 38.73$	$m_8 = 98.76$	0.875	**Total = 4.48**		
$p_{16} = 6.41$	$p_{17} = 4.88$	$\rho_{10} = 46.35$	$m_9 = 32.77$	0.854			
$p_{18} = 5.15$	$p_{19} = 3.77$	$\rho_{11} = 35.32$	$m_{10} = 98.49$	0.885			
	$p_{20} = 2.84$	$\rho_{12} = 31.21$	$m_{11} = 32.77$	0.897			
	$p_{21} = 1.38$	$\rho_{13} = 24.98$	$m_{12} = 32.77$	0.916			
			$m_{13} = 32.77$				

Table B-2: Optimized results for 5% H_2-95% NG mixture of multi-delivery points NG pipeline.

Upstream pressure (MPa)	Downstream pressure (MPa)	Density (kg/m^3)	Mass flow rate (kg/s)	Z	Fuel consumption (kg/s)	Compressor head (kJ/kg)	Compressor required power (kW)
$p_1 = 8.32$	$p_2 = 7.73$	$\rho_1 = 66.21$	$m_0 = 168.05$	0.814	4.06	269.9	63013
$p_3 = 8.28$	$p_4 = 7.68$	$\rho_2 = 65.75$	$m_1 = 163.95$	0.815	0.123	8.41	1914
$p_5 = 8.23$	$p_6 = 7.63$	$\rho_3 = 65.24$	$m_2 = 163.72$	0.816	0.124	8.47	1927
$p_7 = 8.18$	$p_8 = 7.57$	$\rho_4 = 64.69$	$m_3 = 163.50$	0.817	0.125	8.54	1941
$p_9 = 8.12$	$p_{10} = 6.06$	$\rho_5 = 56.95$	$m_4 = 163.28$	0.836	0.128	8.80	1999
	$p_{11} = 6.64$	$\rho_6 = 59.77$	$m_5 = 16.23$	0.829	0.085	7.26	1315
	$p_{12} = 7.15$	$\rho_7 = 62.28$	$m_6 = 16.23$	0.822	0.076	8.67	1181
$p_{13} = 7.58$	$p_{14} = 6.05$	$\rho_8 = 54.32$	$m_7 = 130.6$	0.842	0.081	9.25	1254
	$p_{15} = 2.04$	$\rho_9 = 36.32$	$m_8 = 97.87$	0.889	**Total = 4.80**		
$p_{16} = 6.49$	$p_{17} = 4.88$	$\rho_{10} = 43.93$	$m_9 = 32.464$	0.869			
$p_{18} = 5.25$	$p_{19} = 3.85$	$\rho_{11} = 34.12$	$m_{10} = 97.66$	0.895			
	$p_{20} = 2.89$	$\rho_{12} = 30.15$	$m_{10} = 32.464$	0.906			
	$p_{21} = 1.41$	$\rho_{13} = 24.21$	$m_{11} = 32.464$	0.924			
			$m_{12} = 32.464$				

Table B-3: Optimized results for 10% H_2-90% NG mixture of multi-delivery points NG pipeline.

Upstream pressure (MPa)	Downstream pressure (MPa)	Density (kg/m^3)	Mass flow rate (kg/s)	Z	Fuel consumption (kg/s)	Compressor head (kJ/kg)	Compressor required power (kW)
$p_1 = 8.39$	$p_2 = 7.76$	$\rho_1 = 62.02$	$m_0 = 166.82$	0.835	4.31	291.6	67569
$p_3 = 8.34$	$p_4 = 7.71$	$\rho_2 = 61.56$	$m_1 = 162.48$	0.836	0.136	9.47	2137
$p_5 = 8.29$	$p_6 = 7.66$	$\rho_3 = 61.11$	$m_2 = 162.24$	0.837	0.137	9.54	2151
$p_7 = 8.25$	$p_8 = 7.62$	$\rho_4 = 60.74$	$m_3 = 161.98$	0.838	0.140	9.77	2199
$p_9 = 8.20$	$p_{10} = 6.07$	$\rho_5 = 53.58$	$m_4 = 161.75$	0.855	0.141	9.85	2213
	$p_{11} = 6.66$	$\rho_6 = 56.19$	$m_5 = 16.069$	0.848	0.108	9.49	1705
	$p_{12} = 7.18$	$\rho_7 = 58.52$	$m_6 = 16.069$	0.843	0.102	11.86	1597
$p_{13} = 7.71$	$p_{14} = 5.99$	$\rho_8 = 51.09$	$m_7 = 129.328$	0.860	0.099	11.64	1563
	$p_{15} = 1.89$	$\rho_9 = 34.15$	$m_8 = 96.919$	0.902	**Total = 5.17**		
$p_{16} = 6.55$	$p_{17} = 4.90$	$\rho_{10} = 41.60$	$m_9 = 32.138$	0.883			
$p_{18} = 5.34$	$p_{19} = 3.91$	$\rho_{11} = 32.77$	$m_{10} = 96.65$	0.905			
	$p_{20} = 2.94$	$\rho_{12} = 29.02$	$m_{10} = 32.138$	0.915			
	$p_{21} = 1.41$	$\rho_{13} = 23.26$	$m_{11} = 32.138$	0.931			
			$m_{12} = 32.138$				

Table B-4: Optimized results for 15% H_2-85% NG mixture of multi-delivery points NG pipeline.

Upstream pressure (MPa)	Downstream pressure (MPa)	Density (kg/m^3)	Mass flow rate (kg/s)	Z	Fuel consumption (kg/s)	Compressor head (kJ/kg)	Compressor required power (kW)
$p_1 = 8.45$	$p_2 = 7.78$	$\rho_1 = 57.56$	$m_0 = 165.67$	0.857	4.61	317.34	73020
$p_3 = 8.38$	$p_4 = 7.71$	$\rho_2 = 56.98$	$m_1 = 161.05$	0.858	0.149	10.58	2366
$p_5 = 8.32$	$p_6 = 7.64$	$\rho_3 = 56.45$	$m_2 = 160.77$	0.859	0.153	10.85	2425
$p_7 = 8.29$	$p_8 = 7.61$	$\rho_4 = 56.20$	$m_3 = 160.48$	0.860	0.164	11.65	2598
$p_9 = 8.27$	$p_{10} = 6.04$	$\rho_5 = 49.80$	$m_4 = 160.20$	0.873	0.169	12.06	2684
	$p_{11} = 6.68$	$\rho_6 = 52.35$	$m_5 = 15.893$	0.868	0.138	12.31	2190
	$p_{12} = 7.18$	$\rho_7 = 54.37$	$m_6 = 15.893$	0.863	0.129	15.32	2042
$p_{13} = 7.82$	$p_{14} = 5.96$	$\rho_8 = 47.70$	$m_7 = 128.11$	0.878	0.121	14.41	1913
	$p_{15} = 1.81$	$\rho_9 = 32.02$	$m_8 = 95.96$	0.914	**Total = 5.63**		
$p_{16} = 6.63$	$p_{17} = 4.92$	$\rho_{10} = 39.13$	$m_9 = 31.786$	0.897			
$p_{18} = 5.43$	$p_{19} = 3.97$	$\rho_{11} = 31.19$	$m_{10} = 95.618$	0.916			
	$p_{20} = 2.98$	$\rho_{12} = 27.65$	$m_{10} = 31.786$	0.924			
	$p_{21} = 1.42$	$\rho_{13} = 22.18$	$m_{11} = 31.786$	0.938			
			$m_{12} = 31.786$				

Table B-5: Optimized results for 20% H_2-80% NG mixture of multi-delivery points NG pipeline.

Upstream pressure (MPa)	Downstream pressure (MPa)	Density (kg/m^3)	Mass flow rate (kg/s)	Z	Fuel consumption (kg/s)	Compressor head (kJ/kg)	Compressor required power (kW)
p_1 = 8.49	p_2 = 7.79	ρ_1 = 53.61	m_0 = 164.3	0.877	4.87	342.8	78239
p_3 = 8.41	p_4 = 7.71	ρ_2 = 53.02	m_1 = 159.5	0.878	0.162	11.74	2602
p_5 = 8.35	p_6 = 7.64	ρ_3 = 52.53	m_2 = 159.13	0.879	0.168	12.25	2707
p_7 = 8.32	p_8 = 7.61	ρ_4 = 52.31	m_3 = 158.8	0.880	0.180	13.11	2891
p_9 =8.29	p_{10} = 5.96	ρ_5 = 46.17	m_4 = 158.46	0.892	0.183	13.34	2935
	p_{11} = 6.64	ρ_6 = 48.64	m_5 = 15.704	0.887	0.169	15.46	2722
	p_{12} = 7.16	ρ_7 = 50.54	m_6 = 15.704	0.883	0.157	19.12	2521
p_{13} = 7.91	p_{14} = 5.94	ρ_8 = 44.74	m_7 = 126.74	0.895	0.137	16.76	2200
	p_{15} = 1.73	ρ_9 = 30.11	m_8 = 94.9	0.925	**Total = 6.03**		
p_{16} = 6.72	p_{17} = 4.96	ρ_{10} = 37.08	m_9 = 31.408	0.910			
p_{18} = 5.52	p_{19} = 4.03	ρ_{11} = 29.81	m_{10} = 94.52	0.926			
	p_{20} = 3.03	ρ_{12} = 26.47	m_{10} = 31.408	0.933			
	p_{21} = 1.42	ρ_{13} = 21.21	m_{11} = 31.408	0.945			
			m_{12} = 31.408				

Table B-6: Optimized results for 100% H_2 of multi-delivery points NG pipeline.

Upstream pressure (MPa)	Downstream pressure (MPa)	Density (kg/m^3)	Mass flow rate (kg/s)	Z	Fuel consumption (kg/s)	Compressor head (kJ/kg)	Compressor required power (kW)
p_1 = 8.59	p_2 = 7.34	ρ_1 = 6.43	m_0 = 82.54	1.06	8.53	2813	322500
p_3 = 8.55	p_4 = 7.32	ρ_2 = 6.41	m_1 = 74.03	1.06	0.527	193.8	19930
p_5 = 8.53	p_6 = 7.32	ρ_3 = 6.40	m_2 = 73.23	1.06	0.518	192.5	19585
p_7 = 8.50	p_8 = 7.31	ρ_4 = 6.39	m_3 = 72.46	1.06	0.501	188.0	18921
p_9 = 8.48	p_{10} = 5.22	ρ_5 = 5.59	m_4 = 71.70	1.06	0.487	184.8	18411
	p_{11} = 6.17	ρ_6 = 5.95	m_5 = 6.66	1.05	0.665	313.9	25132
	p_{12} = 6.57	ρ_7 = 6.10	m_6 = 6.66	1.06	1.08	680.7	41121
p_{13} = 8.42	p_{14} = 4.06	ρ_8 = 5.12	m_7 = 57.64	1.05	0.926	603.4	35000
	p_{15} = 1.44	ρ_9 = 4.09	m_8 = 43.49	1.03	**Total = 13.24**		
p_{16} = 6.83	p_{17} = 3.94	ρ_{10} = 4.45	m_9 = 13.32	1.04			
p_{18} = 6.30	p_{19} = 5.81	ρ_{11} = 4.78	m_{10} = 41.76	1.04			
	p_{20} = 4.23	ρ_{12} = 4.36	m_{10} = 13.32	1.03			
	p_{21} = 1.39	ρ_{13} = 3.22	m_{11} = 13.32	1.02			
			m_{12} = 13.32				

Appendix C

MATLAB Code for Single-delivery points NG pipeline:

```
function [f,p1,p3,p5,p7,p9,p11,p13,p15,v1,v2,v3,v4,v5,v6,v7,v8,c1,c2,c3,c4,c5,c6,c7,c8,v_e1,v_e2,v_e3,v_e4,v_e5,
v_e6,v_e7,v_e8] = Fitness_Value(p2,p4,p6,p8,p10,p12,p14,p16)

%% Input parameters
R=8.314;                % J/mol.K
T=283;                  % Kelvine
M=16.5*0.001;           % pure NG kg/mol
roughness=5*10^-5;      % meter

%% Pipeline equations

% Pipeline 1
    D1=0.9;                         % Diameter (m)
    L1=100000;
    m1=163.83+mf-mf1;               % constant mass flow rate (kg/s)
    f1=(-2*log10((roughness/D1)/3.71))^-2;          %Darcy friction factor
e1=@(p1)  ((p2^2-p1^2)-((32*m1^2*Z1*R*T)/(3.1416^2*D1^4*M))*log(p2/p1)  +  ((16*f1*Z1*R  *T*m1^2*
L1)/(3.1416^2*D1^5*M)));
    p1 = fsolve(e1, p2);

% Pipeline 2
    D2=0.9;
    L2=100000;
    m2=163.83+ mf-mf1-mf2;
    f2=(-2*log10((roughness/D2)/3.71))^-2;
    e2 =@(p3) ((p4^2-p3^2)-((32*m2^2*Z2*R*T)/(3.1416^2*D2^4*M))*log(p4/p3)+((16*f2*Z2*R*T*m2^2*
L2)/(3.1416^2*D2^5*M)));
    p3 = fsolve(e2, p4);

% Pipeline 3
    D3=0.9;
    L3=100000;
    m3=163.83+ mf-mf1-mf2-mf3;
    f3=(-2*log10((roughness/D3)/3.71))^-2;
    e3 =@(p5) ((p6^2-p5^2)-((32*m3^2*Z3*R*T)/(3.1416^2*D3^4*M))*log(p6/p5)+((16*f3*Z3*R*T*m3^2*
L3)/(3.1416^2*D3^5*M)));
    p5 = fsolve(e3, p6);

% Pipeline 4
    D4=0.9;
    L4=100000;
    m4=163.83+ mf-mf1-mf2-mf3-mf4;
    f4=(-2*log10((roughness/D4)/3.71))^-2;
    e4 =@(p7) ((p8^2-p7^2)-((32*m4^2*Z4*R*T)/(3.1416^2*D4^4*M))*log(p8/p7)+((16*f4*Z4*R*T*m4^2*
L4)/(3.1416^2*D4^5*M)));
    p7 = fsolve(e4, p8);

% Pipeline 5
    D5=0.9;
    L5=100000;
    m5=163.83+ mf-mf1-mf2-mf3-mf4-mf5;
```

```
    f5=(-2*log10((roughness/D5)/3.71))^-2;
    e5 =@(p9) ((p10^2-p9^2)-((32*m5^2*Z5*R*T)/(3.1416^2*D5^4*M))*log(p10/p9)+((16*f5*Z5*R*T*m5^2*
L5)/(3.1416^2*D5^5*M)));
    p9 = fsolve(e5, p10);

% Pipeline 6
    D6=0.9;
    L6=100000;
    m6=163.83+ mf-mf1-mf2-mf3-mf4-mf5-mf6;
    f6=(-2*log10((roughness/D6)/3.71))^-2;
    e6 =@(p11) ((p12^2-p11^2)-((32*m6^2*Z6*R*T)/(3.1416^2*D6^4*M))*log(p12/p11)+((16*f6*Z6*R*T*
m6^2*L6)/(3.1416^2*D6^5*M)));
    p11 = fsolve(e6, p12);

% Pipeline 7
    D7=0.9;
    L7=100000;
    m7=163.83+ mf-mf1-mf2-mf3-mf4-mf5-mf6-mf7;
    f7=(-2*log10((roughness/D7)/3.71))^-2;
    e7 = @(p13) ((p14^2-p13^2)-((32*m7^2*Z7*R*T)/(3.1416^2*D7^4*M))*log(p14/p13)+ ((16*f7*Z7*R*T
*m7^2*L7)/(3.1416^2*D7^5*M)));
    p13 = fsolve(e7, p14);

% Pipeline 8
    D8=0.9;
    L8=100000;
    m8=163.83+ mf-mf1-mf2-mf3-mf4-mf5-mf6-mf7-mf8;
    f8=(-2*log10((roughness/D8)/3.71))^-2;
    e8 =@(p15) ((p16^2-p15^2)-((32*m8^2*Z8*R*T)/(3.1416^2*D8^4*M))*log(p16/p15) + ((16*f8*Z8*R*T
*m8^2*L8)/(3.1416^2*D8^5*M)));
    p15 = fsolve(e8, p16);

%% Compressibility Calculation
T_c = 190.9;          % Critical temperature of pure natural gas (K)
T_r= (T/T_c);         % Reduced temperature calculation
Z_ini=0.9;            % Initial compressibility factor (assumed 0.9)

P_1 = (p1+p2)/2;      %Pipeline average Pressure (Pa)
P_2 = (p3+p4)/2;
P_3 = (p5+p6)/2;
P_4 = (p7+p8)/2;
P_5 = (p9+p10)/2;
P_6 = (p11+p12)/2;
P_7 = (p13+p14)/2;
P_8 = (p15+p16)/2;

P_c = 4.58*10^6;      % critical pressure for natural gas (Pa)
Pr_1=P_1/P_c;         % reduced pressure equations
Pr_2=P_2/P_c;
Pr_3=P_3/P_c;
Pr_4=P_4/P_c;
Pr_5=P_5/P_c;
Pr_6=P_6/P_c;
Pr_7=P_7/P_c;
Pr_8=P_8/P_c;
```

```
row_r_1 = 0.27*(Pr_1/(Z_ini*T_r));
row_r_2 = 0.27*(Pr_2/(Z_ini*T_r));
row_r_3 = 0.27*(Pr_3/(Z_ini*T_r));
row_r_4 = 0.27*(Pr_4/(Z_ini*T_r));
row_r_5 = 0.27*(Pr_5/(Z_ini*T_r));
row_r_6 = 0.27*(Pr_6/(Z_ini*T_r));
row_r_7 = 0.27*(Pr_7/(Z_ini*T_r));
row_r_8 = 0.27*(Pr_8/(Z_ini*T_r));


Z_1= 1+(0.31506-(1.0467/T_r)-(0.5783/T_r^3))*row_r_1 + (0.5353-(0.6127/T_r)-(0.6185/T_r^3))*row_r_1^2;
Z_2= 1+(0.31506-(1.0467/T_r)-(0.5783/T_r^3))*row_r_2 + (0.5353-(0.6127/T_r)-(0.6185/T_r^3))*row_r_2^2;
Z_3= 1+(0.31506-(1.0467/T_r)-(0.5783/T_r^3))*row_r_3 + (0.5353-(0.6127/T_r)-(0.6185/T_r^3))*row_r_3^2;
Z_4= 1+(0.31506-(1.0467/T_r)-(0.5783/T_r^3))*row_r_4 + (0.5353-(0.6127/T_r)-(0.6185/T_r^3))*row_r_4^2;
Z_5= 1+(0.31506-(1.0467/T_r)-(0.5783/T_r^3))*row_r_5 + (0.5353-(0.6127/T_r)-(0.6185/T_r^3))*row_r_5^2;
Z_6= 1+(0.31506-(1.0467/T_r)-(0.5783/T_r^3))*row_r_6 + (0.5353-(0.6127/T_r)-(0.6185/T_r^3))*row_r_6^2;
Z_7= 1+(0.31506-(1.0467/T_r)-(0.5783/T_r^3))*row_r_7 + (0.5353-(0.6127/T_r)-(0.6185/T_r^3))*row_r_7^2;
Z_8= 1+(0.31506-(1.0467/T_r)-(0.5783/T_r^3))*row_r_8 + (0.5353-(0.6127/T_r)-(0.6185/T_r^3))*row_r_8^2;

%% Denisty Equations
density_1= (P_1*M)/(Z_1*R*T);          % P_1 means average pressure for pipeline 1
density_2= (P_2*M)/(Z_2*R*T);
density_3= (P_3*M)/(Z_3*R*T);
density_4= (P_4*M)/(Z_4*R*T);
density_5= (P_5*M)/(Z_5*R*T);
density_6= (P_6*M)/(Z_6*R*T);
density_7= (P_7*M)/(Z_7*R*T);
density_8= (P_8*M)/(Z_8*R*T);


% volumetric flow rate (m3/sec)
q1 = m1/density_1;              % constant mass flow rate (kg/sec) is converted to volumetric flow rate (m3/s)
q2 = m2/density_2;
q3 = m3/density_3;
q4 = m4/density_4;
q5 = m5/density_5;
q6 = m6/density_6;
q7 = m7/density_7;
q8 = m8/density_8;

% Velocity of Gas (m/s)
v1 = q1/((3.1416*D1^2)/4);      % velocity (m/s) of flowing gas calculated from volumetric flow rate (m3/s) and Area
v2 = q2/((3.1416*D2^2)/4);
v3 = q3/((3.1416*D3^2)/4);
v4 = q4/((3.1416*D4^2)/4);
v5 = q5/((3.1416*D5^2)/4);
v6 = q6/((3.1416*D6^2)/4);
v7 = q7/((3.1416*D7^2)/4);
v8 = q8/((3.1416*D8^2)/4);

%% Inequality constraint (from here)

% Critical velocity (m/s)
k = 1.3;
c1 = sqrt(k*Z_1*R*T/M);  % The flowing gas velocity is less than the half of critical velocity (c, (unit: m/s)) of the
gas
```

```
c2 = sqrt(k*Z_2*R*T/M);
c3 = sqrt(k*Z_3*R*T/M);
c4 = sqrt(k*Z_4*R*T/M);
c5 = sqrt(k*Z_5*R*T/M);
c6 = sqrt(k*Z_6*R*T/M);
c7 = sqrt(k*Z_7*R*T/M);
c8 = sqrt(k*Z_8*R*T/M);

% Erosional velocity (m/s): To avoid erosion of the inside surface of the tubes, elbows and other joints.
v_e1 = 122*sqrt((Z_1*R*T)/(P_1*M));
v_e2 = 122*sqrt((Z_2*R*T)/(P_2*M));
v_e3 = 122*sqrt((Z_3*R*T)/(P_3*M));
v_e4 = 122*sqrt((Z_4*R*T)/(P_4*M));
v_e5 = 122*sqrt((Z_5*R*T)/(P_5*M));
v_e6 = 122*sqrt((Z_6*R*T)/(P_6*M));
v_e7 = 122*sqrt((Z_7*R*T)/(P_7*M));
v_e8 = 122*sqrt((Z_8*R*T)/(P_8*M));

%% Compressor isentropic head (kj/kg)
k=1.3;
p0=1.38e+6;                % Assumed gas pressure from well is 200psi (1.379 MPa)
Z_0=0.79;                  % Initially assume Z_0 = 0.79

h1 =(Z_0*R*T/M)*(k/(k-1))*(((p1/p0)^((k-1)/k))-1)/1000;
h2 =(Z_1*R*T/M)*(k/(k-1))*(((p3/p2)^((k-1)/k))-1)/1000;
h3 =(Z_2*R*T/M)*(k/(k-1))*(((p5/p4)^((k-1)/k))-1)/1000;
h4 =(Z_3*R*T/M)*(k/(k-1))*(((p7/p6)^((k-1)/k))-1)/1000;
h5 =(Z_4*R*T/M)*(k/(k-1))*(((p9/p8)^((k-1)/k))-1)/1000;
h6 =(Z_7*R*T/M)*(k/(k-1))*(((p13/p12)^((k-1)/k))-1)/1000;

%% Fuel consumption Equation
eff_i=0.72;
eff_m=0.9;
eff_d=0.35;
LHV=48830;

%% Compressor fuel consumption calculation
m0=169.04;                 % The fuel enters in the first compressor (total mass delivered + total fuel consumption)
mf1=((m0*h1)/(eff_i*eff_m*eff_d*LHV));
mf2=((m1*h2)/(eff_i*eff_m*eff_d*LHV));
mf3=((m2*h3)/(eff_i*eff_m*eff_d*LHV));
mf4=((m3*h4)/(eff_i*eff_m*eff_d*LHV));
mf5=((m4*h5)/(eff_i*eff_m*eff_d*LHV));
mf6=((m7*h6)/(eff_i*eff_m*eff_d*LHV));

mf = (mf1 + mf2 + mf3+ mf4 + mf5 + mf6);          % Total fuel consumption for all the compressors (kg/s)

%% Objective function
f = (mf);                  % The objective function is to minimize the total fuel consumption of the compressor
end
```

Genetic Algorithm for Single-delivery point NG pipeline:

```
clc
```

```
clear

%% GA Parameters
% Maximum Allowable operating pressure (Pa): The maximum pressure that a pipeline can tolerate
D=0.9;
f_F = 0.4;                          % design factor
f_E = 0.8;                          % seam joint factor is between 1 and 0.6 for the most commonly used material types
f_T = 1;                           % Temperature factor,f_T, is equal to 1 for the gas temperature below 393K
SMYS = 2e+8;                            % specified minimum yield strength (SMYS) of pipe material.
t = 52*10^-3*D + 989*10^-5;                 % meter if other units are in meter
MAOP = SMYS * ((2*t)/(D-t)) * f_F * f_E * f_T;

U= MAOP; L= 1.38;       % Max. and min. value of controller parameters
P= 200;                 % Population size
k= 2;                   % Tournament competitor size
MaxIt=500;              % Maximum Number of iterations
Pc= 0.8;                % Crossover proability
Pm= 0.2;                % Mutation probability
muC= 20;                % Distribution index for crossover
muM= 20;                % Distribution index for mutation
% Fbest= zeros(MaxIt,1);  % Initialize storage for performance index
Fitness= zeros(P,1);    %Initialize fitness storage
nv= 8;                  %No. of variables
PWP= 1000;              % Penalty weight for pressure p1, p3, p5
Gain= ones(1,nv,P);     %Initialize gain storage

%% Initial fitness evaluation for random population

% Initialization of random population
%In general, you can generate N random numbers in the interval (a,b) with the formula r = a + (b-a).*rand(N,1).
InitPop= L+(U-L).*rand(1,nv,P);  %Initialization of population

   for p= 1:P              %Run for each population
      init_Gains= InitPop(:,:,p);
      p2= init_Gains(1)*1e6;
      p4= init_Gains(2)*1e6;
      p6= init_Gains(3)*1e6;
      p8= init_Gains(4)*1e6;
      p10= init_Gains(5)*1e6;
      p12= init_Gains(6)*1e6;
      p14= init_Gains(7)*1e6;
      p16= init_Gains(8)*1e6;

[f,p1,p3,p5,p7,p9,p11,p13,p15,v1,v2,v3,v4,v5,v6,v7,v8,c1,c2,c3,c4,c5,c6,c7,c8,v_e1,v_e2,v_e3,v_e4,v_e5,v_e6,v_e
7,v_e8] = Fitness_Value(p2,p4,p6,p8,p10,p12,p14,p16);

      %% Constraints Start
      if p1>(U*1e6)
         penalty_p1= PWP+(p1/1e6)-U;
      else
         penalty_p1=0;
      end
      if p3>(U*1e6)
         penalty_p2= PWP+(p3/1e6)-U;
      else
         penalty_p2=0;
```

```
    end
    if p5>(U*1e6)
       penalty_p3= PWP+(p5/1e6)-U;
    else
       penalty_p3=0;
    end
    if p7>(U*1e6)
       penalty_p4= PWP+(p7/1e6)-U;
    else
       penalty_p4=0;
    end
    if p9>(U*1e6)
       penalty_p5= PWP+(p9/1e6)-U;
    else
       penalty_p5=0;
    end
    if p11>(U*1e6)
       penalty_p6= PWP+(p11/1e6)-U;
    else
       penalty_p6=0;
    end
    if p13>(U*1e6)
       penalty_p7= PWP+(p13/1e6)-U;
    else
       penalty_p7=0;
    end
    if p15>(U*1e6)
       penalty_p8= PWP+(p15/1e6)-U;
    else
       penalty_p8=0;
    end


    vLim1=v1-(c1/2); vLim2=v2-(c2/2); vLim3=v3-(c3/2);
    vLim4=v4-(c4/2); vLim5=v5-(c5/2); vLim6=v6-(c6/2); vLim7=v7-(c7/2); vLim8=v8-(c8/2);

    veLim1=v1-v_e1; veLim2=v2-v_e2; veLim3=v3-v_e3; veLim4=v4-v_e4; veLim5=v5-v_e5; veLim6=v6-v_e6;
veLim7=v7-v_e7; veLim8=v8-v_e8;
    if vLim1>0
       penalty_v1= vLim1;
    else
       penalty_v1=0;
    end
    if vLim2>0
       penalty_v2= vLim2;
    else
       penalty_v2=0;
    end
    if vLim3>0
       penalty_v3= vLim3;
    else
       penalty_v3=0;
    end
    if vLim4>0
       penalty_v4= vLim4;
    else
```

```
    penalty_v4=0;
end
if vLim5>0
    penalty_v5= vLim5;
else
    penalty_v5=0;
end
if vLim6>0
    penalty_v6= vLim6;
else
    penalty_v6=0;
end
if vLim7>0
    penalty_v7= vLim7;
else
    penalty_v7=0;
end
if vLim8>0
    penalty_v8= vLim8;
else
    penalty_v8=0;
end


if veLim1>0
    penalty_ve1= veLim1;
else
    penalty_ve1=0;
end
if veLim2>0
    penalty_ve2= veLim2;
else
    penalty_ve2=0;
end
if veLim3>0
    penalty_ve3= veLim3;
else
    penalty_ve3=0;
end
if veLim4>0
    penalty_ve4= veLim4;
else
    penalty_ve4=0;
end
if veLim5>0
    penalty_ve5= veLim5;
else
    penalty_ve5=0;
end
if veLim6>0
    penalty_ve6= veLim6;
else
    penalty_ve6=0;
end
if veLim7>0
    penalty_ve7= veLim7;
```

```
        else
            penalty_ve7=0;
        end
        if veLim8>0
            penalty_ve8= veLim8;
        else
            penalty_ve8=0;
        end
        %% Constraints End

Fitness(p)=f+penalty_p1+penalty_p2+penalty_p3+penalty_p4+penalty_p5+penalty_p6+penalty_p7+penalty_p8+pe
nalty_v1+penalty_v2+penalty_v3+penalty_v4+penalty_v5+penalty_v6+penalty_v7+penalty_v8+penalty_ve1+penal
ty_ve2+penalty_ve3+penalty_ve4+penalty_ve5+penalty_ve6+penalty_ve7+penalty_ve8;
        Gain(:,:,p)= init_Gains;

    end

%% Main loop of GA
BestFit= zeros(MaxIt,1);
for it= 1:MaxIt
    pFitness= Fitness;      %Define fitness as parent fitness

    %% Tournament selection (Binary)

    GainS= Gain; % Initialize selected gains
    R= randperm(P); % Randomize population sequence
    for p= 1:P-1    % Each population participates in tournament selection twice except 1 & P
        T= [Fitness(R(p)) Fitness(R(p+1))];
        [sortT, Tindex]= sort(T);
        if Tindex== [1 2]
            GainS(:,:,R(p+1))=Gain(:,:,R(p));
        else
            GainS(:,:,R(p))=Gain(:,:,R(p+1));
        end
    end
    if Fitness(R(P)) <= Fitness(R(1)) % Comparison between population 1 & P left
        GainS(:,:,R(1))=Gain(:,:,R(P));
    else
        GainS(:,:,R(P))=Gain(:,:,R(1));
    end

    %% SBX Crossover

    GainC= GainS;        % Initialize offsprings
    Rc= randperm(P); % Randomize parents for crossover
    beta= zeros(1,nv);
    for p=1:2:P
        if rand < Pc
            for j= 1:nv %beta formation
                u=rand;
                if u<=0.5
                    beta(1,j)= (2*u)^(1/(muC+1));
                else
                    beta(1,j)= (1/(2*(1-u)))^(1/(muC+1));
                end
            end
```

```
        GainC(:,:,Rc(p))= 0.5 .*(((ones(1,nv)+beta).*GainS(:,:,Rc(p)))+((ones(1,nv)-beta).*GainS(:,:,Rc(p+1))));
        GainC(:,:,Rc(p+1))= 0.5 .*(((ones(1,nv)-beta).*GainS(:,:,Rc(p)))+((ones(1,nv)+beta).*GainS(:,:,Rc(p+1))));
    end
end

%% Mutation (Polynomial)

GainM= GainC;  % Initialize mutants
del= zeros(1,nv);
for p=1:P

    if rand < Pm
        for j= 1:nv %del2 formation
            r=rand;
            if r<0.5
                del(1,j)= ((2*r)^(1/(muM+1)))-1;
            else
                del(1,j)= 1-(2*(1-r))^(1/(muM+1));
            end
        end

        GainM(:,:,p)= GainC(:,:,p)+(U-L).*del;
    end
end

%% Do corner bounding here
    GainM= min(GainM,U);
    GainM= max(GainM,L);

%% Function Evaluation
b= zeros(1,nv,P);
for p= 1:P  %Run for each population

    init_Gains= GainM(:,:,p);
    p2= init_Gains(1)*1e6;
    p4= init_Gains(2)*1e6;
    p6= init_Gains(3)*1e6;
    p8= init_Gains(4)*1e6;
    p10= init_Gains(5)*1e6;
    p12= init_Gains(6)*1e6;
    p14= init_Gains(7)*1e6;
    p16= init_Gains(8)*1e6;

[f,p1,p3,p5,p7,p9,p11,p13,p15,v1,v2,v3,v4,v5,v6,v7,v8,c1,c2,c3,c4,c5,c6,c7,c8,v_e1,v_e2,v_e3,v_e4,v_e5,v_e6,v_e
7,v_e8] = Fitness_Value(p2,p4,p6,p8,p10,p12,p14,p16);

    %% Constraints Start
    %% Constraints Start
    if p1>(U*1e6)
        penalty_p1= PWP+(p1/1e6)-U;
    else
        penalty_p1=0;
    end
    if p3>(U*1e6)
        penalty_p2= PWP+(p3/1e6)-U;
    else
```

```
    penalty_p2=0;
end
if p5>(U*1e6)
    penalty_p3= PWP+(p5/1e6)-U;
else
    penalty_p3=0;
end
if p7>(U*1e6)
    penalty_p4= PWP+(p7/1e6)-U;
else
    penalty_p4=0;
end
if p9>(U*1e6)
    penalty_p5= PWP+(p9/1e6)-U;
else
    penalty_p5=0;
end
if p11>(U*1e6)
    penalty_p6= PWP+(p11/1e6)-U;
else
    penalty_p6=0;
end
if p13>(U*1e6)
    penalty_p7= PWP+(p13/1e6)-U;
else
    penalty_p7=0;
end
if p15>(U*1e6)
    penalty_p8= PWP+(p15/1e6)-U;
else
    penalty_p8=0;
end


vLim1=v1-(c1/2); vLim2=v2-(c2/2); vLim3=v3-(c3/2);
vLim4=v4-(c4/2); vLim5=v5-(c5/2); vLim6=v6-(c6/2); vLim7=v7-(c7/2); vLim8=v8-(c8/2);

veLim1=v1-v_e1; veLim2=v2-v_e2; veLim3=v3-v_e3; veLim4=v4-v_e4; veLim5=v5-v_e5; veLim6=v6-v_e6;
veLim7=v7-v_e7; veLim8=v8-v_e8;
if vLim1>0
    penalty_v1= vLim1;
else
    penalty_v1=0;
end
if vLim2>0
    penalty_v2= vLim2;
else
    penalty_v2=0;
end
if vLim3>0
    penalty_v3= vLim3;
else
    penalty_v3=0;
end
if vLim4>0
    penalty_v4= vLim4;
```

```
else
   penalty_v4=0;
end
if vLim5>0
   penalty_v5= vLim5;
else
   penalty_v5=0;
end
if vLim6>0
   penalty_v6= vLim6;
else
   penalty_v6=0;
end
if vLim7>0
   penalty_v7= vLim7;
else
   penalty_v7=0;
end
if vLim8>0
   penalty_v8= vLim8;
else
   penalty_v8=0;
end


if veLim1>0
   penalty_ve1= veLim1;
else
   penalty_ve1=0;
end
if veLim2>0
   penalty_ve2= veLim2;
else
   penalty_ve2=0;
end
if veLim3>0
   penalty_ve3= veLim3;
else
   penalty_ve3=0;
end
if veLim4>0
   penalty_ve4= veLim4;
else
   penalty_ve4=0;
end
if veLim5>0
   penalty_ve5= veLim5;
else
   penalty_ve5=0;
end
if veLim6>0
   penalty_ve6= veLim6;
else
   penalty_ve6=0;
end
if veLim7>0
```

```
        penalty_ve7= veLim7;
    else
        penalty_ve7=0;
    end
    if veLim8>0
        penalty_ve8= veLim8;
    else
        penalty_ve8=0;
    end
    %% Constraints End

Fitness(p)=f+penalty_p1+penalty_p2+penalty_p3+penalty_p4+penalty_p5+penalty_p6+penalty_p7+penalty_p8+pe
nalty_v1+penalty_v2+penalty_v3+penalty_v4+penalty_v5+penalty_v6+penalty_v7+penalty_v8+penalty_ve1+penal
ty_ve2+penalty_ve3+penalty_ve4+penalty_ve5+penalty_ve6+penalty_ve7+penalty_ve8;

  end

  %% Combine population & mutant offsprings
  ComFitness= zeros(2*P,1);                    % Initialize storage for combined fitness
  ComGain= zeros(1,nv,2*P);                    % Initialize storage for combined gains
  ComFitness(1:P)= pFitness(1:P);              % Copy parent fitness to combined fitness
  ComFitness(P+1:2*P)= Fitness(1:P);           % Copy mutant fitness to combined fitness
  ComGain(:,:,1:P)= Gain(:,:,1:P);             % Copy parent gains to combined gains
  ComGain(:,:,1+P:2*P)= GainM(:,:,1:P);        % Copy mutant gains to combined gains
  [sortComFitness,ComFitnessIndex]= sort(ComFitness);
  Fitness(1:P)= ComFitness(ComFitnessIndex(1:P));      % Redefine Fitness as best P values of combined fitness
  Gain(:,:,1:P)= ComGain(:,:,ComFitnessIndex(1:P));

  %Always isolating the overall best generation
  BestFit(it)= Fitness(1)
  Best_Gain= 1e6.*Gain(:,:,1);

end
p2= init_Gains(1)*1e6;
      p4= init_Gains(2)*1e6;
      p6= init_Gains(3)*1e6;
      p8= init_Gains(4)*1e6;
      p10= init_Gains(5)*1e6;
      p12= init_Gains(6)*1e6;
      p14= init_Gains(7)*1e6;
      p16= init_Gains(8)*1e6;

count=1:MaxIt;
plot(count,BestFit)
xlabel('Number of iteration');
ylabel('fuel consumption (kg/s)');
[f,p1,p3,p5,p7,p9,p11,p13,p15,v1,v2,v3,v4,v5,v6,v7,v8,c1,c2,c3,c4,c5,c6,c7,c8,v_e1,v_e2,v_e3,v_e4,v_e5,v_e6,v_e
7,v_e8] = Fitness_Value(p2,p4,p6,p8,p10,p12,p14,p16);
```

MATLAB code for multi-delivery points NG pipeline (File name: Fitness_value):

```
function[f,p1,p3,p5,p7,p9,p11,p12,p13,p15,p16,p18,p20,p21,p22,v1,v2,v3,v4,v5,v6,v7,v8,v9,v10,v11,v12,v13,v14,c
1,c2,c3,c4,c5,c6,c7,c8,c9,c10,c11,c12,c13,c14,v_e1,v_e2,v_e3,v_e4,v_e5,v_e6,v_e7,v_e8,v_e9,v_e10,v_e11,v_e12,
v_e13,v_e14] = Fitness_Value(p2,p4,p6,p8,p10,p14,p17,p19,p23)


%Input parameters
R=8.314;                % J/mol.K
T=283;                  % Kelvine
M=16.5*0.001;           % pure NG kg/mol
roughness=5*10^-5;      % (meter), Pipeline material roughness (50μm)

%% Pipeline equations
    % 1st pipeline
    D1=0.9;             % Diameter (m)
    L1=100000;
    m1=160+mf-mf1;      % constant mass flow rate (kg/s)
    f1=(-2*log10((roughness/D1)/3.71))^-2;  %Darcy friction factor
    e1 =@(p1) ((p2^2-p1^2)-((32*m1^2*Z1*R*T)/(3.1416^2*D1^4*M))*log(p2/p1)+((16*f1*Z1*R*T *m1^2*
L1)/(3.1416^2*D1^5*M)));
    p1 = fsolve(e1, p2);

    % 2nd pipeline
    D2=0.9;
    L2=100000;
    m2=1 60+mf-mf1-mf2;
    f2=(-2*log10((roughness/D2)/3.71))^-2;
    e2 =@(p3) ((p4^2-p3^2)-((32*m2^2*Z2*R*T)/(3.1416^2*D2^4*M))*log(p4/p3)+((16*f2*Z2*R*T*m2^2
*L2)/(3.1416^2*D2^5*M)));
    p3 = fsolve(e2, p4);

    % 3rd pipeline
    D3=0.9;
    L3=100000;
    m3=160+ mf-mf1-mf2-mf3;
    f3=(-2*log10((roughness/D3)/3.71))^-2;
    e3 =@(p5) ((p6^2-p5^2)-((32*m3^2*Z3*R*T)/(3.1416^2*D3^4*M))*log(p6/p5)+((16*f3*Z3*R*T*m3^2
*L3)/(3.1416^2*D3^5*M)));
    p5 = fsolve(e3, p6);

    % 4th pipeline junction
    D4=0.9;
    L4=100000;
    m4=160+ mf-mf1-mf2-mf3-mf4;
    f4=(-2*log10((roughness/D4)/3.71))^-2;
    e4 =@(p7) ((p8^2-p7^2)-
((32*m4^2*Z4*R*T)/(3.1416^2*D4^4*M))*log(p8/p7)+((16*f4*Z4*R*T*m4^2*L4)/(3.1416^2*D4^5*M)));
    p7 = fsolve(e4, p8);

    % 5th pipeline junction
    D5=0.76;
    L5=100000;
    m5=128.86+ mf-mf1-mf2-mf3-mf4-mf5;
    f5=(-2*log10((roughness/D5)/3.71))^-2;
    e5 =@(p9) ((p10^2-p9^2)-((32*m5^2*Z5*R*T)/(3.1416^2*D5^4*M))*log(p10/p9)+((16*f5*Z5*R*T*m5^2
*L5)/(3.1416^2*D5^5*M)));
    p9 = fsolve(e5, p10);
```

```
D6=0.254;
L6=30000;
m6=16;
f6=(-2*log10((roughness/D6)/3.71))^-2;
e6 =@(p11) ((p11^2-p9^2)-((32*m6^2*Z6*R*T)/(3.1416^2*D6^4*M))*log(p11/p9)+((16*f6*Z6*R*T*m6^2
*L6)/(3.1416^2*D6^5*M)));
p11 = fsolve(e6, p9);


D7=0.254;
L7=40000;
m7=16;
f7=(-2*log10((roughness/D7)/3.71))^-2;
e7 =@(p12) ((p12^2-p9^2)-((32*m7^2*Z7*R*T)/(3.1416^2*D7^4*M))*log(p12/p9)+((16*f7*Z7*R*T*m7^2
*L7)/(3.1416^2*D7^5*M)));
p12 = fsolve(e7, p9);


% 6th pipeline junction
D8=0.66;
L8=100000;
m8=96.797++ mf-mf1-mf2-mf3-mf4-mf5;-mf6
f8=(-2*log10((roughness/D8)/3.71))^-2;
e8 =@(p13) ((p14^2-p13^2)-((32*m8^2*Z8*R*T)/(3.1416^2*D8^4*M))*log(p14/p13)+((16*f8*Z8*R*T
*m8^2*L8)/(3.1416^2*D8^5*M)));
p13 = fsolve(e8, p14);


D9=0.254;
L9=20000;
m9=32;
f9=(-2*log10((roughness/D9)/3.71))^-2;
e9 =@(p15) ((p15^2-p13^2)-
((32*m9^2*Z9*R*T)/(3.1416^2*D9^4*M))*log(p15/p13)+((16*f9*Z9*R*T*m9^2*L9)/(3.1416^2*D9^5*M)));
p15 = fsolve(e9, p13);

% 7th Pipeline
D10=0.66;
L10=100000;
m10=96.521+ mf-mf1-mf2-mf3-mf4-mf5-mf6-mf7;
f10=(-2*log10((roughness/D10)/3.71))^-2;
e10 =@(p16) ((p17^2-p16^2)-((32*m10^2*Z10*R*T)/(3.1416^2*D10^4*M))*log(p17/p16)+((16*f10
*Z10*R*T*m10^2*L10)/(3.1416^2*D10^5*M)));
p16 = fsolve(e10, p17);


% Last node pipeline junction
D11=0.3;
L11=10000;
m11=32;
f11=(-2*log10((roughness/D11)/3.71))^-2;
e11 =@(p18) ((p19^2-p18^2)-((32*m11^2*Z11*R*T)/(3.1416^2*D11^4*M))*log(p19/p18)+((16*f11*Z11
*R*T*m11^2*L11)/(3.1416^2*D11^5*M)));
p18 = fsolve(e11, p19);
```

```
D12=0.3;
L12=15000;
m12=32;
f12=(-2*log10((roughness/D12)/3.71))^-2;
e12 =@(p20) ((p20^2-p18^2)-((32*m12^2*Z12*R*T)/(3.1416^2*D12^4*M))*log(p20/p18)+((16*f12*Z12
*R*T*m12^2*L12)/(3.1416^2*D12^5*M)));
p20 = fsolve(e12, p18);


D13=0.3;
L13=20000;
m13=32;
f13=(-2*log10((roughness/D13)/3.71))^-2;
e13 =@(p21) ((p21^2-p18^2)-((32*m13^2*Z13*R*T)/(3.1416^2*D13^4*M))*log(p21/p18)+((16*f13*
Z13*R*T*m13^2*L13)/(3.1416^2*D13^5*M)));
p21 = fsolve(e13, p18);

%% Compressibility Calculation
T_c = 190.9;                % critical temperature of pure natural gas (K)
T_r= (T/T_c);               % reduced temperature
Z_ini=0.9;                  % Initial compressibility factor (assumed 0.9)

P_1 = (p1+p2)/2;            % Pipeline average Pressure (Pa)
P_2 = (p3+p4)/2;
P_3 = (p5+p6)/2;
P_4 = (p7+p8)/2;            % Pipeline average Pressure (Pa)
P_5 = (p9+p11)/2;
P_6 = (p9+p12)/2;
P_7 = (p9+p10)/2;           % Pipeline average Pressure (Pa)
P_8 = (p13+p14)/2;
P_9 = (p13+p15)/2;
P_10 = (p16+p17)/2;         % Pipeline average Pressure (Pa)
P_11 = (p18+p19)/2;
P_12 = (p18+p20)/2;
P_13 = (p18+p21)/2;
P_14 = (p22+p23)/2;

P_c = 4.58*10^6;            % Critical pressure for natural gas (Pa)
Pr_1=P_1/P_c;               % Reduced pressure
Pr_2=P_2/P_c;
Pr_3=P_3/P_c;
Pr_4=P_4/P_c;
Pr_5=P_5/P_c;
Pr_6=P_6/P_c;
Pr_7=P_7/P_c;               % Reduced pressure
Pr_8=P_8/P_c;
Pr_9=P_9/P_c;
Pr_10=P_10/P_c;
Pr_11=P_11/P_c;
Pr_12=P_12/P_c;
Pr_13=P_13/P_c;
Pr_14=P_14/P_c;


row_r_1 = 0.27*(Pr_1/(Z_ini*T_r));
```

```
row_r_2 = 0.27*(Pr_2/(Z_ini*T_r));
row_r_3 = 0.27*(Pr_3/(Z_ini*T_r));
row_r_4 = 0.27*(Pr_4/(Z_ini*T_r));
row_r_5 = 0.27*(Pr_5/(Z_ini*T_r));
row_r_6 = 0.27*(Pr_6/(Z_ini*T_r));
row_r_7 = 0.27*(Pr_7/(Z_ini*T_r));
row_r_8 = 0.27*(Pr_8/(Z_ini*T_r));
row_r_9 = 0.27*(Pr_9/(Z_ini*T_r));
row_r_10 = 0.27*(Pr_10/(Z_ini*T_r));
row_r_11 = 0.27*(Pr_11/(Z_ini*T_r));
row_r_12 = 0.27*(Pr_12/(Z_ini*T_r));
row_r_13 = 0.27*(Pr_13/(Z_ini*T_r));
row_r_14 = 0.27*(Pr_14/(Z_ini*T_r));


Z_1= 1+(0.31506-(1.0467/T_r)-(0.5783/T_r^3))*row_r_1 + (0.5353-(0.6127/T_r)-(0.6185/T_r^3))*row_r_1^2;
Z_2= 1+(0.31506-(1.0467/T_r)-(0.5783/T_r^3))*row_r_2 + (0.5353-(0.6127/T_r)-(0.6185/T_r^3))*row_r_2^2;
Z_3= 1+(0.31506-(1.0467/T_r)-(0.5783/T_r^3))*row_r_3 + (0.5353-(0.6127/T_r)-(0.6185/T_r^3))*row_r_3^2;
Z_4= 1+(0.31506-(1.0467/T_r)-(0.5783/T_r^3))*row_r_4 + (0.5353-(0.6127/T_r)-(0.6185/T_r^3))*row_r_4^2;
Z_5= 1+(0.31506-(1.0467/T_r)-(0.5783/T_r^3))*row_r_5 + (0.5353-(0.6127/T_r)-(0.6185/T_r^3))*row_r_5^2;
Z_6= 1+(0.31506-(1.0467/T_r)-(0.5783/T_r^3))*row_r_6 + (0.5353-(0.6127/T_r)-(0.6185/T_r^3))*row_r_6^2;
Z_7= 1+(0.31506-(1.0467/T_r)-(0.5783/T_r^3))*row_r_7 + (0.5353-(0.6127/T_r)-(0.6185/T_r^3))*row_r_7^2;
Z_8= 1+(0.31506-(1.0467/T_r)-(0.5783/T_r^3))*row_r_8 + (0.5353-(0.6127/T_r)-(0.6185/T_r^3))*row_r_8^2;
Z_9= 1+(0.31506-(1.0467/T_r)-(0.5783/T_r^3))*row_r_9 + (0.5353-(0.6127/T_r)-(0.6185/T_r^3))*row_r_9^2;
Z_10= 1+(0.31506-(1.0467/T_r)-(0.5783/T_r^3))*row_r_10 + (0.5353-(0.6127/T_r)-(0.6185/T_r^3))*row_r_10^2;
Z_11= 1+(0.31506-(1.0467/T_r)-(0.5783/T_r^3))*row_r_11 + (0.5353-(0.6127/T_r)-(0.6185/T_r^3))*row_r_11^2;
Z_12= 1+(0.31506-(1.0467/T_r)-(0.5783/T_r^3))*row_r_12 + (0.5353-(0.6127/T_r)-(0.6185/T_r^3))*row_r_12^2;
Z_13= 1+(0.31506-(1.0467/T_r)-(0.5783/T_r^3))*row_r_13 + (0.5353-(0.6127/T_r)-(0.6185/T_r^3))*row_r_13^2;
Z_14= 1+(0.31506-(1.0467/T_r)-(0.5783/T_r^3))*row_r_14 + (0.5353-(0.6127/T_r)-(0.6185/T_r^3))*row_r_14^2;

%% Denisty Equations
density_1= (P_1*M)/(Z_1*R*T);          % P_1 means average pressure for pipeline 1
density_2= (P_2*M)/(Z_2*R*T);
density_3= (P_3*M)/(Z_3*R*T);
density_4= (P_4*M)/(Z_4*R*T);
density_5= (P_5*M)/(Z_5*R*T);
density_6= (P_6*M)/(Z_6*R*T);
density_7= (P_7*M)/(Z_7*R*T);
density_8= (P_8*M)/(Z_8*R*T);
density_9= (P_9*M)/(Z_9*R*T);
density_10= (P_10*M)/(Z_10*R*T);
density_11= (P_11*M)/(Z_11*R*T);
density_12= (P_12*M)/(Z_12*R*T);
density_13= (P_13*M)/(Z_13*R*T);
density_14= (P_14*M)/(Z_14*R*T);


% volumetric flow rate (m3/sec)
q1 = m1/density_1;                    % constant mass flow rate (kg/sec) is converted to volumetric flow rate (m3/s)
q2 = m2/density_2;
q3 = m3/density_3;
q4 = m4/density_4;
q5 = m5/density_5;
q6 = m6/density_6;
q7 = m7/density_7;
q8 = m8/density_8;
```

```
q9 = m9/density_9;
q10 = m10/density_10;
q11 = m11/density_11;
q12 = m12/density_12;
q13 = m13/density_13;
q14 = m14/density_14;


% Velocity of Gas (m/s)
v1 = q1/((3.1416*D1^2)/4);      % velocity (m/s) of flowing gas calculated from volumetric flow rate (m3/s) and
Area
v2 = q2/((3.1416*D2^2)/4);
v3 = q3/((3.1416*D3^2)/4);
v4 = q4/((3.1416*D4^2)/4);
v5 = q5/((3.1416*D5^2)/4);
v6 = q6/((3.1416*D6^2)/4);
v7 = q7/((3.1416*D7^2)/4);
v8 = q8/((3.1416*D8^2)/4);
v9 = q9/((3.1416*D9^2)/4);
v10 = q10/((3.1416*D10^2)/4);
v11 = q11/((3.1416*D11^2)/4);
v12 = q12/((3.1416*D12^2)/4);
v13 = q13/((3.1416*D13^2)/4);
v14 = q14/((3.1416*D14^2)/4);

%% Inequality constraint

% Critical velocity (m/s)
k = 1.3;
c1 = sqrt(k*Z_1*R*T/M);                 % The flowing gas velocity is less than the half of critical velocity (c, (unit:
m/s)) of the gas
c2 = sqrt(k*Z_2*R*T/M);
c3 = sqrt(k*Z_3*R*T/M);
c4 = sqrt(k*Z_4*R*T/M);
c5 = sqrt(k*Z_5*R*T/M);
c6 = sqrt(k*Z_6*R*T/M);
c7 = sqrt(k*Z_7*R*T/M);
c8 = sqrt(k*Z_8*R*T/M);
c9 = sqrt(k*Z_9*R*T/M);
c10 = sqrt(k*Z_10*R*T/M);
c11 = sqrt(k*Z_11*R*T/M);
c12 = sqrt(k*Z_12*R*T/M);
c13 = sqrt(k*Z_13*R*T/M);
c14 = sqrt(k*Z_14*R*T/M);

% Erosional velocity (m/s): To avoid erosion of the inside surface of the tubes, elbows and other joints.
v_e1 = 122*sqrt((Z_1*R*T)/(P_1*M));
v_e2 = 122*sqrt((Z_2*R*T)/(P_2*M));
v_e3 = 122*sqrt((Z_3*R*T)/(P_3*M));
v_e4 = 122*sqrt((Z_4*R*T)/(P_4*M));
v_e5 = 122*sqrt((Z_5*R*T)/(P_5*M));
v_e6 = 122*sqrt((Z_6*R*T)/(P_6*M));
v_e7 = 122*sqrt((Z_7*R*T)/(P_7*M));
v_e8 = 122*sqrt((Z_8*R*T)/(P_8*M));
v_e9 = 122*sqrt((Z_9*R*T)/(P_9*M));
v_e10 = 122*sqrt((Z_10*R*T)/(P_10*M));
```

```
v_e11 = 122*sqrt((Z_11*R*T)/(P_11*M));
v_e12 = 122*sqrt((Z_12*R*T)/(P_12*M));
v_e13 = 122*sqrt((Z_13*R*T)/(P_13*M));
v_e14 = 122*sqrt((Z_14*R*T)/(P_14*M));
%% Compressor isentropic head (kj/kg)
k=1.3;
p0=1.379e+6;                % Assumed gas pressure from well is 200psi (1.379 MPa)

h1 =(Z_1*R*T/M)*(k/(k-1))*(((p1/p0)^((k-1)/k))-1)/1000;
h2 =(Z_2*R*T/M)*(k/(k-1))*(((p3/p2)^((k-1)/k))-1)/1000;
h3 =(Z_3*R*T/M)*(k/(k-1))*(((p5/p4)^((k-1)/k))-1)/1000;
h4 =(Z_4*R*T/M)*(k/(k-1))*(((p7/p6)^((k-1)/k))-1)/1000;
h5 =(Z_5*R*T/M)*(k/(k-1))*(((p9/p8)^((k-1)/k))-1)/1000;
h6 =(Z_6*R*T/M)*(k/(k-1))*(((p13/p10)^((k-1)/k))-1)/1000;
h7 =(Z_7*R*T/M)*(k/(k-1))*(((p16/p14)^((k-1)/k))-1)/1000;
h8 =(Z_8*R*T/M)*(k/(k-1))*(((p18/p17)^((k-1)/k))-1)/1000;

%% Fuel consumption Equation
eff_i=0.72;
eff_m=0.9;
eff_d=0.35;
LHV=48830;
m0=165.3+mf;

mf1=((m0*h1)/(eff_i*eff_m*eff_d*LHV));
mf2=((m1*h2)/(eff_i*eff_m*eff_d*LHV));
mf3=((m2*h3)/(eff_i*eff_m*eff_d*LHV));
mf4=((m3*h4)/(eff_i*eff_m*eff_d*LHV));
mf5=((m4*h5)/(eff_i*eff_m*eff_d*LHV));
mf6=((m5*h6)/(eff_i*eff_m*eff_d*LHV));
mf7=((m8*h7)/(eff_i*eff_m*eff_d*LHV));
mf8=((m10*h8)/(eff_i*eff_m*eff_d*LHV));

mf = (mf1 + mf2 + mf3+ mf4 + mf5 + mf6+ mf7 + mf8); % Total fuel consumption for all the compressors (kg/s)

%% Objective function

f = (mf);  % The objective function is to minimize the total fuel consumption of the compressor
end
```

Genetic Algorithm for multi-delivery points NG pipeline:

```
clc
clear

%% GA Parameters
% Maximum Allowable operating pressure (Pa): The maximum pressure that a pipeline can
tolerate
D=0.9;
f_F = 0.4;                                  % design factor
f_E = 0.8;                                  % seam joint factor is between 1 and 0.6
for the most commonly used material types
f_T = 1;                                    % Temperature factor,f_T, is equal to 1
for the gas temperature below 393K
```

```
SMYS = 2e+8;                                % specified minimum yield strength
(SMYS) of pipe material.
t = 52*10^-3*D + 989*10^-5;                 % meter if other units are in meter
MAOP = SMYS * ((2*t)/(D-t)) * f_F * f_E * f_T;

U= MAOP; L= 1.38;        % Max. and min. value of controller parameters
P= 200;                  % Population size
k= 2;                   % Tournament competitor size
MaxIt=500;              % Maximum Number of iterations
Pc= 0.8;                % Crossover proability
Pm= 0.2;                % Mutation probability
muC= 20;                % Distribution index for crossover
muM= 20;                % Distribution index for mutation
% Fbest= zeros(MaxIt,1);  % Initialize storage for performance index
Fitness= zeros(P,1);    %Initialize fitness storage
nv= 9;                  %No. of variables
PWP= 1000;                % Penalty weight for pressure p1, p3, p5
Gain= ones(1,nv,P);    %Initialize gain storage

%% Initial fitness evaluation for random population

% Initialization of random population
%In general, you can generate N random numbers in the interval (a,b) with the formula
r = a + (b-a).*rand(N,1).
InitPop= L+(U-L).*rand(1,nv,P);  %Initialization of population

for p= 1:P  %Run for each population
    init_Gains= InitPop(:,:,p);
    p2= init_Gains(1)*1e6;
    p4= init_Gains(2)*1e6;
    p6= init_Gains(3)*1e6;
    p8= init_Gains(4)*1e6;
    p10= init_Gains(5)*1e6;
    p14= init_Gains(6)*1e6;
    p17= init_Gains(7)*1e6;
    p19= init_Gains(8)*1e6;
    p23= init_Gains(9)*1e6;

[f,p1,p3,p5,p7,p9,p11,p12,p13,p15,p16,p18,p20,p21,p22,v1,v2,v3,v4,v5,v6,v7,v8,v9,v10,
v11,v12,v13,v14,c1,c2,c3,c4,c5,c6,c7,c8,c9,c10,c11,c12,c13,c14,v_e1,v_e2,v_e3,v_e4,v_
e5,v_e6,v_e7,v_e8,v_e9,v_e10,v_e11,v_e12,v_e13,v_e14] =
Fitness_Value(p2,p4,p6,p8,p10,p14,p17,p19,p23);

    %% Constraints Start
    if p1>(U*1e6)
        penalty_p1= PWP+(p1/1e6)-U;
    else
        penalty_p1=0;
    end
    if p3>(U*1e6)
        penalty_p2= PWP+(p3/1e6)-U;
    else
        penalty_p2=0;
    end
    if p5>(U*1e6)
```

```
    penalty_p3= PWP+(p5/1e6)-U;
else
    penalty_p3=0;
end
if p7>(U*1e6)
    penalty_p4= PWP+(p7/1e6)-U;
else
    penalty_p4=0;
end
if p9>(U*1e6)
    penalty_p5= PWP+(p9/1e6)-U;
else
    penalty_p5=0;
end
if p11>(U*1e6)
    penalty_p6= PWP+(p11/1e6)-U;
else
    penalty_p6=0;
end
if p12>(U*1e6)
    penalty_p7= PWP+(p12/1e6)-U;
else
    penalty_p7=0;
end
if p13>(U*1e6)
    penalty_p8= PWP+(p13/1e6)-U;
else
    penalty_p8=0;
end
if p15>(U*1e6)
    penalty_p9= PWP+(p15/1e6)-U;
else
    penalty_p9=0;
end
if p16>(U*1e6)
    penalty_p10= PWP+(p16/1e6)-U;
else
    penalty_p10=0;
end
if p18>(U*1e6)
    penalty_p11= PWP+(p18/1e6)-U;
else
    penalty_p11=0;
end
if p20>(U*1e6)
    penalty_p12= PWP+(p20/1e6)-U;
else
    penalty_p12=0;
end
if p21>(U*1e6)
    penalty_p13= PWP+(p21/1e6)-U;
else
    penalty_p13=0;
end
if p22>(U*1e6)
```

```
        penalty_p14= PWP+(p22/1e6)-U;
    else
        penalty_p14=0;
    end


    vLim1=v1-(c1/2); vLim2=v2-(c2/2); vLim3=v3-(c3/2);
    vLim4=v4-(c4/2); vLim5=v5-(c5/2); vLim6=v6-(c6/2);
    vLim7=v7-(c7/2); vLim8=v8-(c8/2); vLim9=v9-(c9/2);
    vLim10=v10-(c10/2); vLim11=v11-(c11/2); vLim12=v12-(c12/2); vLim13=v13-(c13/2);
vLim14=v14-(c14/2);

veLim1=v1-v_e1; veLim2=v2-v_e2; veLim3=v3-v_e3; veLim4=v4-v_e4; veLim5=v5-v_e5;
veLim6=v6-v_e6;
veLim7=v7-v_e7; veLim8=v8-v_e8; veLim9=v9-v_e9; veLim10=v10-v_e10; veLim11=v11-v_e11;
veLim12=v12-v_e12; veLim13=v13-v_e13; veLim14=v14-v_e14;

    if vLim1>0
        penalty_v1= vLim1;
    else
        penalty_v1=0;
    end
    if vLim2>0
        penalty_v2= vLim2;
    else
        penalty_v2=0;
    end
    if vLim3>0
        penalty_v3= vLim3;
    else
        penalty_v3=0;
    end
    if vLim4>0
        penalty_v4= vLim4;
    else
        penalty_v4=0;
    end
    if vLim5>0
        penalty_v5= vLim5;
    else
        penalty_v5=0;
    end
    if vLim6>0
        penalty_v6= vLim6;
    else
        penalty_v6=0;
    end

    if vLim7>0
        penalty_v7= vLim7;
    else
        penalty_v7=0;
    end
    if vLim8>0
        penalty_v8= vLim8;
```

```
else
    penalty_v8=0;
end
if vLim9>0
    penalty_v9= vLim9;
else
    penalty_v9=0;
end
if vLim10>0
    penalty_v10= vLim10;
else
    penalty_v10=0;
end
if vLim11>0
    penalty_v11= vLim11;
else
    penalty_v11=0;
end
if vLim12>0
    penalty_v12= vLim12;
else
    penalty_v12=0;
end
if vLim13>0
    penalty_v13= vLim13;
else
    penalty_v13=0;
end
if vLim14>0
    penalty_v14= vLim14;
else
    penalty_v14=0;
end



if veLim1>0
    penalty_ve1= veLim1;
else
    penalty_ve1=0;
end
if veLim2>0
    penalty_ve2= veLim2;
else
    penalty_ve2=0;
end
if veLim3>0
    penalty_ve3= veLim3;
else
    penalty_ve3=0;
end
if veLim4>0
    penalty_ve4= veLim4;
else
    penalty_ve4=0;
```

```
    end
    if veLim5>0
        penalty_ve5= veLim5;
    else
        penalty_ve5=0;
    end
    if veLim6>0
        penalty_ve6= veLim6;
    else
        penalty_ve6=0;
    end
    if veLim7>0
        penalty_ve7= veLim7;
    else
        penalty_ve7=0;
    end
    if veLim8>0
        penalty_ve8= veLim8;
    else
        penalty_ve8=0;
    end
    if veLim9>0
        penalty_ve9= veLim9;
    else
        penalty_ve9=0;
    end
    if veLim10>0
        penalty_ve10= veLim10;
    else
        penalty_ve10=0;
    end
    if veLim11>0
        penalty_ve11= veLim11;
    else
        penalty_ve11=0;
    end
    if veLim12>0
        penalty_ve12= veLim12;
    else
        penalty_ve12=0;
    end
    if veLim13>0
        penalty_ve13= veLim13;
    else
        penalty_ve13=0;
    end
    if veLim14>0
        penalty_ve14= veLim14;
    else
        penalty_ve14=0;
    end
    %% Constraints End

Fitness(p)=f+penalty_p1+penalty_p2+penalty_p3+penalty_p4+penalty_p5+penalty_p6+penalt
y_p7+penalty_p8+penalty_p9+penalty_p10+penalty_p11+penalty_p12+penalty_p13+penalty_p1
```

```
4+penalty_v1+penalty_v2+penalty_v3+penalty_v4+penalty_v5+penalty_v6+penalty_v7+penalt
y_v8+penalty_v9+penalty_v10+penalty_v11+penalty_v12+penalty_v13+penalty_v14+penalty_v
e1+penalty_ve2+penalty_ve3+penalty_ve4+penalty_ve5+penalty_ve6+penalty_ve7+penalty_ve
8+penalty_ve9+penalty_ve10+penalty_ve11+penalty_ve12+penalty_ve13++penalty_ve14;
    Gain(:,:,p)= init_Gains;

end

%% Main loop of GA

BestFit= zeros(MaxIt,1);
for it= 1:MaxIt
    pFitness= Fitness;      %Define fitness as parent fitness

    %% Tournament selection (Binary)

    GainS= Gain; % Initialize selected gains
    R= randperm(P); % Randomize population sequence
    for p= 1:P-1    % Each population perticipates in tournament selection twice
except 1 & P
        T= [Fitness(R(p)) Fitness(R(p+1))];
        [sortT, Tindex]= sort(T);
        if Tindex== [1 2]
            GainS(:,:,R(p+1))=Gain(:,:,R(p));
        else
            GainS(:,:,R(p))=Gain(:,:,R(p+1));
        end
    end
    if Fitness(R(P)) <= Fitness(R(1)) % Comparison between population 1 & P left
        GainS(:,:,R(1))=Gain(:,:,R(P));
    else
        GainS(:,:,R(P))=Gain(:,:,R(1));
    end

    %% SBX Crossover

    GainC= GainS;        % Initialize offsprings
    Rc= randperm(P); % Randomize parents for crossover
    beta= zeros(1,nv);
    for p=1:2:P
        if rand < Pc
            for j= 1:nv %beta formation
                u=rand;
                if u<=0.5
                    beta(1,j)= (2*u)^(1/(muC+1));
                else
                    beta(1,j)= (1/(2*(1-u)))^(1/(muC+1));
                end
            end
            GainC(:,:,Rc(p))= 0.5
.*(((ones(1,nv)+beta).*GainS(:,:,Rc(p)))+((ones(1,nv)-beta).*GainS(:,:,Rc(p+1))));
            GainC(:,:,Rc(p+1))= 0.5 .*(((ones(1,nv)-
beta).*GainS(:,:,Rc(p)))+((ones(1,nv)+beta).*GainS(:,:,Rc(p+1))));
        end
    end
```

```
    %% Mutation (Polynomial)

    GainM= GainC;  % Initialize mutants
    del= zeros(1,nv);
    for p=1:P

        if rand < Pm
            for j= 1:nv %del2 formation
                r=rand;
                if r<0.5
                    del(1,j)= ((2*r)^(1/(muM+1)))-1;
                else
                    del(1,j)= 1-(2*(1-r))^(1/(muM+1));
                end
            end

            GainM(:,:,p)= GainC(:,:,p)+(U-L).*del;
        end
    end

    %% Do corner bounding here
    GainM= min(GainM,U);
    GainM= max(GainM,L);

    %% Function Evaluation
    b= zeros(1,nv,P);
    for p= 1:P  %Run for each population

        p2= init_Gains(1)*1e6;
        p4= init_Gains(2)*1e6;
        p6= init_Gains(3)*1e6;
        p8= init_Gains(4)*1e6;
        p10= init_Gains(5)*1e6;
        p14= init_Gains(6)*1e6;
        p17= init_Gains(7)*1e6;
        p19= init_Gains(8)*1e6;
        p23= init_Gains(9)*1e6;

[f,p1,p3,p5,p7,p9,p11,p12,p13,p15,p16,p18,p20,p21,p22,v1,v2,v3,v4,v5,v6,v7,v8,v9,v10,
v11,v12,v13,v14,c1,c2,c3,c4,c5,c6,c7,c8,c9,c10,c11,c12,c13,c14,v_e1,v_e2,v_e3,v_e4,v_
e5,v_e6,v_e7,v_e8,v_e9,v_e10,v_e11,v_e12,v_e13,v_e14] =
Fitness_Value(p2,p4,p6,p8,p10,p14,p17,p19,p23);

        %% Constraints Start
        if p1>(U*1e6)
            penalty_p1= PWP+(p1/1e6)-U;
        else
            penalty_p1=0;
        end
        if p3>(U*1e6)
            penalty_p2= PWP+(p3/1e6)-U;
        else
            penalty_p2=0;
        end
```

```
if p5>(U*1e6)
    penalty_p3= PWP+(p5/1e6)-U;
else
    penalty_p3=0;
end
if p7>(U*1e6)
    penalty_p4= PWP+(p7/1e6)-U;
else
    penalty_p4=0;
end
if p9>(U*1e6)
    penalty_p5= PWP+(p9/1e6)-U;
else
    penalty_p5=0;
end
if p11>(U*1e6)
    penalty_p6= PWP+(p11/1e6)-U;
else
    penalty_p6=0;
end
if p12>(U*1e6)
    penalty_p7= PWP+(p12/1e6)-U;
else
    penalty_p7=0;
end
if p13>(U*1e6)
    penalty_p8= PWP+(p13/1e6)-U;
else
    penalty_p8=0;
end
if p15>(U*1e6)
    penalty_p9= PWP+(p15/1e6)-U;
else
    penalty_p9=0;
end
if p16>(U*1e6)
    penalty_p10= PWP+(p16/1e6)-U;
else
    penalty_p10=0;
end
if p18>(U*1e6)
    penalty_p11= PWP+(p18/1e6)-U;
else
    penalty_p11=0;
end
if p20>(U*1e6)
    penalty_p12= PWP+(p20/1e6)-U;
else
    penalty_p12=0;
end
if p21>(U*1e6)
    penalty_p13= PWP+(p21/1e6)-U;
else
    penalty_p13=0;
end
```

```
        if p22>(U*1e6)
            penalty_p14= PWP+(p22/1e6)-U;
        else
            penalty_p14=0;
        end


        vLim1=v1-(c1/2); vLim2=v2-(c2/2); vLim3=v3-(c3/2);
        vLim4=v4-(c4/2); vLim5=v5-(c5/2); vLim6=v6-(c6/2);
        vLim7=v7-(c7/2); vLim8=v8-(c8/2); vLim9=v9-(c9/2);
        vLim10=v10-(c10/2); vLim11=v11-(c11/2); vLim12=v12-(c12/2); vLim13=v13-
(c13/2); vLim14=v14-(c14/2);

        veLim1=v1-v_e1; veLim2=v2-v_e2; veLim3=v3-v_e3; veLim4=v4-v_e4; veLim5=v5-
v_e5; veLim6=v6-v_e6;
        veLim7=v7-v_e7; veLim8=v8-v_e8; veLim9=v9-v_e9; veLim10=v10-v_e10;
veLim11=v11-v_e11; veLim12=v12-v_e12; veLim13=v13-v_e13; veLim14=v14-v_e14;

        if vLim1>0
            penalty_v1= vLim1;
        else
            penalty_v1=0;
        end
        if vLim2>0
            penalty_v2= vLim2;
        else
            penalty_v2=0;
        end
        if vLim3>0
            penalty_v3= vLim3;
        else
            penalty_v3=0;
        end
        if vLim4>0
            penalty_v4= vLim4;
        else
            penalty_v4=0;
        end
        if vLim5>0
            penalty_v5= vLim5;
        else
            penalty_v5=0;
        end
        if vLim6>0
            penalty_v6= vLim6;
        else
            penalty_v6=0;
        end

        if vLim7>0
            penalty_v7= vLim7;
        else
            penalty_v7=0;
        end
        if vLim8>0
```

```
    penalty_v8= vLim8;
else
    penalty_v8=0;
end
if vLim9>0
    penalty_v9= vLim9;
else
    penalty_v9=0;
end
if vLim10>0
    penalty_v10= vLim10;
else
    penalty_v10=0;
end
if vLim11>0
    penalty_v11= vLim11;
else
    penalty_v11=0;
end
if vLim12>0
    penalty_v12= vLim12;
else
    penalty_v12=0;
end
if vLim13>0
    penalty_v13= vLim13;
else
    penalty_v13=0;
end
if vLim14>0
    penalty_v14= vLim14;
else
    penalty_v14=0;
end



if veLim1>0
    penalty_ve1= veLim1;
else
    penalty_ve1=0;
end
if veLim2>0
    penalty_ve2= veLim2;
else
    penalty_ve2=0;
end
if veLim3>0
    penalty_ve3= veLim3;
else
    penalty_ve3=0;
end
if veLim4>0
    penalty_ve4= veLim4;
else
```

```
        penalty_ve4=0;
    end
    if veLim5>0
        penalty_ve5= veLim5;
    else
        penalty_ve5=0;
    end
    if veLim6>0
        penalty_ve6= veLim6;
    else
        penalty_ve6=0;
    end
    if veLim7>0
        penalty_ve7= veLim7;
    else
        penalty_ve7=0;
    end
    if veLim8>0
        penalty_ve8= veLim8;
    else
        penalty_ve8=0;
    end
    if veLim9>0
        penalty_ve9= veLim9;
    else
        penalty_ve9=0;
    end
    if veLim10>0
        penalty_ve10= veLim10;
    else
        penalty_ve10=0;
    end
    if veLim11>0
        penalty_ve11= veLim11;
    else
        penalty_ve11=0;
    end
    if veLim12>0
        penalty_ve12= veLim12;
    else
        penalty_ve12=0;
    end
    if veLim13>0
        penalty_ve13= veLim13;
    else
        penalty_ve13=0;
    end
    if veLim14>0
        penalty_ve14= veLim14;
    else
        penalty_ve14=0;
    end
    %% Constraints End

Fitness(p)=f+penalty_p1+penalty_p2+penalty_p3+penalty_p4+penalty_p5+penalty_p6+penalt
```

```
y_p7+penalty_p8+penalty_p9+penalty_p10+penalty_p11+penalty_p12+penalty_p13+penalty_p1
4+penalty_v1+penalty_v2+penalty_v3+penalty_v4+penalty_v5+penalty_v6+penalty_v7+penalt
y_v8+penalty_v9+penalty_v10+penalty_v11+penalty_v12+penalty_v13+penalty_v14+penalty_v
e1+penalty_ve2+penalty_ve3+penalty_ve4+penalty_ve5+penalty_ve6+penalty_ve7+penalty_ve
8+penalty_ve9+penalty_ve10+penalty_ve11+penalty_ve12+penalty_ve13++penalty_ve14;

    end

    %% Combine population & mutant offsprings

    ComFitness= zeros(2*P,1);                                % Initialize storage for
combined fitness
    ComGain= zeros(1,nv,2*P);                                 % Initialize storage for
combined gains
    ComFitness(1:P)= pFitness(1:P);                          % Copy parent fitness to
combined fitness
    ComFitness(P+1:2*P)= Fitness(1:P);                       % Copy mutant fitness to
combined fitness
    ComGain(:,:,1:P)= Gain(:,:,1:P);                         % Copy parent gains to
combined gains
    ComGain(:,:,1+P:2*P)= GainM(:,:,1:P);                    % Copy mutant gains to
combined gains
    [sortComFitness,ComFitnessIndex]= sort(ComFitness);
    Fitness(1:P)= ComFitness(ComFitnessIndex(1:P));          % Redefine Fitness as best
P values of combined fitness
    Gain(:,:,1:P)= ComGain(:,:,ComFitnessIndex(1:P));

    %Always isolating the overall best generation
    BestFit(it)= Fitness(1)
    Best_Gain= 1e6.*Gain(:,:,1);

end
p2= init_Gains(1)*1e6;
p4= init_Gains(2)*1e6;
p6= init_Gains(3)*1e6;
p8= init_Gains(4)*1e6;
p10= init_Gains(5)*1e6;
p14= init_Gains(6)*1e6;
p17= init_Gains(7)*1e6;
p19= init_Gains(8)*1e6;
p23= init_Gains(9)*1e6;
count=1:MaxIt;

plot(count,BestFit)
xlabel('Number of iteration')
ylabel('Fuel consumption (kg/s)')
[f,p1,p3,p5,p7,p9,p11,p12,p13,p15,p16,p18,p20,p21,p22,v1,v2,v3,v4,v5,v6,v7,v8,v9,v10,
v11,v12,v13,v14,c1,c2,c3,c4,c5,c6,c7,c8,c9,c10,c11,c12,c13,c14,v_e1,v_e2,v_e3,v_e4,v_
e5,v_e6,v_e7,v_e8,v_e9,v_e10,v_e11,v_e12,v_e13,v_e14] =
Fitness_Value(p2,p4,p6,p8,p10,p14,p17,p19,p23);
```

References

1. Chong, Z.R., et al., *Review of natural gas hydrates as an energy resource: Prospects and challenges.* Applied energy, 2016. **162**: p. 1633-1652.
2. Arya, A.K., et al., *Improving natural gas supply chain profitability: A multi-methods optimization study.* Energy, 2023. **282**: p. 128659.
3. Wang, G., et al., *Review on the transport capacity management of oil and gas pipeline network: Challenges and opportunities of future pipeline transport.* Energy Strategy Reviews, 2022. **43**: p. 100933.
4. Wen, K., et al., *Multi-period supply and demand balance of large-scale and complex natural gas pipeline network: Economy and environment.* Energy, 2023. **264**: p. 126104.
5. Xie, M., J. Zhao, and X. Pei, *Maintenance strategy optimization of pipeline system with multi-stage corrosion defects based on heuristically genetic algorithm.* Process Safety and Environmental Protection, 2023. **170**: p. 553-572.
6. *Natural gas consumption worldwide from 1998 to 2022*. 2024; Available from: https://www.statista.com/statistics/282717/global-natural-gas-consumption/.
7. *Assessing the future of Canada's natural gas sector under net zero emissions*. 2022; Available from: https://www.canadianenergycentre.ca/assessing-the-future-of-canadas-natural-gas-sector-under-net-zero-emissions/.
8. Jiao, K., et al., *Study on the multi-objective optimization of reliability and operating cost for natural gas pipeline network.* Oil & Gas Science and Technology–Revue d'IFP Energies nouvelles, 2021. **76**: p. 42.
9. Arya, A.K., *Optimal operation of a multi-distribution natural gas pipeline grid: an ant colony approach.* Journal of Petroleum Exploration and Production Technology, 2021. **11**(10): p. 3859-3878.
10. Zhang, B., et al., *Influence of hydrogen blending on the operation of natural gas pipeline network considering the compressor power optimization.* Applied Energy, 2024. **358**: p. 122594.
11. Liu, E.-B., et al., *Research on low carbon emission optimization operation technology of natural gas pipeline under multi-energy structure.* Petroleum Science, 2022. **19**(6): p. 3046-3058.
12. *U.S. Energy Information Administration*. Natural gas explained-Delivery and storage, June 2024; Available from: https://www.eia.gov/energyexplained/natural-gas/delivery-and-storage.php.
13. Salkuyeh, Y.K., B.A. Saville, and H.L. MacLean, *Techno-economic analysis and life cycle assessment of hydrogen production from natural gas using current and emerging technologies.* International Journal of hydrogen energy, 2017. **42**(30): p. 18894-18909.
14. Gordon, J.A., N. Balta-Ozkan, and S.A. Nabavi, *Socio-technical barriers to domestic hydrogen futures: Repurposing pipelines, policies, and public perceptions.* Applied Energy, 2023. **336**: p. 120850.
15. Brandon, N.P. and Z. Kurban, *Clean energy and the hydrogen economy.* Philosophical Transactions of the Royal Society A: Mathematical, Physical and Engineering Sciences, 2017. **375**(2098): p. 20160400.
16. Kathe, M.V., et al., *Hydrogen production from natural gas using an iron-based chemical looping technology: Thermodynamic simulations and process system analysis.* Applied energy, 2016. **165**: p. 183-201.
17. Antonini, C., et al., *Hydrogen production from natural gas and biomethane with carbon capture and storage–A techno-environmental analysis.* Sustainable Energy & Fuels, 2020. **4**(6): p. 2967-2986.

18. Timmerberg, S., M. Kaltschmitt, and M. Finkbeiner, *Hydrogen and hydrogen-derived fuels through methane decomposition of natural gas–GHG emissions and costs.* Energy Conversion and Management: X, 2020. **7**: p. 100043.
19. Chehade, A.M.E.H., et al., *Simulation and optimization of hydrogen production by steam reforming of natural gas for refining and petrochemical demands in Lebanon.* International Journal of Hydrogen Energy, 2020. **45**(58): p. 33235-33247.
20. Dehdari, L., et al., *Purification of hydrogen from natural gas/hydrogen pipeline mixtures.* Separation and Purification Technology, 2022. **282**: p. 120094.
21. Sun, J., et al., *Investigation of the conversion mechanism for hydrogen production by coal gasification in supercritical water.* International Journal of Hydrogen Energy, 2021. **46**(17): p. 10205-10215.
22. Jiang, L., et al., *Coal decarbonization: A state-of-the-art review of enhanced hydrogen production in underground coal gasification.* Energy Reviews, 2022. **1**(1): p. 100004.
23. Nguyen-Thi, T.X., et al., *Recent advances in hydrogen production from biomass waste with a focus on pyrolysis and gasification.* International Journal of Hydrogen Energy, 2024. **54**: p. 127-160.
24. Wang, S., A. Lu, and C.-J. Zhong, *Hydrogen production from water electrolysis: role of catalysts.* Nano Convergence, 2021. **8**(1): p. 4.
25. Anwar, S., et al., *Recent development in electrocatalysts for hydrogen production through water electrolysis.* International Journal of Hydrogen Energy, 2021. **46**(63): p. 32284-32317.
26. Wang, T., X. Cao, and L. Jiao, *PEM water electrolysis for hydrogen production: fundamentals, advances, and prospects.* Carbon Neutrality, 2022. **1**(1): p. 21.
27. Simoes, S.G., et al., *Water availability and water usage solutions for electrolysis in hydrogen production.* Journal of Cleaner Production, 2021. **315**: p. 128124.
28. Ishaq, H. and I. Dincer, *Comparative assessment of renewable energy-based hydrogen production methods.* Renewable and Sustainable Energy Reviews, 2021. **135**: p. 110192.
29. Hassan, Q., et al., *Renewable energy-to-green hydrogen: A review of main resources routes, processes and evaluation.* International Journal of Hydrogen Energy, 2023.
30. Bora, J., S. Ghosh, and A. Mitra, *Photobiological hydrogen production by microorganisms*, in *Solar-Driven Green Hydrogen Generation and Storage*. 2023, Elsevier. p. 237-257.
31. Touloupakis, E., et al., *Sustained photobiological hydrogen production by Chlorella vulgaris without nutrient starvation.* International Journal of Hydrogen Energy, 2021. **46**(5): p. 3684-3694.
32. Mukherjee, N. and R. Srivastava, *Photobiological hydrogen production: Introduction and fundamental concept*, in *Solar-Driven Green Hydrogen Generation and Storage*. 2023, Elsevier. p. 193-222.
33. Al-Janabi, S., et al., *Advances in hydrogen production from sustainable recourses through biological and thermochemical pathways: Review and bibliometric analysis.* International Journal of Hydrogen Energy, 2024. **60**: p. 28-45.
34. Yadav, S., et al., *Biochemical and thermochemical routes of H2 production from food waste: a comparative review.* Chemical Engineering & Technology, 2023. **46**(2): p. 191-203.
35. Khan, A., et al., *Thermochemical conversion of agricultural waste to hydrogen, methane, and biofuels: A review.* Fuel, 2023. **351**: p. 128947.
36. Machineni, L., et al., *Biohydrogen production from lignocellulosic feedstock: Abiotic and biotic methods.* Renewable and Sustainable Energy Reviews, 2023. **182**: p. 113344.
37. Calise, F., et al., *Solar hydrogen production: processes, systems and technologies*. 2019: Academic Press.
38. Franchi, G., et al., *Hydrogen production via steam reforming: a critical analysis of MR and RMM technologies.* Membranes, 2020. **10**(1): p. 10.

39. Boretti, A., *Production of hydrogen for export from wind and solar energy, natural gas, and coal in Australia.* International Journal of Hydrogen Energy, 2020. **45**(7): p. 3899-3904.
40. Edwards, R.L., C. Font-Palma, and J. Howe, *The status of hydrogen technologies in the UK: A multi-disciplinary review.* Sustainable Energy Technologies and Assessments, 2021. **43**: p. 100901.
41. Yang, C. and J. Ogden, *Determining the lowest-cost hydrogen delivery mode.* International Journal of Hydrogen Energy, 2007. **32**(2): p. 268-286.
42. Witkowski, A., et al., *Comprehensive analysis of hydrogen compression and pipeline transportation from thermodynamics and safety aspects.* Energy, 2017. **141**: p. 2508-2518.
43. Schoots, K., et al., *Historical variation in the capital costs of natural gas, carbon dioxide and hydrogen pipelines and implications for future infrastructure.* International Journal of Greenhouse Gas Control, 2011. **5**(6): p. 1614-1623.
44. Wang, A., et al., *European hydrogen backbone: How a dedicated hydrogen infrastructure can be created.* 2020.
45. Kuczyński, S., et al., *Thermodynamic and technical issues of hydrogen and methane-hydrogen mixtures pipeline transmission.* Energies, 2019. **12**(3): p. 569.
46. Ogden, J., et al., *Natural gas as a bridge to hydrogen transportation fuel: Insights from the literature.* Energy Policy, 2018. **115**: p. 317-329.
47. Colorado, A., V. McDonell, and S. Samuelsen, *Direct emissions of nitrous oxide from combustion of gaseous fuels.* international journal of hydrogen energy, 2017. **42**(1): p. 711-719.
48. Melaina, M.W., O. Antonia, and M. Penev, *Blending hydrogen into natural gas pipeline networks: a review of key issues.* 2013.
49. Abad, A.V. and P.E. Dodds, *Green hydrogen characterisation initiatives: Definitions, standards, guarantees of origin, and challenges.* Energy Policy, 2020. **138**: p. 111300.
50. Ruth, M.F., et al., *The technical and economic potential of the H2@ Scale hydrogen concept within the United States*. 2020, National Renewable Energy Lab.(NREL), Golden, CO (United States).
51. Sorgulu, F. and I. Dincer, *Analysis and techno-economic assessment of renewable hydrogen production and blending into natural gas for better sustainability.* International Journal of Hydrogen Energy, 2022. **47**(46): p. 19977-19988.
52. Faye, O., J. Szpunar, and U. Eduok, *A critical review on the current technologies for the generation, storage, and transportation of hydrogen.* International journal of hydrogen energy, 2022. **47**(29): p. 13771-13802.
53. Rasul, M., et al., *The future of hydrogen: Challenges on production, storage and applications.* Energy Conversion and Management, 2022. **272**: p. 116326.
54. Arya, A.K., et al., *A multi-objective model for optimizing hydrogen injected-high pressure natural gas pipeline networks.* International Journal of Hydrogen Energy, 2023. **48**(76): p. 29699-29723.
55. Erdener, B.C., et al., *A review of technical and regulatory limits for hydrogen blending in natural gas pipelines.* International Journal of Hydrogen Energy, 2023. **48**(14): p. 5595-5617.
56. Koo, B., Y. Ha, and H. Kwon, *Preliminary evaluation of hydrogen blending into high-pressure natural gas pipelines through hydraulic analysis.* Energy, 2023. **268**: p. 126639.
57. Deymi-Dashtebayaz, M., et al., *Investigating the effect of hydrogen injection on natural gas thermo-physical properties with various compositions.* Energy, 2019. **167**: p. 235-245.
58. Mukherjee, U., et al., *Optimal sizing of an electrolytic hydrogen production system using an existing natural gas infrastructure.* International Journal of Hydrogen Energy, 2015. **40**(31): p. 9760-9772.
59. Cristello, J.B., et al., *Feasibility analysis of blending hydrogen into natural gas networks.* International Journal of Hydrogen Energy, 2023. **48**(46): p. 17605-17629.

60. Liu, J., et al., *Analysis of hydrogen gas injection at various compositions in an existing natural gas pipeline.* Frontiers in Energy Research, 2021. **9**: p. 685079.
61. Wang, B., et al., *An MILP model for the reformation of natural gas pipeline networks with hydrogen injection.* International Journal of Hydrogen Energy, 2018. **43**(33): p. 16141-16153.
62. Wang, B., et al., *An MILP model for optimal design of multi-period natural gas transmission network.* Chemical engineering research and design, 2018. **129**: p. 122-131.
63. Üster, H. and Ş. Dilaveroğlu, *Optimization for design and operation of natural gas transmission networks.* Applied Energy, 2014. **133**: p. 56-69.
64. da Silva Alves, F., J.N.M. de Souza, and A.L.H. Costa, *Multi-objective design optimization of natural gas transmission networks.* Computers & Chemical Engineering, 2016. **93**: p. 212-220.
65. Sanaye, S. and J. Mahmoudimehr, *Optimal design of a natural gas transmission network layout.* Chemical Engineering Research and Design, 2013. **91**(12): p. 2465-2476.
66. Wu, X., et al., *Optimal operation of trunk natural gas pipelines via an inertia-adaptive particle swarm optimization algorithm.* Journal of Natural Gas Science and Engineering, 2014. **21**: p. 10-18.
67. Chebouba, A., et al., *Optimization of natural gas pipeline transportation using ant colony optimization.* Computers & Operations Research, 2009. **36**(6): p. 1916-1923.
68. Guandalini, G., P. Colbertaldo, and S. Campanari, *Dynamic modeling of natural gas quality within transport pipelines in presence of hydrogen injections.* Applied energy, 2017. **185**: p. 1712-1723.
69. Saedi, I., S. Mhanna, and P. Mancarella, *Integrated electricity and gas system modelling with hydrogen injections and gas composition tracking.* Applied Energy, 2021. **303**: p. 117598.
70. Eames, I., M. Austin, and A. Wojcik, *Injection of gaseous hydrogen into a natural gas pipeline.* International Journal of Hydrogen Energy, 2022. **47**(61): p. 25745-25754.
71. Haeseldonckx, D. and W. D'haeseleer, *The use of the natural-gas pipeline infrastructure for hydrogen transport in a changing market structure.* International Journal of Hydrogen Energy, 2007. **32**(10-11): p. 1381-1386.
72. Zhou, D., et al., *Modeling and simulation of the hydrogen blended gas-electricity integrated energy system and influence analysis of hydrogen blending modes.* Energy, 2022. **239**: p. 121629.
73. Kazi, S.R., et al., *Modeling and optimization of steady flow of natural gas and hydrogen mixtures in pipeline networks.* International Journal of Hydrogen Energy, 2024. **54**: p. 14-24.
74. Weymouth, T., *Measurement of natural gas.* Journal of Fluids Engineering, 1912. **34**: p. 1091-1104.
75. Cullender, M. and R. Smith, *Practical solution of gas-flow equations for wells and pipelines with large temperature gradients.* Transactions of the AIME, 1956. **207**(01): p. 281-287.
76. Beggs, H.D., *An experimental study of two-phase flow in inclined pipes*. 1972: The University of Tulsa.
77. Osiadacz, A.J. and M. Chaczykowski, *Comparison of isothermal and non-isothermal pipeline gas flow models.* Chemical Engineering Journal, 2001. **81**(1-3): p. 41-51.
78. Khabbazi, A.J., et al., *Mixing hydrogen into natural gas distribution pipeline system through Tee junctions.* International Journal of Hydrogen Energy, 2024. **49**: p. 1332-1344.
79. Hai, W., L. Xiaojing, and Z. Weiguo, *Transient flow simulation of municipal gas pipelines and networks using semi implicit finite volume method.* Procedia Engineering, 2011. **12**: p. 217-223.
80. Sletfjerding, E. and J.S. Gudmundsson, *Friction factor directly from roughness measurements.* J. Energy Resour. Technol., 2003. **125**(2): p. 126-130.
81. Tabkhi, F., et al., *Improving the performance of natural gas pipeline networks fuel consumption minimization problems.* AIChE journal, 2010. **56**(4): p. 946-964.
82. Arya, A.K., et al., *A multi-objective model for optimizing hydrogen injected-high pressure natural gas pipeline networks.* International Journal of Hydrogen Energy, 2023.

83. Wu, S., et al., *Model relaxations for the fuel cost minimization of steady-state gas pipeline networks.* Mathematical and Computer Modelling, 2000. **31**(2-3): p. 197-220.
84. Khan, M.A., C. Young, and D.B. Layzell, *The techno-economics of hydrogen pipelines.* Transition Accelerator Technical Briefs, 2021. **1**(2): p. 1-40.
85. Clees, T., et al., *Efficient method for simulation of long-distance gas transport networks with large amounts of hydrogen injection.* Energy Conversion and Management, 2021. **234**: p. 113984.
86. Cerniauskas, S., et al., *Options of natural gas pipeline reassignment for hydrogen: Cost assessment for a Germany case study.* International Journal of Hydrogen Energy, 2020. **45**(21): p. 12095-12107.
87. Tabkhi, F., et al., *A mathematical framework for modelling and evaluating natural gas pipeline networks under hydrogen injection.* International journal of hydrogen energy, 2008. **33**(21): p. 6222-6231.
88. Adeyanju, O. and L. Oyekunle, *Optimization of natural gas transportation in pipeline.* 2015.
89. Zhang, X., C. Wu, and L. Zuo, *Minimizing fuel consumption of a gas pipeline in transient states by dynamic programming.* Journal of Natural Gas Science and Engineering, 2016. **28**: p. 193-203.
90. Goldberg, D.E., *Computer-aided pipeline operation using genetic algorithms and rule learning. PART I: Genetic algorithms in pipeline optimization.* Engineering with Computers, 1987. **3**: p. 35-45.
91. Li, T., P. Liu, and Z. Li, *Modelling and optimization of a natural gas supply system at a transient stage: a case study of China.* BMC Energy, 2019. **1**: p. 1-17.
92. Botros, K., et al. *Multi-objective optimization of large pipeline networks using genetic algorithm*. in *International Pipeline Conference*. 2004.
93. Habibvand, G. and R.M. Behbahani, *Using genetic algorithm for fuel consumption optimization of a natural gas transmission compressor station.* International Journal of Computer Applications, 2012. **43**(1): p. 1-6.
94. Kashani, A.H.A. and R. Molaei, *Techno-economical and environmental optimization of natural gas network operation.* Chemical Engineering Research and Design, 2014. **92**(11): p. 2106-2122.
95. Farrokhifar, M., Y. Nie, and D. Pozo, *Energy systems planning: A survey on models for integrated power and natural gas networks coordination.* Applied Energy, 2020. **262**: p. 114567.
96. Liu, S., et al., *Optimizing large-scale hydrogen storage: A novel hybrid genetic algorithm approach for efficient pipeline network design.* International Journal of Hydrogen Energy, 2024. **66**: p. 430-444.
97. Das, P., et al., *Evaluating the prospect of utilizing excess energy and creating employments from a hybrid energy system meeting electricity and freshwater demands using multi-objective evolutionary algorithms.* Energy, 2022. **238**: p. 121860.
98. Katoch, S., S.S. Chauhan, and V. Kumar, *A review on genetic algorithm: past, present, and future.* Multimedia tools and applications, 2021. **80**: p. 8091-8126.
99. Davis, M., et al., *Greenhouse gas reduction potential and cost-effectiveness of economy-wide hydrogen-natural gas blending for energy end uses.* Renewable and Sustainable Energy Reviews, 2023. **171**: p. 112962.
100. *About natural gas*. 2024 [cited May 2024; Available from: https://www.alberta.ca/about-natural-gas#:~:text=Alberta's%20residential%20and%20commercial%20sectors,and%20electric%20power%2Dgeneration%20industries.
101. *Alberta Energy Regulator*. Natural Gas Production May 2024; Available from: https://www.aer.ca/providing-information/data-and-reports/statistical-reports/st98/natural-gas/production.

102. Yu, Q., et al., *Techno-economic analysis of hydrogen pipeline network in China based on levelized cost of transportation.* Energy Conversion and Management, 2024. **301**: p. 118025.
103. *Emission factors and reference values, Government of Canada.* . June, 2024; Available from: https://www.canada.ca/en/environment-climate-change/services/climate-change/pricing-pollution-how-it-will-work/output-based-pricing-system/federal-greenhouse-gas-offset-system/emission-factors-reference-values.html
104. Compare FortisBC natural gas rates with gas marketers' rates, F., June 13, 2024.
105. *Coastal GasLink*. June 2024; Available from: https://www.coastalgaslink.com/.